CATALOGED BY ASTIA
AS AD No. 296188

INVESTIGATION OF THEORETICAL AND PRACTICAL ASPECTS OF THE THERMAL EXPANSION OF CERAMIC MATERIALS

Prepared for:
Department Of The Navy
Bureau Of Weapons

296 188

FINAL REPORT
Contract No. NOrd – 18419
CAL Report No. P1 – 1273 – M – 12
July 1962

A.S.T.I.A.
DEC 15 1963
TISIA

CORNELL AERONAUTICAL LABORATORY, INC.
OF CORNELL UNIVERSITY, BUFFALO 21, N. Y.

19990604257

NOTICE: When government or other drawings, specifications or other data are used for any purpose other than in connection with a definitely related government procurement operation, the U. S. Government thereby incurs no responsibility, nor any obligation whatsoever; and the fact that the Government may have formulated, furnished, or in any way supplied the said drawings, specifications, or other data is not to be regarded by implication or otherwise as in any manner licensing the holder or any other person or corporation, or conveying any rights or permission to manufacture, use or sell any patented invention that may in any way be related thereto.

Qualified requesters may obtain copies of this report from ASTIA.

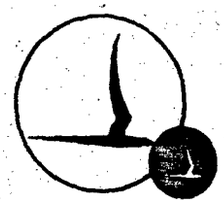

CORNELL AERONAUTICAL LABORATORY, INC.
BUFFALO 21, NEW YORK

FINAL REPORT

INVESTIGATION OF THEORETICAL AND PRACTICAL ASPECTS OF THE THERMAL EXPANSION OF CERAMIC MATERIALS

REPORT NO. PI-1273-M-12

CONTRACT NO. NOrd-18419

JULY 1962

PREPARED BY:

Henry P. Kirchner
Howard A. Scheetz
W. Richard Brown
Harold T. Smyth

H. P. Kirchner
H. P. Kirchner
Project Engineer

APPROVED BY:

H. P. Kirchner
H. P. Kirchner, Staff Scientist
Computer Research Department

W. St. Holmes
W. St. Holmes, Head
Computer Research Department

PREPARED FOR:

DEPARTMENT OF THE NAVY
BUREAU OF WEAPONS

ABSTRACT

Several methods were used to predict the thermal expansion coefficients of pure, single-phase ceramics. The predictions were extended to cover 1700 pure phases. Based upon these calculations a number of phases, predicted to have low values of thermal expansion coefficient, were synthesized and the thermal expansion properties of these materials were measured. Several of these were found to be low-expansion materials. The thermal expansion properties of cubic UP_2O_7 are particularly interesting. This material expands with increasing temperature up to about 400°C. Above this temperature the crystal contracts, returning to its room temperature length at about 1000°C. These properties are believed to be unique.

Variation of the thermal expansion anisotropy by addition of solid solution atoms to several base crystals was attempted. Addition of vanadium to rutile (TiO_2) resulted in a significant decrease in thermal expansion anisotropy. Vanadium additions to cassiterite (SnO_2) which has the same structure as rutile, also caused a significant decrease in thermal expansion anisotropy.

Two principal methods were used to predict the thermal expansion of two-phase ceramic bodies knowing the thermoelastic properties of the individual phases. Kerner's method was applied to ceramic bodies for the first time. Satisfactory predictions were made for several two-phase systems.

ABSTRACT

Several methods were used to predict the thermal expansion coefficients of pure, single-phase ceramics. The predictions were extended to cover 1700 pure phases. Based upon these calculations a number of phases, predicted to have low values of thermal expansion coefficient, were synthesized and the thermal expansion properties of these materials were measured. Several of these were found to be low-expansion materials. The thermal expansion properties of cubic UP_2O_7 are particularly interesting. This material expands with increasing temperature up to about 400°C. Above this temperature the crystal contracts, returning to its room temperature length at about 1000°C. These properties are believed to be unique.

Variation of the thermal expansion anisotropy by addition of solid solution atoms to several base crystals was attempted. Addition of vanadium to rutile (TiO_2) resulted in a significant decrease in thermal expansion anisotropy. Vanadium additions to cassiterite (SnO_2) which has the same structure as rutile, also caused a significant decrease in thermal expansion anisotropy.

Two principal methods were used to predict the thermal expansion of two-phase ceramic bodies knowing the thermoelastic properties of the individual phases. Kerner's method was applied to ceramic bodies for the first time. Satisfactory predictions were made for several two-phase systems.

FOREWORD

This final technical report covers research performed on a program sponsored by the Department of the Navy, Bureau of Weapons, under Contract NOrd-18419. The report includes significant sections from reports previously submitted for the period June, 1958 to September, 1960 and complete coverage of research performed during the period September, 1960 to July, 1962.

This research was performed under the general technical direction of Mr. S. J. Matesky of the Bureau of Weapons.

TABLE OF CONTENTS

		Page
	ABSTRACT	iii
	FOREWORD	iv
	LIST OF TABLES	vii
	LIST OF FIGURES	ix
I.	INTRODUCTION	1
II.	PREDICTION OF THE THERMAL EXPANSION COEFFICIENTS OF PURE CERAMIC CRYSTALS	3
	A. Introduction	3
	B. The Openness Method	3
	C. Openness of Homologous Series Method	13
	D. Prediction of the Thermal Expansion Coefficient Based Upon Atomic Spacing at Minimum Free Energy	22
	1. Independent Lattice Vibrations	23
	2. Vibrations of the Lattice as a Whole	34
	3. Method of Attack	34
	4. Ionic Forces	34
	5. Reciprocal Lattice	35
	6. Expansion Coefficient	35
	7. Discussion	36
III.	THE THERMAL EXPANSION OF SOLID SOLUTIONS	41
	A. Introduction	41
	B. Experimental	42
	1. Specimen Preparation	42
	2. Experimental Procedures	43

TABLE OF CONTENTS

		Page
	C. Discussion of Results	49
IV.	THE THERMAL EXPANSION OF TWO-PHASE BODIES	65
	A. Introduction	65
	B. Relationships Between Elastic Moduli and Stress Wave Velocities in Isotropic Bodies	65
	C. Applications of Ultrasonic Measurements	70
	1. Stress Wave Velocity Measurements	70
	D. Elastic Moduli of Polycrystalline Ceramics . . .	76
	E. Theoretical Thermal Expansion of Multiple-Phase Ceramic Bodies	79
	F. Comparisons Between Theoretical and Empirical Thermal Expansion in Two-Phase Materials	84
	1. Aluminum-Silica System	84
	2. Magnesium Oxide-Spinel System	84
	3. Pyrex-Spinel System	89
	G. Thermoelastic Anisotropy	95
	H. Elevated Temperature Effects	96
	I. Conclusions	
V.	CONCLUSIONS AND RECOMMENDATIONS	101
	A. Conclusions	101
	APPENDIX A: "Openness" Ratios of Some Ceramic Phases	A-1
	APPENDIX B: The Effect of Porosity on the Elastic Properties of Ceramics	B-1
	APPENDIX C: Relationships Between Single Crystal and Polycrystalline Elastic Constants, Including Data for Several Ceramic Phases	C-1
	APPENDIX D: References	D-1

LIST OF TABLES

Table		Page
I	Methods Used for Prediction of the Thermal Expansion Coefficients of Crystals	4
II	The Openness Ratio and Coefficient of Thermal Expansion of One and Two Component Oxides	7
III	The Openness Ratio and Coefficient of Thermal Expansion of Some Silicates	9
IV	Thermal Expansion of Phases Having Open Structures	10
V	Thermal Expansion of Cubic Rare Earth Oxides	16
VI	Thermal Expansion Coefficients for the Alkali Halides at 27°C; Calculated and Literature Values	33
VII	Thermal Expansion Coefficients for the Alkali Halides at 27°C; Calculated and Literature Values	37
VIII	Data On Preparation of Rutile Specimens	44
IX	Room Temperature Lattice Constants of Rutile Solid Solutions	47
X	Thermal Expansion Data for Rutile Solid Solutions (Room Temperature to 1000°C)	50
XI	Thermal Expansion Data for Al_2O_3-Cr_2O_3 Solid Solutions (400°C to 1000°C)	57
XII	Thermal Expansion Data for SnO_2-V_2O_5 Solid Solutions 23 - 800°C	60
XIII	Shear Wave Measurements for Pyrex-Spinel Specimens at Room Temperature (23°-28°C)	73
XIV	Shear Wave Transit Times for Test Specimen Components	75
XV	Elastic Properties of Fully Dense Polycrystalline Ceramics at Room Temperature	80
XVI	Comparison of Thermal Expansion Relations for Composite Media	86

LIST OF TABLES (CONT'D)

Table		Page
XVII	Thermal Expansion in the MgO-$MgO{\cdot}Al_2O_3$ System	88
XVIII	Forming Conditions For Hot-Pressed Pyrex-Spinel Disks	90
XIX	Thermal Expansion of $MgO{\cdot}Al_2O_3$ Spinel	97
B-I	Dimensionless Elastic Constant of Oxide Ceramics (Used in Porous Body Computations)	B-1
B-II	Shear Modulus Dependence on Porosity Based on Mackenzie's Relation	B-2
C-I	Elastic Constants of Oxide-Ceramic Single Crystals	C-3

LIST OF FIGURES

Figures		Page
1	Openness Ratio Vs. Linear Thermal Expansion Coefficient For One and Two Component Oxides at Room Temperature	6
2	Openness Ratio Vs. Linear Thermal Expansion Coefficient For Some Silicates at Room Temperature	8
3	Thermal Expansion of UP_2O_7	11
4	Alkali Halides	15
5	Thermal Expansion Coefficient Vs. Openness Ratio of Cubic Rare Earth Oxides	17
6	Linear Thermal Expansion of Sc_2O_3	18
7	Linear Thermal Expansion of Yb_2O_3	19
8	Linear Thermal Expansion of Er_2O_3	20
9	Linear Thermal Expansion of Dy_2O_3	21
10	Locations of the Atoms In A Simple Example Used For Calculations of Interatomic Forces	24
11	Lattice Constant a_o at Various Temperatures Vs. Composition for 1200°C Firing Temperature	48
12	Linear Thermal Expansion of Pure Rutile (TiO_2). .	52
13	Linear Thermal Expansion of TiO_2+(10 Mole %)ZrO_2	53
14	Linear Thermal Expansion of TiO_2 + 7.7 Mole % Vanadium	54
15	Linear Thermal Exparsion of TiO_2 + (10 Mole %)V_2O_5	55
16	Linear Thermal Expansion of TiO_2 + 21.4 Mole % Vanadium	56
17	Linear Thermal Expansion of Pure Cr_2O_3	58
18	Percent Linear Expansion of ZrO_2	61

LIST OF FIGURES (CONT'D)

Figures		Page
19	Percent Linear Expansion of SnO_2 + 10 Mole Percent V_2O_5	62
20	Block Diagram of CAL Ultrasonic Test System For Stress-Wave Pulse-Transmission Measurements	67
21	Ultrasonic Transducer and Test Specimen Assembly	71
22	Deformation of a Two-Phase Model Subjected to Compressive Loading	77
23	Elastic Moduli of Magnesia-Spinel Ceramics Based On Kerner's Theory	83
24	Thermal Expansion in the Aluminum-Silica System	85
25	Thermal Expansion in the Magnesia-Spinel System	87
26	Dilatometer Thermal Expansion Measurements For Pyrex-Spinel Bars	92
27	Elastic Moduli of Pyrex-Spinel Bodies Based On Kerner's Theory	93
28	Thermal Expansion in the Pyrex-Spinel System	94
B-1	Shear Modulus of Porous Alumina	B-4
B-2	Young's Modulus of Porous Alumina	B-8
B-3	Young's Modulus of Porous Magnesia	B-9
B-4	Shear Modulus of Porous Magnesia	B-10
B-5	Young's Modulus of Porous Spinel ($MgO \cdot Al_2O_3$)	B-11
B-6	Shear Modulus of Porous Spinel ($MgO \cdot Al_2O_3$)	B-12
B-7	Elastic Moduli of Porous Mullite	B-13
B-8	Elastic Moduli of Porous Thoria	B-14
B-9	Bulk Modulus of Pyrex-Spinel Mixtures	B-16

I. INTRODUCTION

The thermal expansion of solids is one of several phenomena included in the general concept of the equation of state of solids. Several aspects of the thermal expansion of ceramic materials were investigated in this program. Among these were the following:

1. Prediction of the thermal expansion properties of pure ceramic crystals. Crude prediction methods useful in the search for low expansion materials were investigated along with more sophisticated methods useful for calculating expansion coefficients.
2. Investigation of the thermal expansion anisotropy of solid solutions.
3. Prediction of the thermal expansion coefficients of two-phase ceramic bodies, knowing the thermoelastic properties of the individual phases.

In recent years rapid progress has been made toward understanding thermal expansion phenomena in terms of atomic vibration mechanisms. The objective of this research has been to indicate ways in which this knowledge can be used to solve practical problems. In addition, several new low-expansion phases were found and previously unavailable thermal expansion and elastic property data were determined.

II. PREDICTION OF THE THERMAL EXPANSION COEFFICIENTS OF PURE CERAMIC CRYSTALS

A. Introduction

Several methods can be used to predict the thermal expansion coefficients of pure ceramic crystals. The choice of a method depends to a great extent on the amount of available information and the accuracy required in the prediction. Since both of these factors may be subject to wide variations, it is desirable to have several different prediction methods. The methods investigated in this program are listed in Table I together with listings of the information required for prediction. The predictions made in the program and the evaluations made of these predictions using our measurements and those of other investigators are described in the following paragraphs.

B. The Openness Method

The relationship between the openness of the crystal structure and the thermal expansion coefficient has been noted by several authors.[1-5] Several measures of the openness of crystals can be calculated with little prior knowledge of crystal properties. One such measure is the openness ratio (R).

$$R = \frac{V_{FW} - V_I}{V_{FW}}$$

in which V_{FW} is the volume of a formula weight of the solid and V_I is the volume of a formula weight of ions or atoms

The openness ratios of a number of materials having known values of thermal expansion coefficient were calculated as part of the CAL sponsored research program which preceded this contract.[5] The effects of various assumptions concerning the degree of ionic binding, on the volume of the atoms, were determined. Calculations using Pauling's[6] electronegativity concept to determine the ionic radius, with the additional assumption that there is a linear variation of ionic radius with percent ionic binding, seemed to

TABLE I

METHODS USED FOR PREDICTION OF THE THERMAL EXPANSION COEFFICIENTS OF CRYSTALS

METHOD	INFORMATION REQUIRED
1. OPENNESS	CHEMICAL FORMULA, SPECIFIC GRAVITY
2. OPENNESS OF HOMOLOGOUS SERIES	CHEMICAL FORMULA, SPECIFIC GRAVITY STRUCTURE TYPE
3. ATOMIC SPACING AT MINIMUM FREE ENERGY ASSUMPTION OF INDEPENDENT VIBRATIONS	CHEMICAL FORMULA, STRUCTURE TYPE INTERATOMIC DISTANCE (LIMITED TO IONIC CRYSTALS WITH ONE BOND TYPE)
4. ATOMIC SPACING AT MINIMUM FREE ENERGY USING EWALD'S METHOD: VIBRATIONS NOT INDEPENDENT	CHEMICAL FORMULA, STRUCTURE TYPE INTERATOMIC DISTANCE (LIMITED TO IONIC CRYSTALS WITH ONE BOND TYPE)

give the best correlation between the openness ratio and the thermal expansion coefficient. The results for some ceramic phases are plotted in Figures 1 and 2 from data given in Tables II and III. At high values of the openness ratio there is a good correlation. At lower values of openness ratio other factors become important. For example, the phases falling farthest from the curve on the high R side are those which have relatively weak bonds between cations and isolated silicate groups (wollastonite, pseudo-wollastonite, forsterite, etc.). Those falling farthest from the curve on the low R side are phases such as corundum (Al_2O_3) which have especially strong bonds. Therefore, it seems likely that this approach can be used most successfully when applied to the search for low-expansion materials.

The more rigorous theoretical approaches to prediction of the thermal expansion of ceramic phases provide some confirmation for these statements. Smyth[2] and others who have investigated the thermal expansion of materials which have low or negative thermal expansion coefficients have attributed the low expansion of some materials to the greater freedom for transverse vibrations in materials having open structures. The observed changes in vibration frequency for internal oscillations (vibrations within groups) and lattice oscillations described by Ganesan[7] for the case of sodium chlorate and sodium bromate, indicate the greater importance of the lattice oscillations, over that of internal oscillations in determining the thermal expansion of crystals with group formation. The importance of the strength of bonds is recognizable in expressions derived by Gruneisen[8], Kontorova[9], Cartz[10], Borelius[11], Kumar[12,13] and others.

The openness ratios of many phases have been calculated. The results of about 1400 of these calculations were presented previously[14]. The results of additional calculations are presented in Appendix A of this report. Based upon the results of the first series of these calculations, a number of phases having open structures were selected for synthesis and thermal expansion measurement. The results are summarized in Table IV. As a result of these measurements, several new low-expansion phases are available.

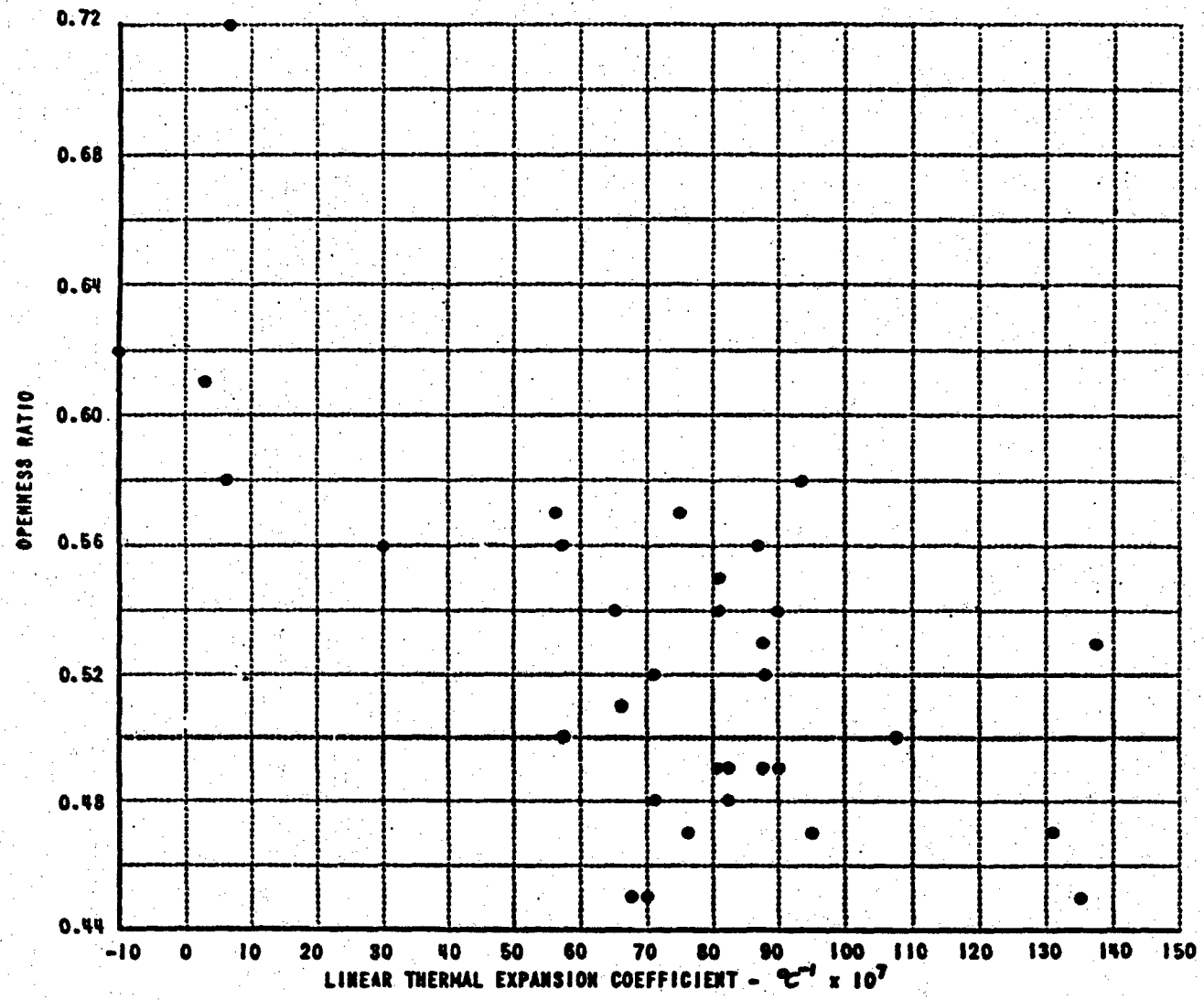

Figure 1 OPENNESS RATIO VS. LINEAR THERMAL EXPANSION COEFFICIENT FOR ONE AND TWO COMPONENT OXIDES AT ROOM TEMPERATURE

Table II

THE OPENNESS RATIO AND COEFFICIENT OF THERMAL EXPANSION OF ONE AND TWO COMPONENT OXIDES

CHEMICAL FORMULA	CONSTITUTION AND METHOD	OPENNESS RATIO	MEAN LINEAR COEFFICIENT OF THERMAL EXPANSION $\alpha_{C^{-1}}$	NOTE 1
Al_2O_3	CORUNDUM, SINGLE CRYST., HEX. INTERFEROMETER	0.45	70×10^{-7}	20-300°C AUSTIN (1006)
$Al_2O_3.TiO_2$	POLYCRYST., ORTHORHOMBIC, X-RAY	0.47	95×10^{-7}	NOTE 2 20-1000°C
			APPROX. SAME AS	20-300°C BUESSEM(1028)
$BaO.Al_2O_3$	POLYCRYST., CUBIC AND HEX.(?) DILATOMETER	0.57	75×10^{-7}	20-300°C THIELKE(1239) NOTE 3
BeO	BROMELITE, POLYCRYST., HEX. X-RAY (203 REFLECTION ONLY)	0.48	82×10^{-7}	20-300°C BEALS(1015)
$BeO.Al_2O_3$	SPINEL STRUCTURE, POLYCRYST., CUBIC DILATOMETER	0.45	68×10^{-7}	20-300°C THIELKE(1239) NOTE 4
CaO	POLYCRYST., CUBIC X-RAY	0.47	131×10^{-7}	20-300° BEALS(1015)
$CaO.Al_2O_3$	POLYCRYST., ORTHORHOMBIC OR MONOCLINIC DILATOMETER	0.57	56×10^{-7}	100-300°C RIGBY(1171)
$3CaO.Al_2O_3$	POLYCRYST., PSEUDO CUBIC, DILATOMETER	0.55	81×10^{-7}	100-300°C RIGBY(1171)
$2CaO.Fe_2O_3$	POLYCRYST., DILATOMETER	0.53	88×10^{-7}	100-300°C RIGBY(1171)
$CaO.ZrO_2$	POLYCRYST., MONOCLINIC	0.49	90×10^{-7}	20-300°C HABLER(1151)
CeO_2	POLYCRYST., CUBIC	0.49	82×10^{-7}	20-300°C HUMMEL(1110)
Fe_2O_3	SINGLE CRYST., TRIGONAL, HEMATITE INTERFEROMETER	0.54	94×10^{-7}	160°C SHARMA(1201)
Fe_3O_4	SINGLE CRYST., CUBIC, MAGNETITE INTERFEROMETER	0.56	87×10^{-7}	41.5°C SHARMA(1198)
$Li_2O.Al_2O_3$	POLYCRYST., DILATOMETER	0.58	93×10^{-7}	20-300°C BUNNEL(1106)
$Li_2O.5Al_2O_3$	POLYCRYST., CUBIC, SPINEL STR. DILATOMETER	0.48	71×10^{-7}	20-300°C HUMMEL(1106)
$MgO.Cr_2O_3$	POLYCRYST., CUBIC, SPINEL STR., X-RAY	0.54	60×10^{-7}	20-300°C BEALS(1015)
MgO	POLYCRYST., CUBIC, PERICLASE, X-RAY	0.45	135×10^{-7}	20-300°C BEALS(1015)
$MgO.2TiO_2$	POLYCRYST., ORTHORHOMBIC, X-RAY	0.52	88×10^{-7}	20-300°C BUSH, SARAKAUSKAS NOTE 5
$MgO.Al_2O_3$	POLYCRYST., SPINEL., X-RAY	0.49	88×10^{-7}	20-300°C BEALS(1015)

CHEMICAL FORMULA	CONSTITUTION AND METHOD	OPENNESS RATIO	MEAN LINEAR COEFFICIENT OF THERMAL EXPANSION $^{\circ}C^{-1}$	NOTE 1
$4MgO.Nb_2O_5$	POLYCRYST., INTERFEROMETER	0.51	66×10^{-7}	25-300°C DURBIN(1061)
Nb_2O_5	POLYCRYST., RHOMBIC, INTERFEROMETER	0.62	-10×10^{-7}	25-300°C DURBIN(1061) NOTE 6
SrO	POLYCRYST., CUBIC, X-RAY	0.53	137×10^{-7}	20-300°C BEALS(1015)
SiO_2	VITREOUS SILICA, TELEMICROSCOPE	0.72	7×10^{-7}	25-300°C WHITTEMORE(1265)
Ta_2O_5	POLYCRYST., RHOMBIC, INTERFEROMETER	0.57	6×10^{-7}	20-300°C DURBIN(1061)
ThO_2	POLYCRYST., CUBIC, TELEMICROSCOPE	0.52	71×10^{-7}	25-300°C WHITTEMORE(1265)
SnO_2	POLYCRYST., TETRAGONAL, CASSITERITE DILATOMETER	0.56	30×10^{-7}	20-300°C HUMMEL(1110)
TiO_2	POLYCRYST., TETRAGONAL, RUTILE, X-RAY	0.58	107×10^{-7}	20-300°C BEALS(1015)
V_2O_4	POLYCRYST., DILATOMETER	0.50	57×10^{-7}	20-300°C KING(1115)
V_2O_5	POLYCRYST., DILATOMETER	0.61	9×10^{-7}	20-300°C KING(1115)
ZnO	POLYCRYST., HEXAGONAL, X-RAY	0.56	57×10^{-7}	20-300°C BEALS(1015
$ZnO.Al_2O_3$	POLYCRYST., CUBIC, SPINEL STR., X-RAY	0.48	81×10^{-7}	20-300 C BEALS(1015)
$ZnO.Cr_2O_3$	POLYCRYST., CUBIC, SPINEL STR., X-RAY	0.54	90×10^{-7}	20-300 C BEALS(1015)
ZrO_2	POLYCRYST., MONOCLINIC, DILATOMETER	0.47	57×10^{-7}	25-300 C DUWEZ(1062)

NOTES

NOTE 1 THERMAL EXPANSION COEFFICIENT, TEMPERATURE RANGE AUTHOR'S NAME AND REFERENCE NUMBER GIVEN IN THAT ORDER. THE REFERENCES ARE LISTED BY NUMBER IN VOLUME I, CAL REPORT NO. PI-1273-M-4 AUGUST 31, 1959.

NOTE 2 THE THERMAL EXPANSION OF POLYCRYSTALINE AGGREGATES OF $Al_2O_3.TiO_2$ IS NEGATIVE AND SHOWS SUBSTANTIAL THERMAL EXPANSION HYSTERESIS.

NOTE 3 SEE ALSO PENNSYLVANIA STATE COLLEGE MEMO. REPORT NO. 16, AT 137225, MAY 15, 1948.

NOTE 4 SEE ALSO PENNSYLVANIA STATE COLLEGE MEMO. REPORT NO. 15, CONTRACT NO. 33-038ac-16374 (17284) FEBRUARY 16, 1948

NOTE 5 $MgO.2TiO_2$ HAS A HIGH DEGREE OF THERMAL EXPANSION ANISOTROPY AND SHOWS SUBSTANTIAL THERMAL EXPANSION HYSTERESIS. E.A. BUSH AND F.A. HUMMEL, J. AM. CERAM. SOC. 41 (6) 186-195 (1958). R.V. SARAKAUSKAS, "STUDY OF COMPOUNDS ISOMORPHOUS WITH ALUMINUM TITANATE", THESIS, THE PENNSYLVANIA STATE UNIVERSITY (1952).

NOTE 6 POLYCRYSTALLINE AGGREGATES OF Nb_2O_5 MAY SHOW THERMAL EXPANSION HYSTERESIS.

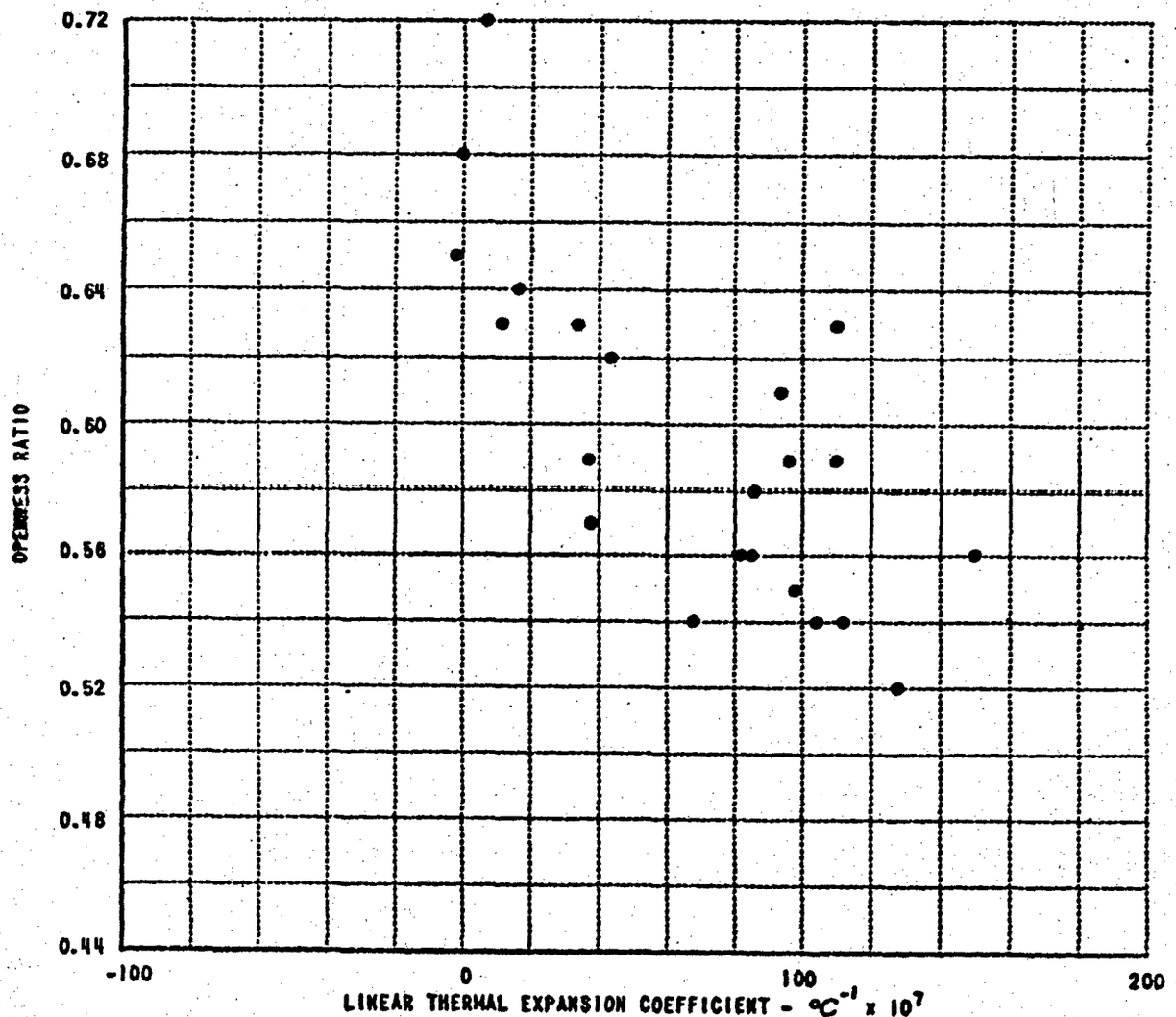

Figure 2 OPENNESS RATIO VS. LINEAR THERMAL EXPANSION COEFFICIENT FOR SOME SILICATES AT ROOM TEMPERATURE

PI-1277-R-12

Table III

THE OPENNESS RATIO AND COEFFICIENT OF THERMAL EXPANSION OF SOME SILICATES

CHEMICAL FORMULA	CONSTITUTION AND METHOD	OPENNESS RATIO	MEAN LINEAR COEFFICIENT OF THERMAL EXPANSION $^{\circ}C^{-1}$	NOTE I
$3Al_2O_3.2SiO_2$	POLYCRYST., ORTHORHOMBIC, MULLITE INTERFEROMETER (MASS OF ORIENTED CRYSTALS)	0.57	38×10^{-7}	25-300°C AUSTIN(1006)
$BaO.Al_2O_3.2SiO_2$	POLYCRYST., 90% CELSIAN, MONOCLINIC INTERFEROMETER	0.63	32×10^{-7}	25-200°C GELLER(1078)
$3BaO.Al_2O_3.6SiO_2$	SINGLE CRYSTAL, BERYL, HEXAGONAL INTERFEROMETER	0.64	16×10^{-7}	25-225°C GELLER(1078)
$CaO.SiO_2$	POLYCRYST., PSEUDO-WOLLASTONITE MONOCLINIC, DILATOMETER	0.58	96×10^{-7}	100-300°C RIEBY(1173)
$CaO.SiO_2$	POLYCRYST., PSEUDO-WOLLASTONITE MONOCLINIC, DILATOMETER	0.58	96×10^{-7}	100-300°C RIEBY(1173)
$CaO.SiO_2$	POLYCRYST., WOLLASTONITE INTERFEROMETER	0.58	110×10^{-7}	20-300°C ANDERS(1061)
$2CaO.SiO_2$	POLYCRYST., $2CaO.SiO_2$ RHOMBIC, DILATOMETER	0.52	120×10^{-7}	100-300°C RIEBY(1173)
$2CaO.Al_2O_3.SiO_2$	POLYCRYST., TETRAGONAL, GEHLENITE DILATOMETER	0.56	82×10^{-7}	100-300°C RIEBY(1172)
$CaO.Al_2O_3.2SiO_2$	POLYCRYST., TRICLINIC, ANORTHITE INTERFEROMETER	0.62	43×10^{-7}	20-300°C GELLER(1072)
$CaO.MgO.2SiO_2$	POLYCRYST., MONOCLINIC, DIOPSIDE DILATOMETER	0.54	68×10^{-7}	100-300°C RIEBY(1173)
$CaO.MgO.SiO_2$	POLYCRYST., ORTHORHOMBIC, MONTICELLITE, DILATOMETER	0.54	111×10^{-7}	100-300°C RIEBY(1173)
$2CaO.MgO.2SiO_2$	POLYCRYST., TETRAGONAL, AKERMANITE DILATOMETER	0.58	86×10^{-7}	100-300°C RIEBY(1172)
$3CaO.MgO.2SiO2$	POLYCRYST., MONOCLINIC, HERWINITE DILATOMETER	0.54	104×10^{-7}	100-300°C RIEBY(1172)
$2FeO.SiO_2$	POLYCRYST., ORTHORHOMBIC, FAYALITE DILATOMETER	0.61	93×10^{-7}	20-300°C RIEBY(1173)
$Li_2O.Al_2O_3.2SiO_2$	POLYCRYST., HEXAGONAL EUCRYPTITE DILATOMETER	0.65	-6×10^{-7}	20-300°C GILLERY & BUSH NOTE I
$Li_2O.Al_2O_3.6SiO_2$ or $Li_2O.Al_2O_3.8SiO_2$	POLYCRYST., MONOCLINIC, PETALITE(?) DILATOMETER	0.68	0×10^{-7}	20-300°C RUMMEL(1105, 1108) NOTE I
$MgO.SiO_2$	POLYCRYST., MONOCLINIC, CLINOENSTATITE	0.56	82×10^{-7}	100-300°C RIEBY(1174)
$2MgO.SiO_2$	POLYCRYST., ORTHORHOMBIC, FORSTERITE, DILATOMETER	0.55	98×10^{-7}	100-300°C RIEBY(1174)
$2MgO.2Al_2O_3$	POLYCRYST., 90% CORDIERITE INTERFEROMETER	0.63	11×10^{-7}	25-300°C GELLER(1078)
$Na_2O.Al_2O_3.2SiO_2$	POLYCRYST., TRICLINIC, CARNEGIEITE, DILATOMETER	0.63	110×10^{-7}	20-300°C RUMMEL(1104)
$Na_2O.CaO.SiO_2$	POLYCRYST., CUBIC, DILATOMETER	0.56	150×10^{-7}	20-300°C RUMMEL(1104)
SiO_2	VITREOUS SILICA, TELEMICROSCOPE	0.72	7×10^{-7}	25-300°C WHITTEMORE(1265)
$ZrO_2.SiO_2$	POLYCRYST., TETRAGONAL, ZIRCON,	0.59	37×10^{-7}	25-300°C WHITTEMORE(1265)

NOTE I

THE LITHIUM ALUMINUM SILICATES ARE WIDELY KNOWN TO HAVE LOW VALUES OF THERMAL EXPANSION COEFFICIENT. THEY ARE ALSO NOTED FOR LOW VALUES OF MODULUS OF RUPTURE WHICH ARE THOUGHT TO BE DUE TO INTERNAL CRACKS FORMED AS A RESULT OF ANISOTROPIC THERMAL EXPANSION. THE X-RAY DETERMINATION OF THE THERMAL EXPANSION COEFFICIENT β-EUCRYPTITE IS REPORTED IN THE FOLLOWING REFERENCE.

F.H. GILLERY AND E.A. BUSH, "THERMAL CONTRACTION OF β-EUCRYPTITE ($Li_2O.Al_2O_3.2SiO_2$) BY X-RAY AND DILATOMETER METHODS". J. AM. CERAM. SOC. 42 (4) 175-77. (1959).

Table IV

THERMAL EXPANSION OF PHASES HAVING OPEN STRUCTURES

FORMULA	DESCRIPTION	OPENNESS RATIO	THERMAL EXPANSION COEFFICIENT TEMP. $\alpha_C \times 10^7$	RANGE °C	REFERENCE
$Al_2O_3.As_2O_5$	SAMPLE DECOMPOSED; X-RAY EVIDENCE OF NON-CRYSTALLINE MATERIAL.	0.69	——	——	KIRCHNER ET AL (1959)
$CdO.CeO_2$	SAMPLE DECOMPOSED	0.70	——	——	KIRCHNER ET AL (1959)
$3CoO.P_2O_5$	X-RAY ANAL. INDICATED SAMPLE WAS MAINLY $3CoO.P_2O_5$	0.78	80.8	20-700	KIRCHNER ET AL (1959)
$Li_2O.2SiO_2$	X-RAY ANAL. INDICATED $Li_2O.2SiO_2$ PLUS $Li_2O.SiO_2$ AND QUARTZ	0.63	105	20-700	KIRCHNER ET AL (1959)
$MnO.SiO_2$	NO X-RAY DIFFRACTION ANAL.	0.66	83.3	20-900	KIRCHNER ET AL (1959)
$ThO_2.SiO_2$	X-RAY ANAL. INDICATED ONLY $ThO_2.SiO_2$	0.66	61.8	25-1015	MERZ ET AL (1960)
$3SnO.P_2O_5$	X-RAY ANAL. INDICATED MAINLY $3SnO.P_2O_5$ WITH SMALL AMOUNTS OF $SnSO_4$ AND $Na_3P_2O_5$	0.74	96.7	20-700	KIRCHNER ET AL (1959)
$3BaO.Al_2O_3$	X-RAY ANAL. INDICATED PRESENCE OF $BaO.Al_2O_3$ AND BaO. NO PATTERN WAS AVAILABLE FOR $3BaO.Al_2O_3$	0.57	52.5	20-1032	MERZ ET AL (1960)
$SrO.2Al_2O_3$	X-RAY ANAL. INDICATED MAINLY $SrO.2Al_2O_3$ SOME FREE SrO AND Al_2O_3 ALSO PRESENT.	0.62	67.0	25-1052	MERZ ET AL (1960)
$SrO.Al_2O_3.2SiO_2$	X-RAY PATTERN SIMILAR TO $BaO.Al_2O_3.2SiO_2$ HOMOLOG	0.62	52.3	25-1000	MERZ ET AL (1960)
$CaO.CuO.4SiO_2$	X-RAY PATTERN INDICATED ONLY $CaO.CuO.4SiO_2$	0.64*	29.7	39-1015	MERZ ET AL (1960)
$SrO.CuO.4SiO_2$	X-RAY PATTERN INDICATED ONLY $SrO.CuO.4SiO_2$	——	19.0	26-1013	MERZ ET AL (1960)
$BaO.CuO.4SiO_2$	X-RAY PATTERN INDICATED ONLY $BaO.CuO.4SiO_2$	——	36.6	38-1007	MERZ ET AL (1960)
$UO_2.P_2O_5$	X-RAY ANAL. INDICATES CUBIC UP_2O_7 WITH A POSSIBLE TRACE OF $(UO)_2P_2O_7$	0.72	48.8 -32.3 - 6.66	20-400 400-1200 29-1200	MERZ ET AL (1960)

*THIS COMPOUND WAS SELECTED FOR MEASUREMENT BASED UPON THE OPEN SHEET SILICATE STRUCTURE. THE OPENNESS RATIO R WAS CALCULATED AFTER THE MEASUREMENT OF THE THERMAL EXPANSION COEFFICIENT.

The most unusual low-expansion phase studied in this program is cubic UP_2O_7. Expansion measurements were made using both the x-ray and dilatometer methods. The results for both methods are presented in Figure 3. The material

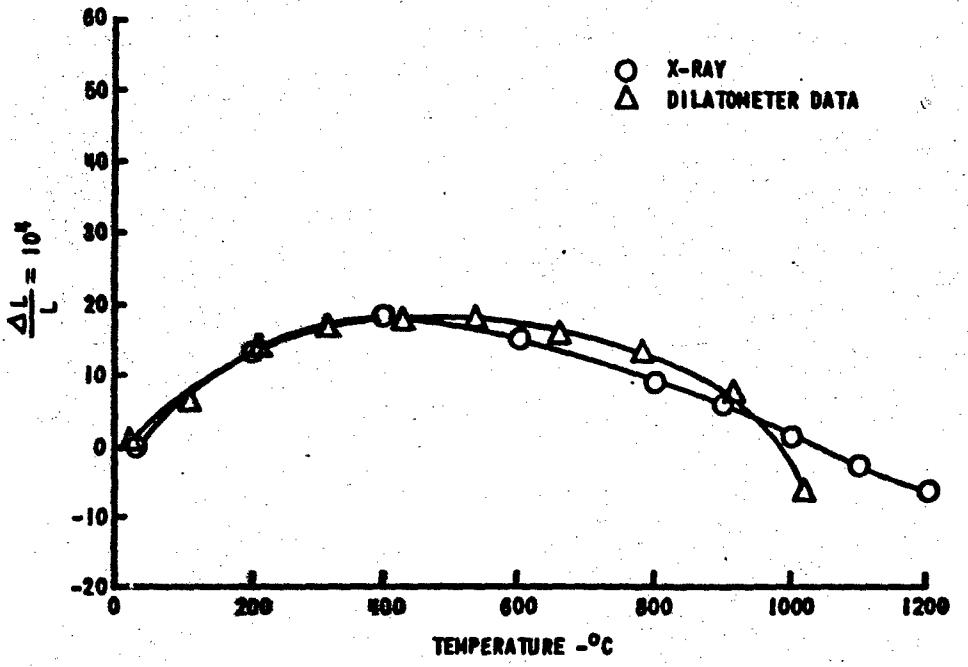

Figure 3 THERMAL EXPANSION OF UP_2O_7

expands up to about 400°C and then contracts, returning to the room temperature dimensions at about 1000°C. Agreement between the two methods of measuring the thermal expansion is good up to about 400°C. Above 400°C, the dilatometer gives slightly higher results. Between 900 and 1000°C the curves cross again so that at 1000°C the dilatometer measurement is lower than the x-ray measurement. The lack of good agreement at 1000°C and above may be due to the presence of a small percentage of $(UO)_2P_2O_7$. The presence of this material would affect the dilatometer measurement since this method measures the overall expansion of both phases, whereas the x-ray method is

sensitive only to changes in the cubic UP_2O_7 phase and not to other phases. Comparison of the x-ray patterns for UP_2O_7 at room temperature and 1000°C (the temperature at which the unit cell of UP_2O_7 has almost returned to its room temperature dimensions) shows close agreement in both "d" spacings and intensities. The pattern taken at 1000°C is excellent and gives no indication of structural changes. Only two weak lines not characteristic of cubic UP_2O_7 were observed. This type of expansion followed by contraction without a phase transformation is unique. Curvature of the thermal expansion curve in the other direction is not uncommon (Si, Ge, InSb and vitreous SiO_2 at low temperatures) but the reverse has not previously been observed.

The thermal expansion of uranium pyrophosphate can be compared with the results for the similar titanium and zirconium compounds measured by Harrison and Hummel.[15,16] TiP_2O_7 has a rather typical thermal expansion curve. The material expands almost linearly from room temperature to 1000°C and has a thermal expansion coefficient of approximately 122 x 10^{-7}/°C. for the temperature range from 50°C to 1000°C. These crystals are weakly birefringent. On the other hand, zirconium pyrophosphate (ZrP_2O_7) expands slightly more than the titanium compound in the range from room temperature to 400°C, but above this temperature the thermal expansion coefficient decreases so that little expansion is observed. These crystals are isotropic. Harrison and Hummel[15] state that the "normal" zirconium phosphate, ZrP_2O_7, has a reversible inversion from a low temperature cubic form to a high temperature cubic form at 300°C and dissociates to the zirconyl compound $(ZrO)_2P_2O_7$ at 1550°C. The thermal expansion of UP_2O_7 seems to be related to that of ZrP_2O_7 in that the material expands to temperatures in the range from 300 to 400°C and then there is a change in the shape of the thermal expansion curve. In the case of UP_2O_7, the thermal expansion coefficient gradually decreases becoming negative at temperatures in the range from 400-500°C so that the sample contracts with increasing temperature in the range from 400°C to 1200°C.

Smyth[2] has explained the negative thermal expansion of vitreous silica and the high temperature forms of quartz, tridymite, and crystobalite on the basis of the variation with temperature of the transverse vibrational frequency of the oxygen atoms vibrating between two silicon atoms. As the

volume decreases, the transverse vibrational frequency of the oxygen decreases due to an increase in the high order repulsion forces which resist restoration of the oxygen to its original position. This increase in the high order repulsion forces is only partially offset by an increase in the electrostatic attraction forces which tend to pull the oxygen back into its position. According to Smyth there is always the possibility of negative expansion if one or more of the lattice frequencies can decrease in this way as the volume decreases. Perhaps the negative expansion of UP_2O_7 can be explained on this basis. Wyckoff[17] describes the structure of ZrP_2O_7 (which is the same as the structure of UP_2O_7) as made up of an undistorted array of Zr^{+4} and $P_2O_7^{4-}$ ions. The P_2O_7 ion consists of a pair of PO_4 tetrahedra which share an oxygen ion with a P-O separation of 1.56 angstroms. The other P-O separations are 1.52 angstroms. Each Zr^{+4} ion is surrounded by six octahedrally distributed oxygen neighbors at a distance of 2.02 Å. Relatively large holes run through the structure bordering the oxygens shared by two phosphorous atoms. Since there are no close neighbors in the transverse directions, a displaced oxygen atom is drawn back into position by electrostatic attractions of its pair of phosphorous neighbors. This is opposed somewhat by the high order repulsion of the same phosphorous atoms. As the lattice shrinks there is a decrease of the restoring force on the transversely displaced oxygen atoms and a decrease in the transverse vibration frequency. This is the condition required for negative expansion.

C. Openness of Homologous Series Method

Many authors including Hummel[18], Austin[19], Megaw[20], Rigby[1] and Smyth[2] have stressed the importance of considering the crystal structure type in any attempt to systematize the thermal expansion properties of materials. Since structure type is an important factor in determining the thermal expansion properties, it is likely that variations among the phases within one structure type will be substantially less than the variations observed in groups of phases having several different structure types. Therefore, the effect of variations other than structure type can be studied in series of

compounds having the same structure type. For this reason, an attempt was made to correlate thermal expansion coefficients and openness ratios for homologous series of compounds. Chemical homologs are compounds having the same structure and similar chemical formulas; for example, the series of cubic compounds TiP_2O_7, ZrP_2O_7 and UP_2O_7.

The thermal expansion properties of several homologous series have been studied.[21,22] These studies were handicapped by lack of data for many phases. In some cases Megaw's rule ($\alpha = Ap^2/\varepsilon^2$ in which p is the coordination number, ε is the ionic charge and A is a constant) was approximately obeyed (cubic alkaline earth oxides, oxides with the CaF_2 structure, and carbides with the NaCl structure). That is, within homologous series the thermal expansion coefficients are the same. In other cases, the presence of displacive transformations or other processes made application of this method of uncertain validity (the cubic pyrophosphates TiP_2O_7, ZrP_2O_7 and UP_2O_7). In the case of the alkali halides there is a reciprocal relationship between the thermal expansion coefficients and the openness ratios for the alkali metal and halogen series. This is shown in Figure 4. In these calculations 100% ionic binding was assumed. The thermal expansion decreases with increasing openness ratio for the halogen series F^-, Cl^-, Br^- and I^-. This relationship is also observed for the alkali metal series Li^+, Na^+, K^+, etc. Exceptions occur for the fluoride series LiF, NaF, KF and CsF. The halides with the cesium chloride structure (CsCl, CsBr, CsI) also show a small decrease in thermal expansion coefficient with increasing openness ratio. The phases with the cesium chloride structure have high values of thermal expansion coefficient relative to those with the sodium chloride structure due to an increase in coordination number.

The cubic rare earth sesquioxides represent an interesting homologous series because variations in chemical bonding are minimized while at the same time there are substantial variations in the openness ratios. Available data on the thermal expansion of these crystals are given in Table V. The openness ratio is plotted vs. thermal expansion coefficient for two temperature ranges in Figure 5. The thermal expansion curves for four members of this series measured by the x-ray method are given in Figures 6 - 9. It is

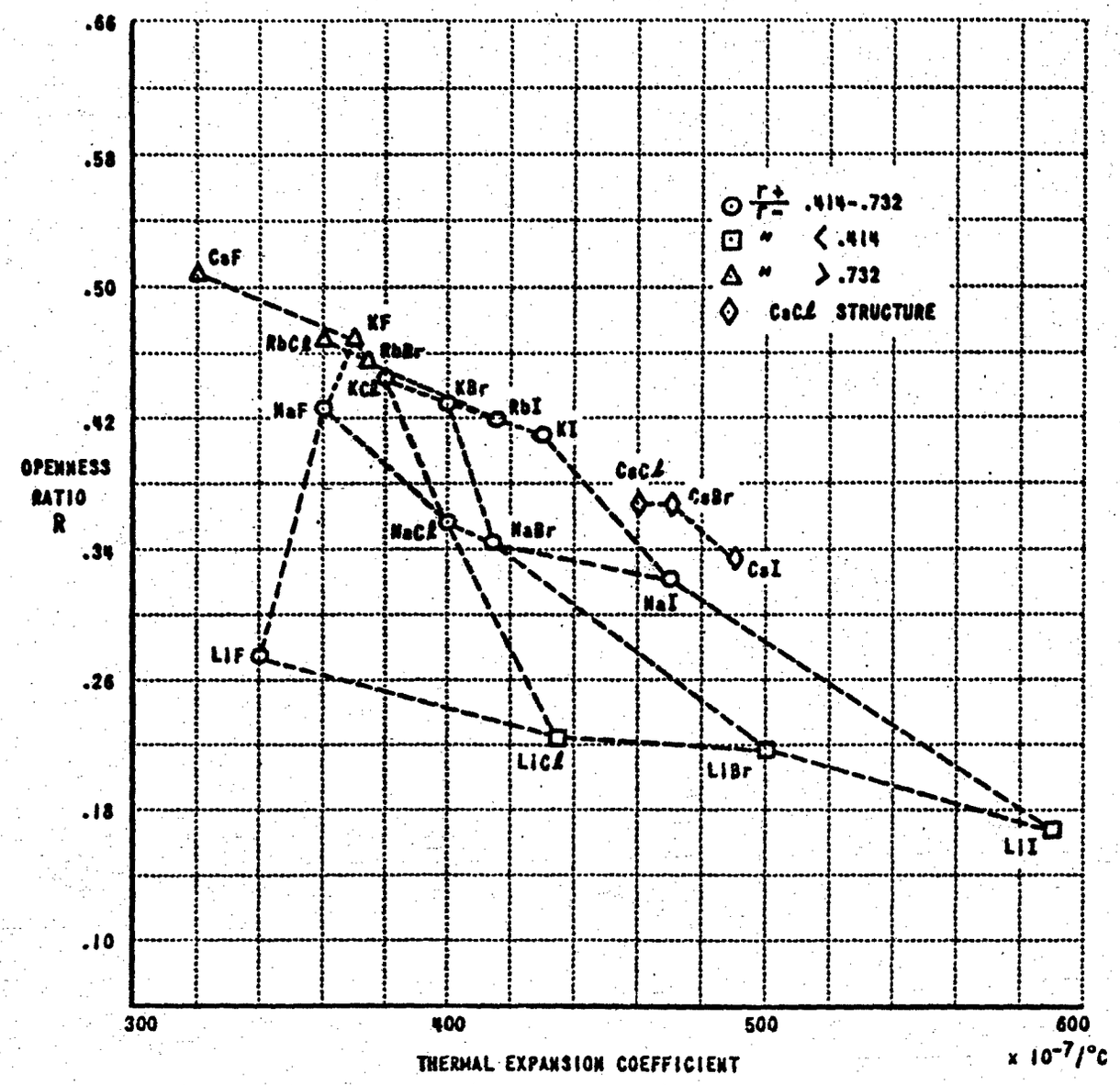

Figure 4 ALKALI HALIDES

Table V

THERMAL EXPANSION OF CUBIC RARE EARTH OXIDES

OXIDE	SAMPLE DESCRIPTION	THERMAL EXPANSION COEFFICIENT $10^7/°C$	TEMPERATURE	REFERENCE
Sc_2O_3	CUBIC	85	0-999°C	STECURA & CAMPBELL (1961)[62]
Y_2O_3	CUBIC	85	0-993°C	STECURA & CAMPBELL (1961)[62]
	CUBIC	88	20-1000°C	WARSHAW & ROY (1961)[60]
Sm_2O_3	CUBIC	88	0-950°C	STECURA & CAMPBELL (1961)[62]
Eu_2O_3	CUBIC	78	0-1011°C	STECURA & CAMPBELL (1961)[62]
Gd_2O_3	CUBIC	86	0-1062°C	STECURA & CAMPBELL (1961)[62]
Dy_2O_3	CUBIC	82.9	25-1200°C	BROWN & KIRCHNER (1961)[61]
	CUBIC	82	0-985°C	STECURA & CAMPBELL (1961)[62]
		83	30-840°C	PLOETZ, KRYSTYNIAK & DUMES (1957)[71]
Ho_2O_3	CUBIC	82	0-969°C	STECURA & CAMPBELL (1961)[62]
Er_2O_3	CUBIC	82.1	25-1200°C	BROWN & KIRCHNER (1961)[61]
	CUBIC	79	0-1038°C	STECURA & CAMPBELL (1961)[62]
Tm_2O_3	CUBIC	82	0-1031°C	STECURA & CAMPBELL (1961)[62]
Yb_2O_3	CUBIC	82.1	25-1200°C	BROWN & KIRCHNER (1961)[61]
	CUBIC	81	0-1021°C	STECURA & CAMPBELL (1961)[62]
Lu_2O_3	CUBIC	78	0-1045°C	STECURA & CAMPBELL (1961)[62]

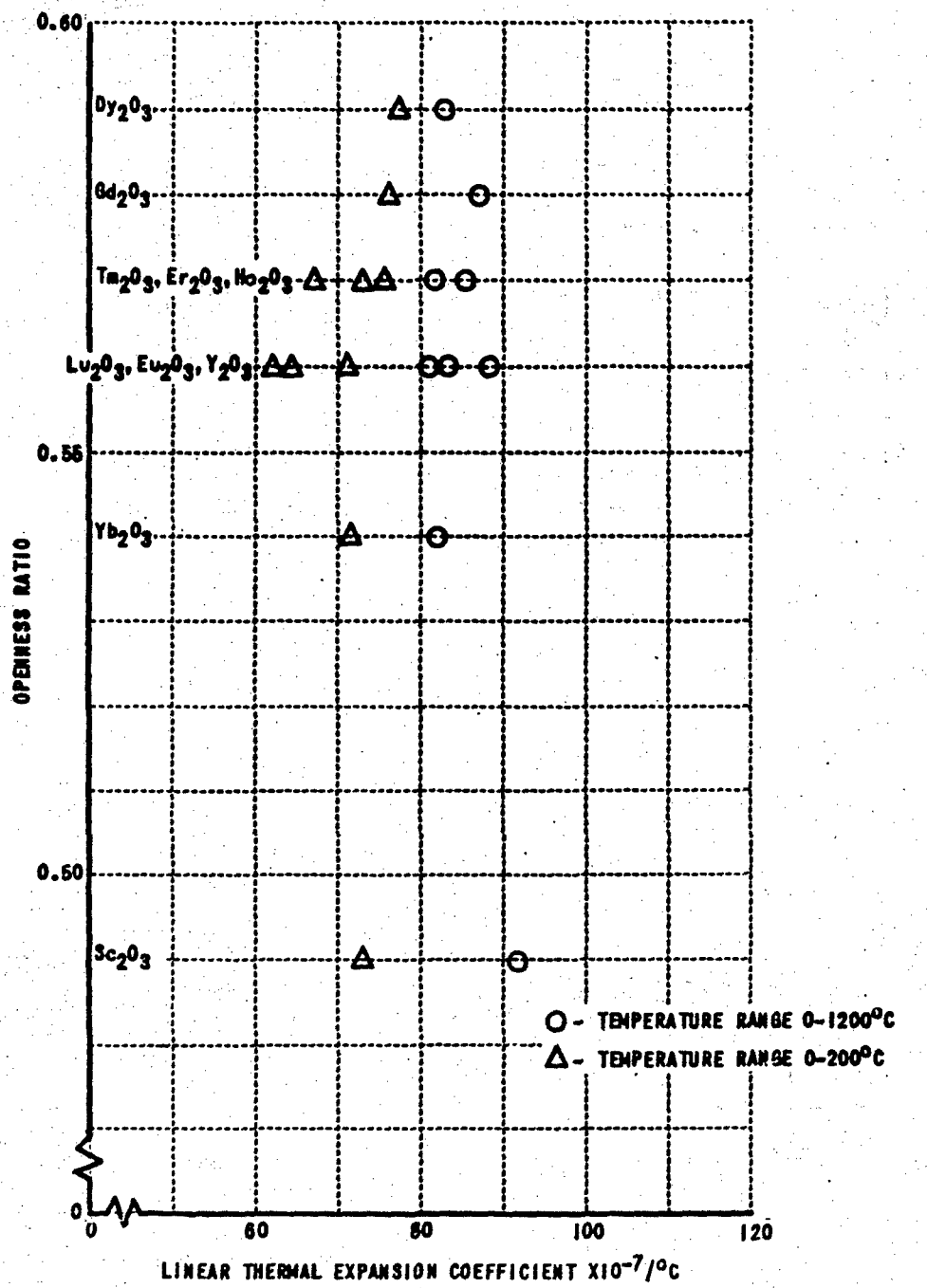

Figure 5 THERMAL EXPANSION COEFFICIENT VS. OPENNESS RATIO OF CUBIC RARE EARTH OXIDES

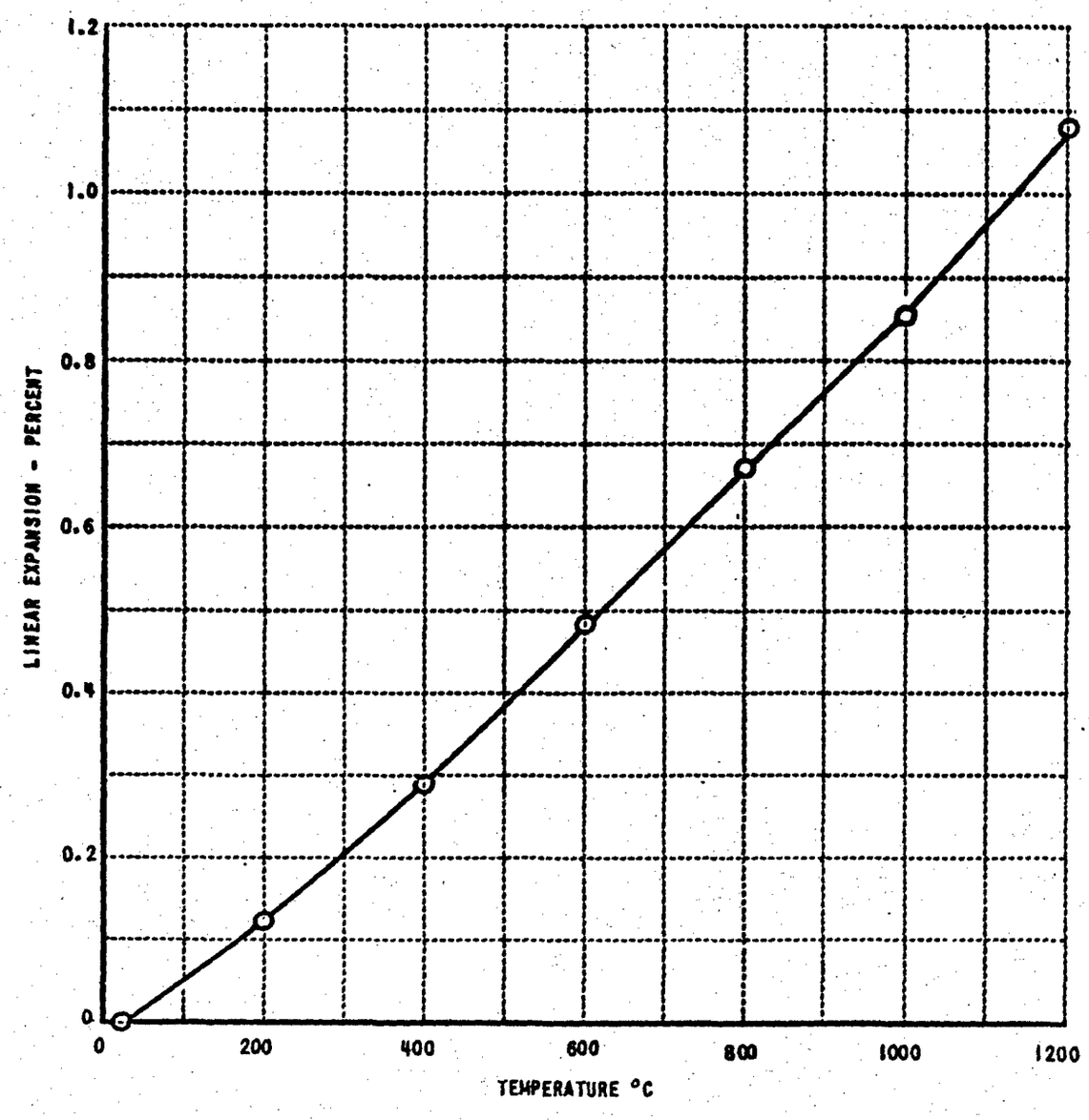

Figure 6 LINEAR THERMAL EXPANSION OF Sc_2O_3

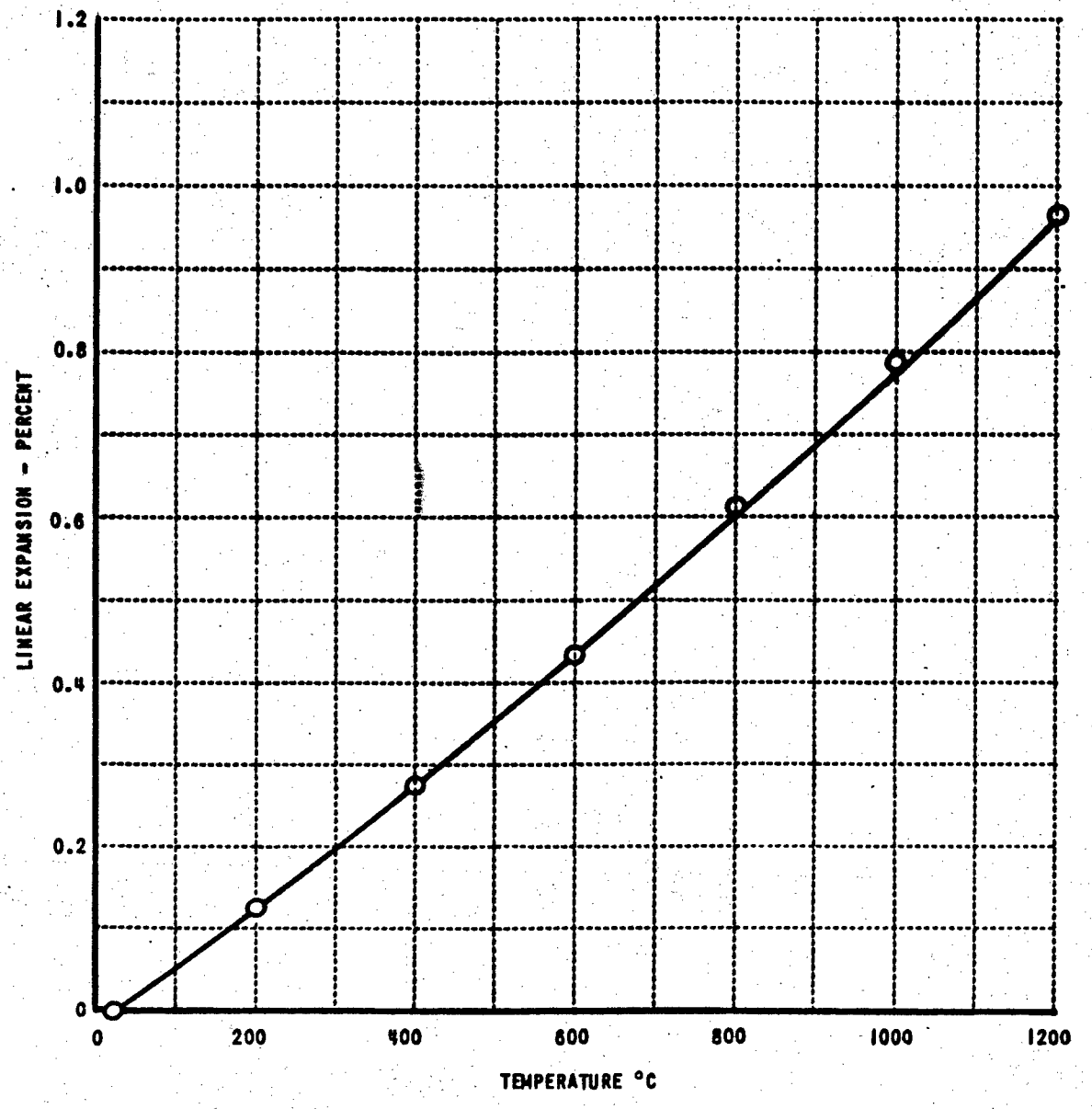

Figure 7 LINEAR THERMAL EXPANSION OF Yb_2O_3

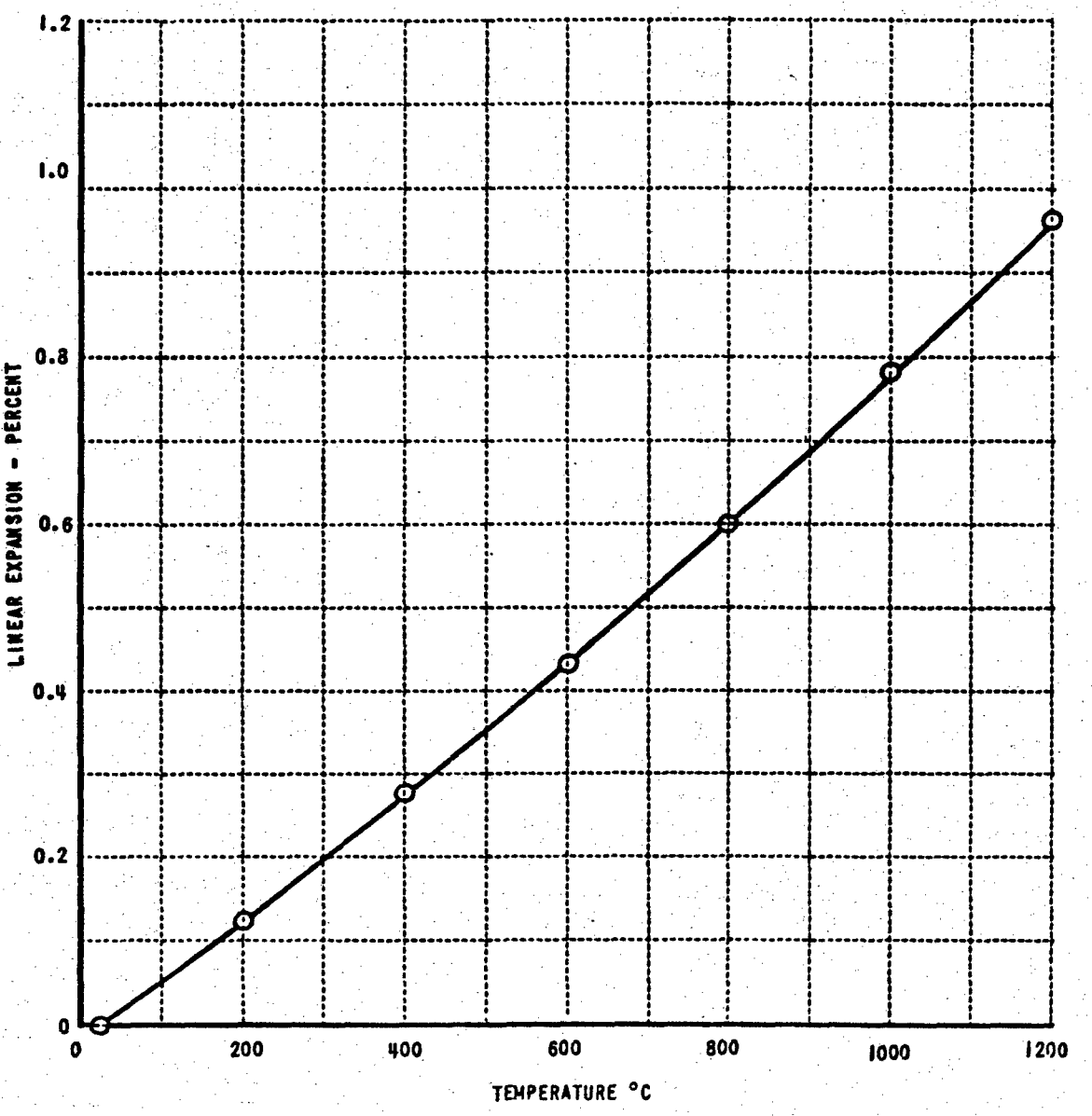

Figure 8 LINEAR THERMAL EXPANSION OF Er_2O_3

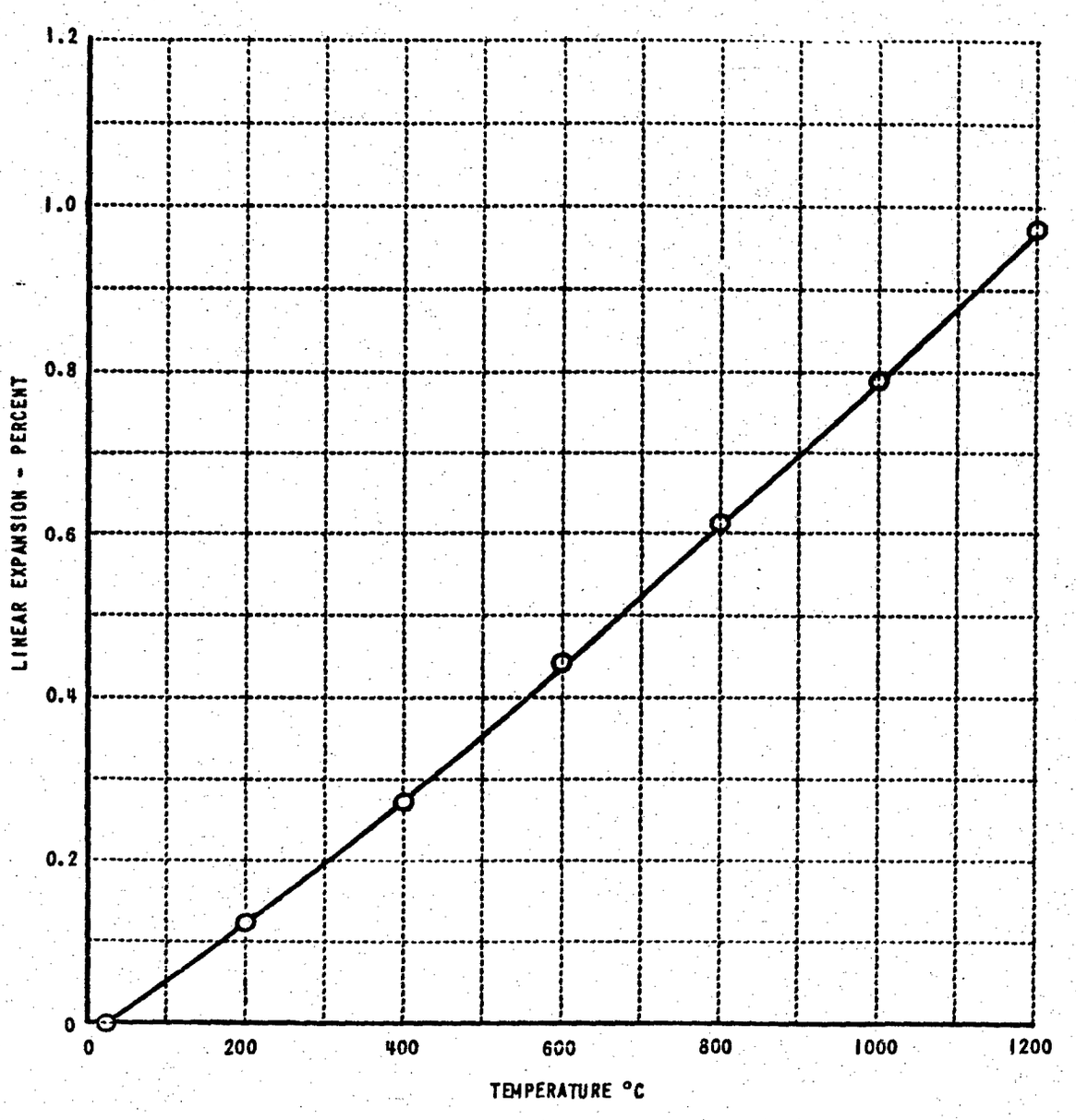

Figure 9 LINEAR THERMAL EXPANSION OF Dy_2O_3

evident that there is little variation in thermal expansion coefficient among these phases. The thermal expansion coefficient of Sc_2O_3 increases more rapidly with increasing temperature, than that of the other phases.

The conclusion to be drawn from these observations is that the openness ratio does not provide a method for predicting the thermal expansion within homologous series except in the case of series like the alkali halides in which there are very large variations in ionic radius, ionic polarizability and openness ratio. In series like the cubic rare earth oxides, carbides with the sodium chloride structure, alkaline earth oxides with the sodium chloride structure, etc., little variation in the thermal expansion coefficient is observed.

D. Prediction of the Thermal Expansion Coefficient Based Upon Atomic Spacing at Minimum Free Energy

Our study of various methods of predicting the thermal expansion of materials included an investigation of the atomic spacing at minimum free energy utilizing statistical mechanics. In this research some relationships which exist between the atomic structure of solids and thermal expansion are pointed out. This approach is important because our principal approach to the prediction of the thermal expansion using the openness concept does not involve direct knowledge of the atomic structure. Therefore, it seems likely that many of the inconsistencies in the predictions will have to be explained in terms of the atomic structure. In the following paragraphs are presented some explanations of the effect of crystal structure on the thermal expansion and a summary of calculations of the thermal expansion values for some alkali halides having the sodium chloride structure. The complete calculations are presented by Kirchner[14] based upon Smyth's research.

The purpose of this work is to show how the structure of some crystals and glasses can be related in a qualitative and even semi-quantitative way to the expansion characteristics of the materials. Two different methods were used. The first method is not mathematically rigorous since the vibrations of the individual atoms are considered as independent of each other rather than treating the crystal as a whole and computing the proper modes of

vibration. The latter is possible but extremely time consuming while the treatment of the individual atoms, although not rigorously correct, can be very helpful in leading to a better understanding of the relations between expansion and structure. It has been shown [2,8] that a mode of vibration, the frequency of which increases with the expansion of the lattice, makes a negative contribution to expansion and vice-versa. Some of the ways in which this principle can work will be illustrated below.

1. Independent Lattice Vibrations

In order to compute the frequency of vibration of an atom or ion about its equilibrium position, it is necessary to know the forces which act on it when it has been displaced by a known amount from this position. Since the atom at rest is in a position in which all the forces acting on it add up to zero, it is necessary only to calculate the amount by which the force of each neighboring atom is altered when the atom in question is displaced by a known amount. In order to allow actual calculation of some of the forces involved, the interactions are treated as purely ionic with Coulomb attractions or repulsions modified by higher power repulsions. The equations for calculating the restoring forces are indicated below. These apply when the magnitudes of the displacements are small as compared with the interatomic distances.

If an ion at the origin has a neighbor at x, y, z, attracting it with a force

$$\frac{e_1 e_2}{r^2} \qquad \text{(II-1)}$$

in which e_1 and e_2 are the charges of the 2 ions and r is the distance between them, and if the atom at the origin is given a small displacement to u, v, w, the change in the x-component of the force exerted on the displaced ion by virtue of its displacement is

$$\frac{e_1 e_2}{r^3}\left\{-u + 3\,\frac{ux^2 + vxy + wxz}{r^2}\right\} \qquad \text{(II-2)}$$

in which $r^2 = x^2 + y^2 + z^2$

The y and z components have the same form. If the ions have charges of the same sign, the results are the same with the opposite sign.

If the ions repel each other with a force

$$\frac{A}{r^n} \qquad \text{(II-3)}$$

in which A is a constant

then the change in the x-component of the force acting on the displaced atom will be

$$\frac{A}{r^{n+1}} \cdot \left\{ u - (n+1) \frac{ux^2 + vxy + wxz}{r^2} \right\} \qquad \text{(II-4)}$$

The y and z components have the same form.

The effects of these forces can be illustrated by a simple example. In Figure 10 an ion P is located at the origin between a pair of ions Q_1 at $(-a, 0, 0)$ and Q_2 at $(a, 0, 0)$. If it is assumed that the electrostatic attractions between P and Q are of the form (1) and the higher order repulsions are of the form (3) then, if P is displaced to $(u, 0, 0)$, the force acting on P by virtue of its displacement will be, on applying (2) and (4)

$$-\frac{A}{a^{n+1}} \, 2nu + \frac{4e_1 e_2}{a^3} \, u \qquad \text{(II-5)}$$

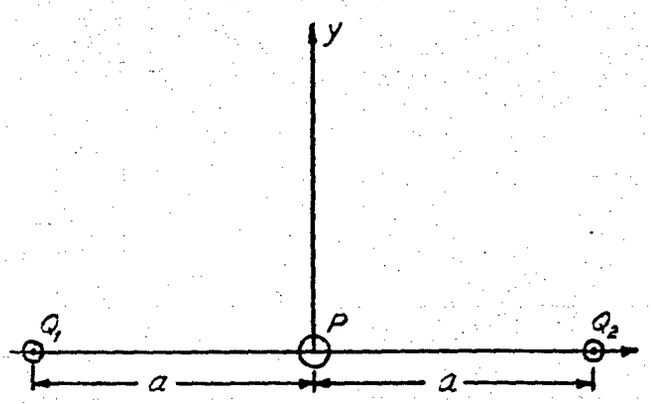

Figure 10 LOCATIONS OF THE ATOMS IN A SIMPLE EXAMPLE USED FOR CALCULATIONS OF INTERATOMIC FORCES

If the ions were originally at their equilibrium separations, the first term will predominate giving a positive restoring force. As a decreases, the first term increases more rapidly than the second giving a greater restoring force per unit displacement or a higher frequency of vibration. In this case the restoring force has come from the high order repulsions diminished somewhat by the Coulomb attractions.

If, on the other hand, the ion at the origin is moved to (o, v, o) which means a transverse displacement, the force, now in the y direction, is

$$\frac{A}{a^{n+1}} 2v - \frac{e_1 e_2}{a^3} 2v \qquad \text{(II-6)}$$

If the original separation is the equilibrium separation, the second term will predominate and there will be a positive restoring force. As a decreases the first term increases more rapidly than the second, diminishing the restoring force per unit displacement and decreasing the frequency. Here the restoring force comes from the Coulomb attractions diminished by the high order repulsions. This accounts for the different behavior from the previous case. A vibration of this kind contributes to a negative expansion and one of the former kind to a positive expansion.

The conditions for the existence of a vibration of the type leading to a negative expansion are that in the structure there must be some atoms connected only to a pair of neighbors about 180 degrees apart and so arranged as to have considerable freedom of transverse vibration. These conditions are met in several of the forms of silica and other materials which crystallize with comparable structures. Vitreous silica shows a negative expansion at very low temperatures and very low expansion at room temperature. The high temperature form of cristobalite shows a negative expansion. The more compact forms, such as quartz, where the more efficient packing inhibits the freedom of transverse vibration, show positive expansions.

If the vibrations of individual atoms or ions are considered as taking place independently of each other, it is possible to develop a fairly simple quantitative treatment for crystals of cubic symmetry. The examples considered will be phases having the sodium chloride structure. Phases

having this structure include most of the alkali halides and crystals of ceramic interest such as magnesium oxide and other alkaline earth oxides.

In the sodium chloride structure, a cation at the origin is surrounded by six anions at $(a,0,0)$, $(-a,0,0)$, $(0,a,0)$, $(0,-a,0)$, $(0,0,a)$ and $(0,0,a)$ where a is the closest cation-anion distance and is one-half of the edge of the unit cube. Equation 2 may be used to find the restoring force on the ion at the origin when it is given a small displacement to (u,v,w) where u, v and w are small compared with a. The total effect is zero and in the same way it can be shown that the complete group of ions at any one distance of separation from any one of the cations or anions makes a zero contribution to the restoring force on that ion when it is displaced in any direction. This, of course, applies only to that part of the restoring force arising from the Coulomb interactions and applies only in the case of surroundings of high symmetry. It applies, for instance, to the vibrations of a silicon in the cristobalite structure but not to an oxygen ion in the same structure. Therefore, for independent vibrations in crystals having the sodium chloride structure, the restoring force on any displaced ion can be computed entirely in terms of the high order repulsion forces.

The repulsion forces fall off very rapidly with increasing separation and not much error will be introduced by considering only interactions between nearest neighbors and second nearest neighbors. If the force of repulsion between any ion at the origin and any of the six nearest neighbors at distance a from this, is of the form

$$\frac{A_1}{r^n} \qquad \text{(II-7)}$$

then the x-component of the restoring force on the atom at the origin arising from a displacement to (u, v, w) can be written using the equation 4. Adding the six equations and simplifying gives

$$\frac{2A_1}{a^{n+1}}(2-n)u \qquad \text{(II-8)}$$

If n is greater than 2 this force is always negative for a positive displacement u indicating that it really is of the nature of a restoring force. The x-component of the restoring force depends only on u which means that the vibrations in the x, y and z directions are independent of each other.

If the force of repulsion between the ion at the origin and any of the twelve ions at a distance $a\sqrt{2}$ is of the form

$$\frac{A_2}{r^n} \qquad \text{(II-9)}$$

the x-component of the force on the atom at the origin when displaced to (u, v, w) can be determined using the equation 4. Adding the twelve equations and simplifying gives

$$\frac{4A_2}{(a\sqrt{2})^{n+1}}(2-n)u \qquad \text{(II-10)}$$

Some reasonable estimate now has to be made for A_1, A_2 and n for the different alkali halides. The method of treatment implies the following model. Each ion has three independent modes of vibration, all with the same frequency. Just enough interaction between the different modes is assumed to allow the attainment of thermodynamic equilibrium so that the usual laws of statistical mechanics can be employed. This allows the calculation and use of the free energy of the system and the condition that this free energy of the system is a minimum determines the state of exparsion or contraction of the crystal at any given temperature.

The energy per mole can be written in the form

$$E = E_s + \sum_{i=1}^{3N}\left(n_i + \frac{1}{2}\right)h\nu_+ + \sum_{j=1}^{3N}\left(n_j + \frac{1}{2}\right)h\nu_- \qquad \text{(II-11)}$$

where n_i is the quantum number describing the state of vibration of the ith mode of vibration of the cation, and ν_+ is the frequency of vibration of the cation, n_j and ν_- describe the jth mode of the anion, and E_s is the potential energy of the lattice at rest. E_s, ν_+ and ν_- are all functions of the cation-anion separation. In the usual method of attacking such a problem, the partition function Q is set up and this has the form[2,23]

$$Q = e^{\frac{-E_s}{KT}} \left\{ \frac{e^{\frac{-h\nu_+}{2KT}}}{1 - e^{\frac{-h\nu_+}{KT}}} \right\}^{3N} \left\{ \frac{e^{\frac{-h\nu_-}{2KT}}}{1 - e^{\frac{-h\nu_-}{KT}}} \right\}^{3N} \qquad \text{(II-12)}$$

The Helmholtz free energy U is given by

$$U = -KT \ln Q \qquad \text{(II-13)}$$

Hence

$$U = E_s + 3NKT \left[\frac{h\nu_+}{2KT} + \ln\left(1 - e^{\frac{-h\nu_+}{KT}}\right) + \frac{h\nu_-}{2KT} + \ln\left(1 - e^{\frac{-h\nu_-}{KT}}\right) \right] \qquad \text{(II-14)}$$

In the absence of stress or external pressure, the cation-anion separation will be such as to make U a minimum. The quantities

$$\Theta_+ = \frac{h\nu_+}{K} \quad \text{and} \quad \Theta_- = \frac{h\nu_-}{K}$$

are the Einstein characteristic temperatures.

E_s has the form

$$E_s = \frac{-NMe^2}{r} + \frac{Be^2N}{r^n} \qquad \text{(II-15)}$$

and may be expanded about r_o , the value of r for which E_s is a minimum. M is the Madelung constant for the lattice and B is a constant characteristic of the lattice. r_o is given by

$$\frac{Me^2}{r_o^2} = \frac{nBe^2}{r_o^{n+1}} \qquad \text{(II-16)}$$

If $r = r_o + \Delta r$, then E_s takes the following form using the usual Taylor series expansion and omitting terms containing powers of Δr higher than the second.

$$E_s = \frac{-NMe^2}{r_o}\left(1 - \frac{1}{n}\right) + \frac{NMe^2}{2r_o^3}(n-1)(\Delta r)^2 \qquad \text{(II-17)}$$

Here Δr is assumed to be the amount by which the value of the cation-anion separation at any temperature varies from what this separation would be in the absence of thermal motion. The quantity Δr is determined by choosing that value which minimizes U so that

$$\frac{dE_s}{d(\Delta r)} + \frac{3Rd}{dr}\left[\frac{\Theta_+}{2} + \frac{\Theta_-}{2} + T\ln\left(1 - e^{\frac{-\Theta_+}{T}}\right) + T\ln\left(1 - e^{\frac{-\Theta_-}{T}}\right)\right] = 0 \qquad \text{(II-18)}$$

The substituting of the derivative of E_s with respect to Δr and solving for Δr gives

$$\Delta r = \frac{-3Rr_o^3}{NMe^2(n-1)}\frac{d}{dr}\left[\frac{\Theta_+}{2} + \frac{\Theta_-}{2} + T\ln\left(1 - e^{\frac{-\Theta_+}{T}}\right) + T\ln\left(1 - e^{\frac{-\Theta_-}{T}}\right)\right] \qquad \text{(II-19}$$

Taking the derivative and simplifying

$$\Delta r = \frac{-3Rr_o^3}{NMe^2(n-1)}\left[\frac{1}{2}\frac{d\Theta_+}{dr} + \frac{1}{2}\frac{d\Theta_-}{dr} + \frac{1}{e^{\frac{\Theta_+}{T}}-1}\frac{d\Theta_+}{dr} + \frac{1}{e^{\frac{\Theta_-}{T}}-1}\frac{d\Theta_-}{dr}\right] \quad \text{(II-20)}$$

But

$$\alpha = \frac{1}{r_o}\frac{d(\Delta r)}{dT} \quad \text{(II-21)}$$

and if $d\Theta_+/dr$ and $d\Theta_-/dr$ can be considered as constants independent of the state of expansion and therefore of the temperature, then

$$\alpha = \frac{-3Rr_o^2}{NMe^2(n-1)}\left[\frac{e^{\frac{\Theta_+}{T}}\frac{\Theta_+}{T^2}}{\left(e^{\frac{\Theta_+}{T}}-1\right)^2}\frac{d\Theta_+}{dr} + \frac{e^{\frac{\Theta_-}{T}}\frac{\Theta_-}{T^2}}{\left(e^{\frac{\Theta_-}{T}}-1\right)^2}\frac{d\Theta_-}{dr}\right] \quad \text{(II-22)}$$

$$\alpha = \frac{-3Rr_o^2}{NMe^2(n-1)}\left[\frac{1}{\Theta_+}E\left(\frac{\Theta_+}{T}\right)\frac{d\Theta_+}{dr} + \frac{1}{\Theta_-}E\left(\frac{\Theta_-}{T}\right)\frac{d\Theta_-}{dr}\right]$$

where $E\left(\frac{\Theta}{T}\right)$ is the Einstein Function of $\frac{\Theta}{T}$

In order to compute the quantities Θ_+ and Θ_-, it is necessary to know the frequency of vibration of the cation and the anion. This can be determined by differentiating the potential energy functions suggested by Pauling [6] to give the force

$$F = \frac{e^2}{r^2} - \frac{B_o n e^2 (r_+ + r_-)^{n-1}}{r^{n+1}} \quad \text{(II-23)}$$

for the cation and anion and equations of similar form for the forces between cation and cation, and anion and anion. Comparing these with equations II-7, 8, 9 and 10, it can be seen that by equating II-7 and the second term of II-23, we can solve for A_1 . In a similar way we can find A_2 . Then, by substituting the values of A_1 and A_2 in II-8 and II-10 and adding the two terms we have an expression for the restoring force per unit displacement as follows.

For the cation this is

$$\frac{2n(n-1)B_0e^2(r_+ + r_-)^{n-1}}{r^{n+2}} + \frac{5n(n-1)B_0e^2(2r_+)^{n-1}}{(\sqrt{2}\,r)^{n+2}} = \frac{C_+}{r^{n+2}} \qquad \text{(II-24)}$$

and for the anion

$$\frac{2n(n-1)B_0e^2(r_+ + r_-)^{n-1}}{r^{n+2}} + \frac{3n(n-1)B_0e^2(2r_-)^{n-1}}{(\sqrt{2}\,r)^{n+2}} = \frac{C_-}{r^{n+2}} \qquad \text{(II-25)}$$

The frequencies of vibration of the cation and anion are given by

$$\nu_+ = \frac{1}{2\pi}\sqrt{\frac{C_+}{m_+ r^{n+2}}} \qquad \nu_- = \frac{1}{2\pi}\sqrt{\frac{C_-}{m_- r^{n+2}}} \qquad \text{(II-26)}$$

where m_+ and m_- are the respective masses of the cation and anion. Since

$$\textcircled{H}_+ = \frac{h}{2\pi K}\sqrt{\frac{C_+}{m_+}}\;\frac{1}{r^{\frac{n+2}{2}}} \text{ and } \textcircled{H}_- = \frac{h}{2\pi K}\sqrt{\frac{C_-}{m_-}}\;\frac{1}{r^{\frac{n+2}{2}}} \qquad \text{(II-27)}$$

and

$$\frac{d\textcircled{H}_+}{dr} = \frac{-h}{2\pi K}\sqrt{\frac{C_+}{m_+}}\;\frac{n+2}{2}\;\frac{1}{r^{\frac{n+4}{2}}} \qquad \text{(II-28)}$$

and

$$\frac{d\Theta_-}{dr} = \frac{-\hbar}{2\pi K}\sqrt{\frac{c_-}{m_-}}\ \frac{n+2}{2}\ \frac{1}{r^{\frac{n+4}{2}}} \qquad \text{(II-29)}$$

$$\frac{1}{\Theta_+}\ \frac{d\Theta_+}{dr} = \frac{1}{\Theta_-}\ \frac{d\Theta_-}{dr} = -\frac{n+2}{2r} \qquad \text{(II-30)}$$

Equations II-24 and 25 can be used to evaluate c_+ and c_-. B_o can be evaluated using equation 13-13 from Pauling[6]. In this equation B_o must be chosen so that $F(\rho)$ has a value of unity for $\rho = 0.75$. Here ρ is the radius ratio. When this is solved, it gives for B_o the value 0.029 for $n = 9$. This choice of B_o allows the use of Pauling's ionic radii for r_+ and r_- and gives the proper value for r (the cation-anion distance for all of the alkali halides).

Combining equations II-22 and 30, the expansion coefficient can be written in the form

$$\alpha = \frac{3}{2}\ \frac{R(n+2)\,r_o}{NMe^2(n-1)}\left\{E\left(\frac{\Theta_+}{T}\right) + E\left(\frac{\Theta_-}{T}\right)\right\} \qquad \text{(II-31)}$$

Using $n = 9$

$R = 8.314 \times 10^{-7}$ ergs per mole per degree

$M = 1.748$

$e = 4.77 \times 10^{-10}$ e.s.u.

The first factor which is common to all the alkali halides has the value 711. Using this, the known values of the cation-anion separations (r_o) and the values of the Einstein functions, Table VI was prepared showing the computed expansions. The experimental values for the alkali halides are given for comparison. These are the "best" values from the literature as given by Thielke.[24]

Table VI

THERMAL EXPANSION COEFFICIENTS FOR THE ALKALI HALIDES AT 27°C CALCULATED AND LITERATURE VALUES

		F	Cl	Br	I
Li	CALCULATED	210	320	360	410
	EXPERIMENTAL*	340	435	500	590
Na	CALCULATED	270	380	410	450
	EXPERIMENTAL	360	400	415	470
K	CALCULATED	350	430	460	490
	EXPERIMENTAL	370	380	400	430
Rb	CALCULATED	390	460	480	520
	EXPERIMENTAL	-	360	375	415
Ca	CALCULATED	420	-	-	-
	EXPERIMENTAL	320	460	470	490

* THIELKE'S (1953) BEST VALUES

The agreement between the theoretical and experimental values seems to be quite good considering the assumptions that have been made. It may be possible to improve the calculated thermal expansion values by using experimental values for the exponent of the repulsion term rather than the ninth power function which has been assumed.

2. Vibrations of the Lattice As a Whole

The previous computations of thermal expansion of alkali halide crystals were based on calculation of the frequency of oscillation of the ions under the assumption that the ions are free to vibrate independently without disturbing neighboring ions. The present study is undertaken to investigate the feasibility, in calculations of this kind, of treating somewhat more rigorously the vibrations of the lattice as a whole. The assumptions are still made that these vibrations are simple harmonic vibrations and the polarization of individual ions is completely neglected. Because of the great volume of work involved, the calculations were limited to six alkali halides which are lithium fluoride, lithium chloride, sodium fluoride, sodium bromide, sodium iodide and potassium fluoride.

3. Method of Attack

The forces between the ions were taken to be those used by Pauling in his calculation of the interionic separations in the alkali halides. The high order repulsions were all assumed to vary so that the potential energy of a pair of ions varies inversely as the ninth power of the separation and the constant of proportionality was taken to be proportional to the eighth power of the sum of the radii and to have the general form postulated by Pauling. This completely specifies all the parameters necessary for a description of the dynamics of the lattice.

4. Ionic Forces

The role of the Coulomb forces was handled by the method of Ewald which gives the value of the vector at any ion location for a wave described by any wave number vector in the reciprocal lattice. The method was modified to give directly the components of electric field instead of the Hertz vector.

The high order repulsions were considered by calculating the forces arising from the displacements of nearest neighbors and second nearest neighbors only.

The frequency of a wave travelling with a wave number vector described by a point in the reciprocal lattice was computed by assuming a frequency for this wave and then writing down the equations of motion for each of the two ions in each of the x, y and z directions. This gave six equations which, on elimination of the amplitudes, gave a determinant which was a sixth degree equation in the square of the frequency. Most of these determinantal equations could be rather easily broken down into, at the most, second degree equations yielding easy solutions. The equations were all solved by electronic computer.

5. Reciprocal Lattice

To minimize the number of calculations, sixty four points uniformly distributed in one unit cell of the reciprocal lattice were taken to describe the wave numbers of travelling waves. Because of the high symmetry of the lattice, this involved only eight different calculations each yielding six values for the frequency.

6. Expansion Coefficient

If there are n_1 modes of vibration with frequency ν_1, n_2 modes with frequency ν_2, etc. then for one mole of the alkali halide crystal

$$n_1 + n_2 \cdots\cdots = 6N \qquad \text{(II-32)}$$

where N is Avogadro's number.

As was shown by Smyth[2], the coefficient of expansion α of the whole crystal will be given by

$$\alpha = -\frac{1}{\frac{d^2 E_s}{dr^2}} \frac{R}{r}\left\{\frac{n_1}{\nu_1} E\left(\frac{h\nu_1}{kT}\right)\frac{d\nu_1}{dr} + \frac{n_2}{\nu_2} E\left(\frac{h\nu_2}{kT}\right)\frac{d\nu_2}{dr} + - - -\right\} \qquad \text{(II-33)}$$

where R is the gas constant in ergs per mole per degree, E_S is the potential energy of a mole of the crystal when the ions are at rest, r is the cation-anion separation in centimeters and $E(\chi)$ is the Einstein function of χ.

For each of the modes considered, the frequency ν was computed as described above and $\frac{d\nu}{dr}$ was found by increasing r by one percent, keeping all of the force constants the same, and redetermining each frequency ν. The value of $\frac{d\nu}{dr}$ was considered to be given by $\frac{\Delta\nu}{.01r}$.

Equation II-17 showed that E_S could be expressed as follows

$$E_S = -\frac{NMe^2}{r}\left(1-\frac{1}{n}\right) + \frac{NMe^2}{2r^3}(n-1)(\Delta r)^2 \qquad \text{(II-34)}$$

where Δr is the amount by which the cation-anion separation at any temperature varies from the equilibrium value it would have in the absence of thermal motion. From this

$$\frac{dE_S}{dr^2} = \frac{NMe^2(n-1)}{r^3} \qquad \text{(II-35)}$$

If the cation-anion separation is known, as it is for each alkali halide, everything is known to determine the value of the coefficient of expansion for each alkali halide. Table VII gives the values of the calculated and experimental coefficients of exparsion at 300°K for each of the compounds studied.

7. Discussion

The accuracy of the calculated expansion coefficients depends upon a number of assumptions including:

1. Negligible ionic polarizability.
2. Simple harmonic vibrations.
3. Degree of interdependence of lattice vibrations.
4. Choice of the exponent in the term representing the repulsion forces.

Table VII

THERMAL EXPANSION COEFFICIENTS FOR THE ALKALI HALIDES AT 27°C CALCULATED AND LITERATURE VALUES

COMPOUND	CALCULATED THERMAL EXPANSION COEFFICIENT BASED UPON EWALD'S METHOD $^{o}C^{-1} \times 10^{7}$	EXPERIMENTAL DATA*
LiF	280	340
LiCl	710	435
NaF	340	360
NaBr	580	415
NaI	674	470
KF	338	370

*THIELKE'S (1953) BEST VALUES

The choice of the Ewald method for allowing some interdependence of lattice vibrations, requires extensive calculations which, in turn, limits the number of results. The predicted expansion coefficients are of the correct order of magnitude and vary in accordance with the experimental values. However, further calculations of this sort for the alkali halides do not seem to be worthwhile.

Variations in ionic polarization seem to account for many of the differences between the calculated and the experimental expansion coefficients (Table VI). The influence of polarization on the thermal expansion of the alkali halides has been studied by Weyl.[25] Using Weyl's approach, we note first that the theory gives reasonably correct results for NaCl and NaBr. Substitution of Li for sodium leads to calculated results that are too small whereas substitution of K and Rb leads to calculated results that are too large. The principle forces determining the arrangement of the ions in the structure are the attractions between anions and cations and the repulsions between the anions. Neglecting the polarization of the cations, as a first approximation we note that polarization of anions results in higher electron densities between anions and cations. At the same time, the electron density between neighboring anions is decreased. Therefore, the effective charge is greater for coulomb forces between anions and cations and less for coulomb forces between anions. As the temperature increases, the electrons become more symmetrically arranged around the anions. This results in a decreased effective charge for the anion-cation attraction forces and an increased effective charge for the anion-anion repulsion forces. Therefore, the lattice constants increase more with increasing temperature, than would be expected without polarization of the anions and the experimental expansion coefficient is larger than the calculated expansion coefficient. Since the Li^+ polarizes the anions to a greater degree than the other cations, this polarization effect increases the experimental values for the lithium halides to a greater extent than the other compounds. Within the group of lithium halides the polarization effect increases with increasing anion size and polarizability so that LiI has the highest expansion coefficient of the alkali halides. On the other hand decreasing the polarizing power of the cation, for example

by substituting K or Rb for Na results in a decrease in the polarization effect and the calculated expansion coefficients are larger than the experimental values.

III. THE THERMAL EXPANSION OF SOLID SOLUTIONS

A. Introduction

There is a large difference in the thermal expansion coefficients along different crystallographic directions in many anisotropic materials.[26,27] Single phase ceramic bodies prepared from materials having a high thermal expansion anisotropy tend to form internal cracks upon cooling. The hysteresis observed in the thermal expansion curve of TiO_2 is probably caused by these internal microcracks[28]. Other polycrystalline ceramic bodies such as those composed of $MgO.2TiO_2$, $Al_2O_3 \cdot TiO_2$ and $Li_2O \cdot Al_2O_3 \cdot 2SiO_2$ (β -eucryptite) have low thermal expansion coefficients but are very weak because of a high expansion anisotropy.[27] Reduction of the thermal expansion anisotropy of the crystals used in these bodies should result in stronger, more useful bodies.

The effect of solid solutiom atoms on the thermal expansion of ceramic materials has been studied in a few cases. Austin[19] has suggested on the basis of literature data, that extended solid solution lowers the expansion coefficient. For instance Rigby, Lovell and Green[29] showed that the addition of $FeO \cdot SiO_2$ to $CaO \cdot SiO_2$ reduced the thermal expansion. On continued addition of $FeO \cdot SiO_2$, however, the thermal expansion coefficient began to increase somewhat. Kozu and Ueda[30] have found in their study of plagioclase that the relative amount of albite and anorthite strongly influences the magnitude of the thermal expansion anisotropy. These authors[31] have also studied the effect of impurities on the thermal expansion of diopside minerals from various localities. The thermal expansion anisotropy of one of these diopside crystals which contained a relatively large amount of iron was found to be considerably less than that of pure diopside ($CaMgSi_2O_6$). Ricker and Hummel[32] have reported that the solid solution of SiO_2 in TiO_2 decreases the thermal expansion coefficient.

The papers cited above indicate that the thermal expansion of crystals can be varied by addition of solid solution atoms. In the case of one naturally occuring mineral sample, variation of thermal expansion anisotropy

with composition was noted. The objective of this investigation was to study the variation of thermal expansion anisotropy with composition for several ceramic solid solutions. Since this effect has not been studied in series of prepared solid solutions, it was decided to begin a study of the influence on the thermal expansion anisotropy of the replacement of Ti^{+4} in rutile with ions of differing size and charge such as Zr^{+4} and Mn^{+2}. TiO_2 was chosen for study since there are approximately 40 cations which are within 15% of the size of the Ti^{+4} ion so that substantial solid solution is possible with many ions. Also, rutile possesses the relatively simple tetragonal structure and, therefore, the thermal expansion anisotropy can be determined by high-temperature x-ray diffraction methods. Later in the investigation, samples in the SnO_2-V_2O_5 and Al_2O_3-Cr_2O_3 systems were investigated to determine whether these solid solutions also obey the rules that appear to hold for rutile solid solutions.

B. Experimental

1. Specimen Preparation

Except for Nb^{+5},[33] Sn^{+4},[34] Zr^{+4},[35] and Be^{+2},[36] there is little information in the literature on the extent of solid solution in TiO_2. Most of the additives were selected for the present study on the basis of ion size since it is generally considered necessary for the substituting ion to have an ionic radius within about 15% of the substituted ion in order for extensive substitutional solid solution to take place. Ti^{+4} has an ionic radius of 0.68 Å so that the radii of the substituting ions should lie in the range of 0.58 - 0.78 Å.

Because of the lack of information on the extent of solid solution in TiO_2, 10 mole per cent of the oxide additive (based on the cation) was usually used. If this amount of substitution takes place on firing the specimen, a relatively large change in lattice constants is expected. The samples containing 0.5 and 1.0 mole percent additive were based on Johnson's research.[37] It should be noted that the actual extent of solid solution was not known in most cases.

A standard firing temperature of 1500°C was selected on the basis of the Nb_2O_5-TiO_2, ZrO_2-TiO_2 and BeO-TiO_2 phase diagrams, all of which show considerable solid solution at this temperature. In the case of the additives Li_2CO_3, Sb_2O_3 and V_2O_5, a temperature of 1200°C was used because of the high vapor pressure of these compounds at higher temperatures.

These additives were all reagent grade materials. The TiO_2 was Titanium Pigment Corporation's Titanox TG. The analysis of this material is < 0.01% CaO, < 0.1% WO_3, < 0.008% Nb, < 0.007% Sb_2O_3, < 0.04% SiO_2, 0.006% Fe_2O_3, 10 ppm V, 0.5 ppm Mn, 5 ppm Cu, 4 ppm Cr and 10-20 ppm Pb. In Table VIII the additives are given together with the relative weights of TiO_2 and additive, and the firing temperature and time.

The rutile solid solutions were prepared by ball-milling the weighed additive and TiO_2 for four hours. The powder was passed through a 4 mesh standard screen, mixed with 15% binder solution and dried at 110°C for an hour. After passing the dried mix through a 16 mesh screen, it was pressed at 7000 psi into 1" discs about 1/4" thick. These discs were fired to temperature and then cooled to room temperature in less than 30 minutes to avoid possible precipitation. The x-ray powder specimens were prepared by crushing the discs in an alumina mortar to pass a 325 mesh screen. A sample of pure TiO_2 for use as a standard was given the above treatment. The SnO_2-V_2O_5 samples were prepared as described above using a firing temperature of 1000°C for 16 hours. Also, solid solution specimens in the Cr_2O_3-Al_2O_3 system were prepared as described above using a firing temperature of 1500°C for 17 hours. Additional experiments were performed using the phases VO_2, GeO_2, MgF_2, $MgO.2TiO_2$ and Al_2O_3·TiO_2. These latter experiments were unsuccessful for a variety of reasons such as decomposition of the desired phases, lack of stoichiometry or inability to get the compound in the desired crystal form.

2. Experimental Procedures

The equipment used for the x-ray thermal expansion measurements consisted of a G. E. XRD-5 spectrogoniometer and a Tem-Pres high temperature x-ray diffraction furnace. The sample holder was a platinum plate with a

Table VIII

DATA ON THE PREPARATION OF RUTILE SPECIMENS

ADDITIVE USED	MOLE % ADDITIVE (CATION BASIS)	WEIGHT OF ADDITIVE (g)	WEIGHT OF TiO_2 (g)	FIRING TEMPERATURE °C	FIRING TIME HRS.
ZnO	10	11.3	100	1500	17
Li_2CO_3	10	5.14	100	1200	18
MgO	10	5.8	100	1500	17
Cr_2O_3	10	10.57	100	1500	17
Sb_2O_3	10	20.25	100	1200	18
MnO_2	10	12.08	100	1500	17
V_2O_5	10	12.64	100	1200	18
WO_3	10	33.2	100	1500	17
WO_3	1.0	5.7	194.3	1500	15
Nb_2O_5	9.2	42	240	1400	3
ZrO_2	10	17.15	100	1500	17
PbO	10	23.66	76.34	1500	17
Y_2O_3	0.5	0.71	99.29	1500	17
CaO	0.5	0.35	99.65	1500	17
BeO	1.0	0.31	99.69	1500	17
MoO_3	1.0	3.58	196.4	1500	17
SiO_2	30	48	152	1500	15
SnO_2	10	16.75	80	1500	17
SnO_2	20	37.7	80	1500	17
SnO_2	30	64.7	80	1500	17

milled depression 13 x 16 x 0.75 mm deep. Because of the high thermal conductivity of platinum, the maximum difference in temperature across the sample holder was found to be 2°C over the range 25-1000°C. Using a precision potentiometer, it was possible to maintain the temperature within ± 0.5°C during a diffraction peak measurement.

The sample holder mounting was provided with rotational, tilting and translational adjustments so that the specimen surface could be aligned on, and parallel to the spectrometer axis.

Copper radiation (λ = 1.54050 Å for K_α) was used for all measurements. The x-ray tube was operated at 50 KV and 16 ma with a 0.0007" nickel filter. A 3° beam slit and 0.2° detector slit were used with a scanning rate of 0.2° (2θ) per minute and a chart speed of 30 inches per hour. The peak positions were taken as the midpoint of the diffraction curves at one-half peak height. Precision in measurement of the peak position was within ± 0.01°(2θ). To attain precision and accuracy in the determination of lattice constants, use was made of lines in the back reflection region. These were: for TiO_2 (303), 2θ = 134.7°, (521)2θ = 138.8° and (213) 2θ = 119.7°; for SnO_2 (323) 2θ = 137.7° and (512) 2θ = 147.3; for Al_2O_3 (0, 4, 10)2θ = 145.2°, and (416)2θ = 136.0°; and for Cr_2O_3 (330) 2θ = 137.5°, and (3, 2, 10) = 149.8°.

An analysis was made of the precision and accuracy of the x-ray measurements. At 24°C, considering diffraction lines for 130° 2θ, or above, random errors due to angular measurement and specimen centering were estimated to be within ± 0.0004 Å. This was checked by making a series of nine measurements on a sample of Fisher precipitated silver (99.99% Ag) using the (511) and (422) lines. All of the measurements fell within the estimated precision. The accuracy of the measurements was estimated by comparing the extrapolated ASTM card value for the a_o of silver at 24.0°C (4.859 Å) with the observed values. Agreement between the values was also within ± 0.0004 Å. The accuracy was therefore within the limits of the precision. The effect of x-ray absorption on accuracy was estimated by comparing the diffraction peaks of pure silver and a mixture of silver and graphite in the ratio 1/3. The mixture had an a_o value of 0.0001 Å greater than pure silver. The absorption difference of these two compositions is considered to be much

greater than those between the oxide solid solutions investigated so that errors due to x-ray absorption are considered to be negligible. At high temperatures the data are less precise because of a temperature variation across the specimen surface of $\pm$ 2.0°C. This is equivalent to an error of $\pm$ 0.00016 Å. Added to the random errors ($\pm$ 0.0004 Å) at room temperature, the total precision is $\pm$ 0.0006 Å for high angle lines up to 1000°C.

Concerning accuracy at high temperature, systematic errors in temperature measurement and sintering of the sample or sample movement due to expansion of the furnace parts must be estimated. Considering the latter, a displacement of the specimen of 0.001" was found to change a_o of rutile by 0.00006 Å. Assuming the maximum movement of the sample surface to be 5 mils, an error of $\pm$ 0.0003 Å is introduced which is added to the estimated room temperature accuracy of $\pm$ 0.0004 Å to give a total high temperature accuracy of $\pm$ 0.0007 Å.

To obtain an overall estimate of the accuracy of the measurements including temperature, the a_o of silver was measured to 600°C and compared with the values of Hume-Rothery and Reynolds (1938).[70] The observed values agreed with those of Hume-Rothery within $\pm$ 0.0003 Å.

The room temperature lattice constants were measured for each rutile solid solution specimen. These are presented in Table IX. If there was a significant change in the lattice constants, it was assumed that a considerable amount of solid solution had taken place and x-ray thermal expansion measurements were made. In the case of rutile, the peak positions for the (303) and (521) lines were measured as a function of temperature up to 1000°C. These data were then used to obtain the variation of the lattice constants with temperature.

In order to obtain information on the extent of solid solution of vanadium in TiO_2, a series of samples was prepared with various percentages of vanadium. As can be seen from Figure 11, the a_o lattice constant varies linearly with composition up to about 17-20 mole % vanadium. The results are plotted in terms of the compositions originally prepared and do not take into account changes due to volatilization of V_2O_5. A chemical analysis of the 14.8 mole percent vanadium sample indicated the presence of 16.1 mole percent

Table IX

ROOM TEMPERATURE LATTICE CONSTANTS OF RUTILE SOLID SOLUTIONS

ADDITIVE MOLE %	TEMP. °C	LATTICE CONSTANTS A° a_o	c_o	c/a
PURE TiO_2	25	4.5937	2.9593	.6442
1 Li^{+1}	29	4.5946	2.9587	.6440
10 Li^{+1}	28	4.5944	2.9588	.6440
10 Pb^{+2}	22	4.5933	2.9598	.6444
9.2 Nb^{+5}	28	4.6128	2.9632	.6424
0.5 Y^{+3}	29	4.5940	2.959	.6440
0.5 Ca^{+2}	26	4.5933	2.9589	.6442
1 Be^{+2}	27	4.5934	2.9589	.6442
10 Mg^{+2}	29	4.5940	2.9591	.6441
10 Zn^{+2}	27	4.5937	2.9589	.6441
10 Sb^{+3}	27	4.5957	2.9629	.6447
10 V^{+5}	27	4.5859	2.9583	.6451
10 Cr^{+3}	28	4.5989	2.9580	.6432
10 Mn^{+2}	27	4.5973	2.9579	.6434
1 W^{+6}	28.5	4.5946	2.9586	.6439
10 W^{+6}	26	4.5946	2.9598	.6442
10 Zr^{+4}	24	4.6180	2.9899	.6474
1 Mo^{+6}	28	4.5937	2.9585	.6440
30 Si^{+4}	26.5	4.5933	2.9583	.6451
10 Sn^{+4}	26	4.6099	2.9817	.6481
20 Sn^{+4}	26	4.6258	3.0059	.6498
30 Sn^{+4}	25	4.6406	3.0282	.6525

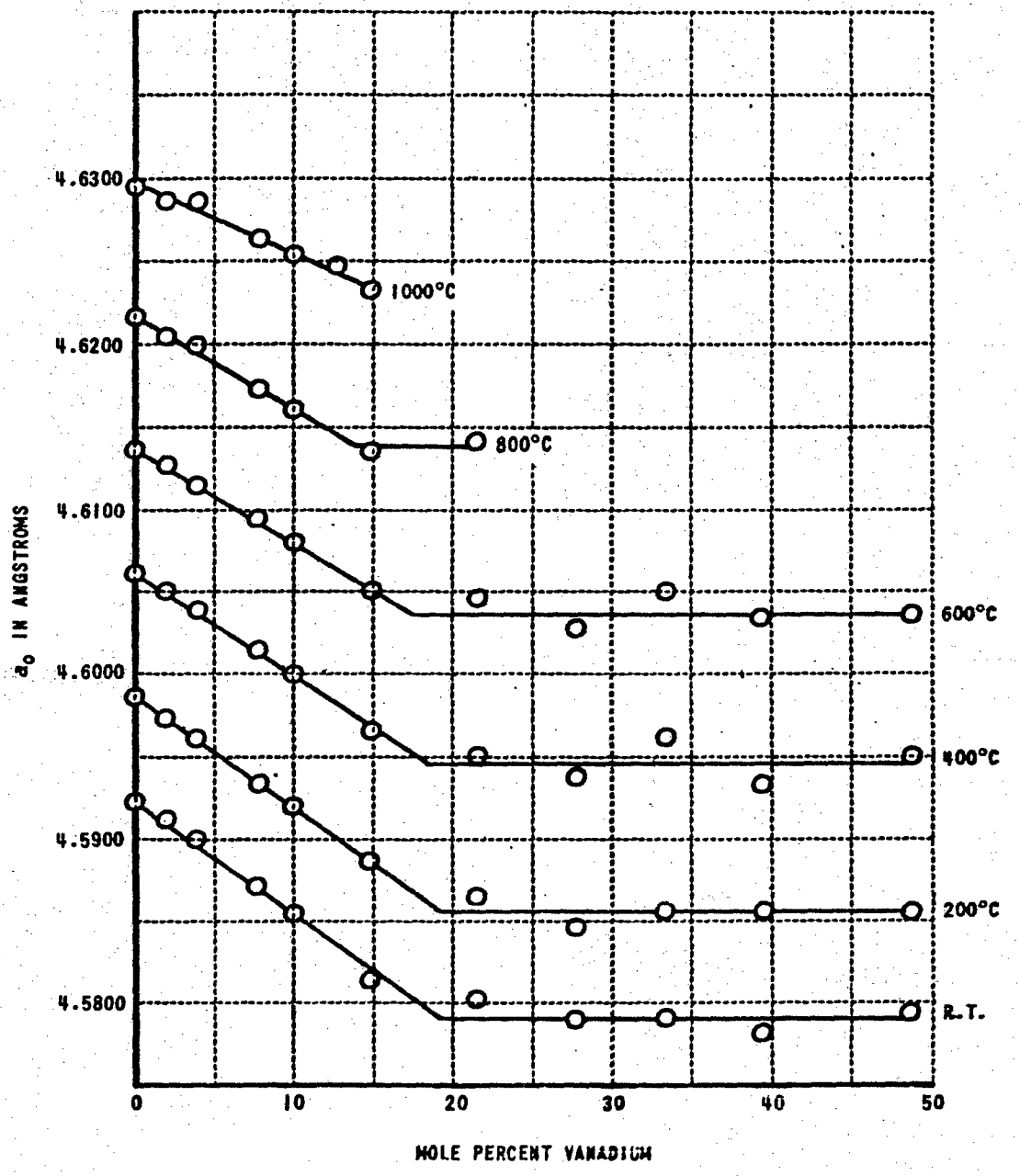

Figure 11 LATTICE CONSTANT a_o AT VARIOUS TEMPERATURES vs. COMPOSITION FOR 1200°C FIRING TEMPERATURE

vanadium after heating to form the solid solution. While an increase in the ratio of vanadium to titanium is unlikely (an error in chemical analysis is more probable), the analysis does provide assurance that a substantial fraction of the vanadium does remain in the material after heating.

C. Discussion of Results

In discussing the results, several things should be kept in mind. First, except for the case of vanadium and tin in TiO_2, the extent of solid solution in the titania specimens is not known. Second, the valence of the additive is not definitely known in some cases. Some work has indicated that there is a tendency for solid solution atom to assume the oxidation state of the host lattice.[38] This "valence inductivity" effect has been investigated for the case of low concentrations of Mn in Al_2O_3, where the Mn at first assumes a +3 oxidation state in imitation of Al^{+3} but then changes to a +4 state at higher concentrations. Recent electron spin resonance experiments reported by Gerritsen and Lewis[39] indicate that vanadium replaces titanium and is present in the four valent state, at least at small concentrations.

The question of valence is not only important because of its bearing on ion size, but also because electrical neutrality must be maintained in the lattice. For instance, ions with a valence greater than four would require the formation of Ti^{+3} ions. Since Ti^{+3} has an ionic radius of 0.76 Å, the overall effect might be similar to the addition of an ion larger than Ti^{+4} (0.68 Å). Similarly, the addition of ions with valences less than four requires the formation of oxygen vacancies (O^{-2} radius is 1.40 Å). Mauer and Bolz[40] have measured the thermal expansion anisotropy of an oxygen deficient sample of TiO_2 with the composition of $TiO_{1.97}$ up to a temperature of 400°C. In such a sample each oxygen vacancy requires the formation of two Ti^{+3} ions in order to maintain electrical neutrality. There are, then, two factors operating; cations of larger size and lower charge than Ti^{+4} are created and many anion vacancies are introduced into the lattice. In Table X, data based on Mauer and Bolz' work are given which show that the $TiO_{1.97}$ sample has a much larger expansion anisotropy ($\Delta\alpha$) and a somewhat decreased volume expansion coefficient (α_v) and average expansion coefficient (α_{av}) than

Table X

THERMAL EXPANSION DATA FOR RUTILE SOLID SOLUTIONS

(ROOM TEMPERATURE TO 1000°C)

MOLE % ADDITIVE	LINEAR EXPANSION COEFFICIENT /°C		EXPANSION ANISOTROPHY /°C	VOLUME EXPANSION COEFFICIENT /°C	AVERAGE LINEAR EXPANSION COEFFICIENT /°C
	a_o α_{a_o}	c_o α_{c_o}	$\alpha_{c_o} - \alpha_{a_o} = \Delta\alpha$	α_v	α_{av}
PURE TiO_2	83.4×10^{-7}	107.7×10^{-7}	24.3×10^{-7}	274.5×10^{-7}	91.5×10^{-7}
10 V_2O_5	89.2×10^{-7}	94.6×10^{-7}	5.4×10^{-7}	273.0×10^{-7}	91.0×10^{-7}
10 ZrO_2	77.7×10^{-7}	110.7×10^{-7}	33.0×10^{-7}	266.0×10^{-7}	88.7×10^{-7}
10 Sb_2O_3	81.1×10^{-7}	103.0×10^{-7}	21.9×10^{-7}	265.2×10^{-7}	88.4×10^{-7}
9.2 Nb_2O_5	82.6×10^{-7}	111.1×10^{-7}	28.6×10^{-7}	276.1×10^{-7}	92.0×10^{-7}
10 WO_3	79.4×10^{-7}	105.7×10^{-7}	26.3×10^{-7}	264.5×10^{-7}	88.2×10^{-7}
30 SiO_2	82.5×10^{-7}	104.8×10^{-7}	22.3×10^{-7}	269.8×10^{-7}	89.9×10^{-7}
10 MnO_2	77.6×10^{-7}	111.0×10^{-7}	33.4×10^{-7}	266.2×10^{-7}	88.7×10^{-7}
10 Li_2CO_3	82.2×10^{-7}	108.0×10^{-7}	25.8×10^{-7}	272.4×10^{-7}	90.8×10^{-7}
10 SnO_2*	75.5×10^{-7}	104.0×10^{-7}	28.4×10^{-7}	248.6×10^{-7}	85.0×10^{-7}
20 SnO_2*	70.9×10^{-7}	93.0×10^{-7}	22.1×10^{-7}	234.8×10^{-7}	78.2×10^{-7}
30 SnO_2*	68.4×10^{-7}	92.0×10^{-7}	23.6×10^{-7}	228.8×10^{-7}	76.3×10^{-7}
10 Cr_2O_3	75.1×10^{-7}	109.7×10^{-7}	34.6×10^{-7}	264.0×10^{-7}	84.7×10^{-7}
DATA OF MAUER AND BOLZ (1957)					
PURE TiO_2#	78.6×10^{-7}	99.2×10^{-7}	20.6×10^{-7}	256.4×10^{-7}	85.5×10^{-7}
$TiO_{1.97}$#	68.0×10^{-7}	104.5×10^{-7}	36.5×10^{-7}	240.5×10^{-7}	80.0×10^{-7}
PURE TiO_2#	84.7×10^{-7}	105.0×10^{-7}	20.3×10^{-7}	274.4×10^{-7}	91.4×10^{-7}

ROOM TEMPERATURE TO 400°C

* ROOM TEMPERATURE TO 800°C

stoichiometric TiO_2. In Table X the thermal expansion data from room temperature to 1000°C are listed for the specimens studied. Those ions which produced relatively small changes in the lattice constants, Li, Si, Sb and W, also produced little change in the thermal expansion anisotropy ($\Delta\alpha$). Except for Sn, ions which increased the lattice constants (Zr, Nb and Mn) also increased $\Delta\alpha$. And finally, vanadium which decreased the lattice constants, also decreased $\Delta\alpha$ to a remarkable degree. It appears that most of these data can be systematized on the basis of ionic radii; if there are no valence changes or vacancies formed, the substitution of an ion of larger radius increases $\Delta\alpha$, and conversely, an ion of smaller atomic radius decreases $\Delta\alpha$. According to this interpretation, Cr^{3+}, with the same ionic radius as V^{+4} produces a larger increase in $\Delta\alpha$ because of the formation of anion vacancies. The result here is similar to that obtained by Mauer and Bolz for oxygen deficient rutile. In the case of Sn^{+4}, the ionic radius is only slightly larger than that of Ti^{+4} and there is almost complete solid solution formation between SnO_2 and TiO_2.[34] Figures 12 to 16 show the thermal expansion curves obtained for pure TiO_2 and for zirconium and vanadium additions to TiO_2.

To provide additional evidence for the above explanation for changes in $\Delta\alpha$, further work was done in the Al_2O_3-Cr_2O_3 system. These oxides are completely miscible in all proportions. Unfortunately, however, the addition of only a small amount of one into the other causes a large broadening and loss in intensity of the diffraction peaks. Besides pure Al_2O_3-Cr_2O_3, only two solid solution specimens were measurable. The results are indicated in Table XI and Figure 17. Since the Curie temperature of Cr_2O_3 is just above room temperature and this causes a discontinuity in the thermal expansion properties[41,42] the thermal expansion anisotropy has been calculated for the temperature range 400-1000°C. The observed changes of thermal expansion anisotropy are too small to be considered significant. The fact that the sign of the thermal expansion anisotropy of Al_2O_3 is positive, while that of Cr_2O_3 is negative, leads to the conclusion that significant changes in thermal expansion anisotropy will be found for larger additions and a composition with zero thermal expansion anisotropy (defined for a particular temperature range) will be found in the intermediate composition range.

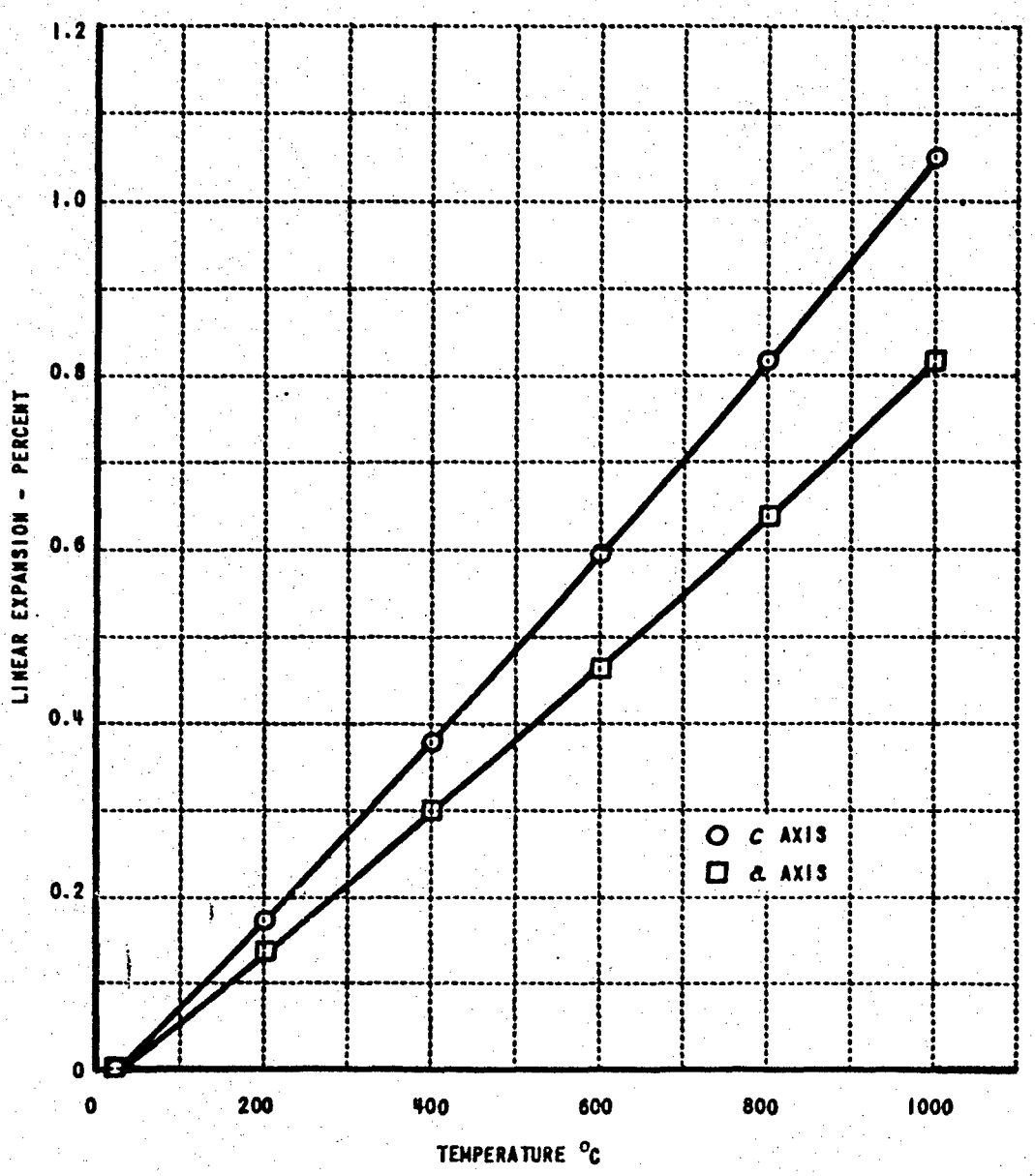

Figure 12 LINEAR THERMAL EXPANSION OF PURE RUTILE (TiO_2)

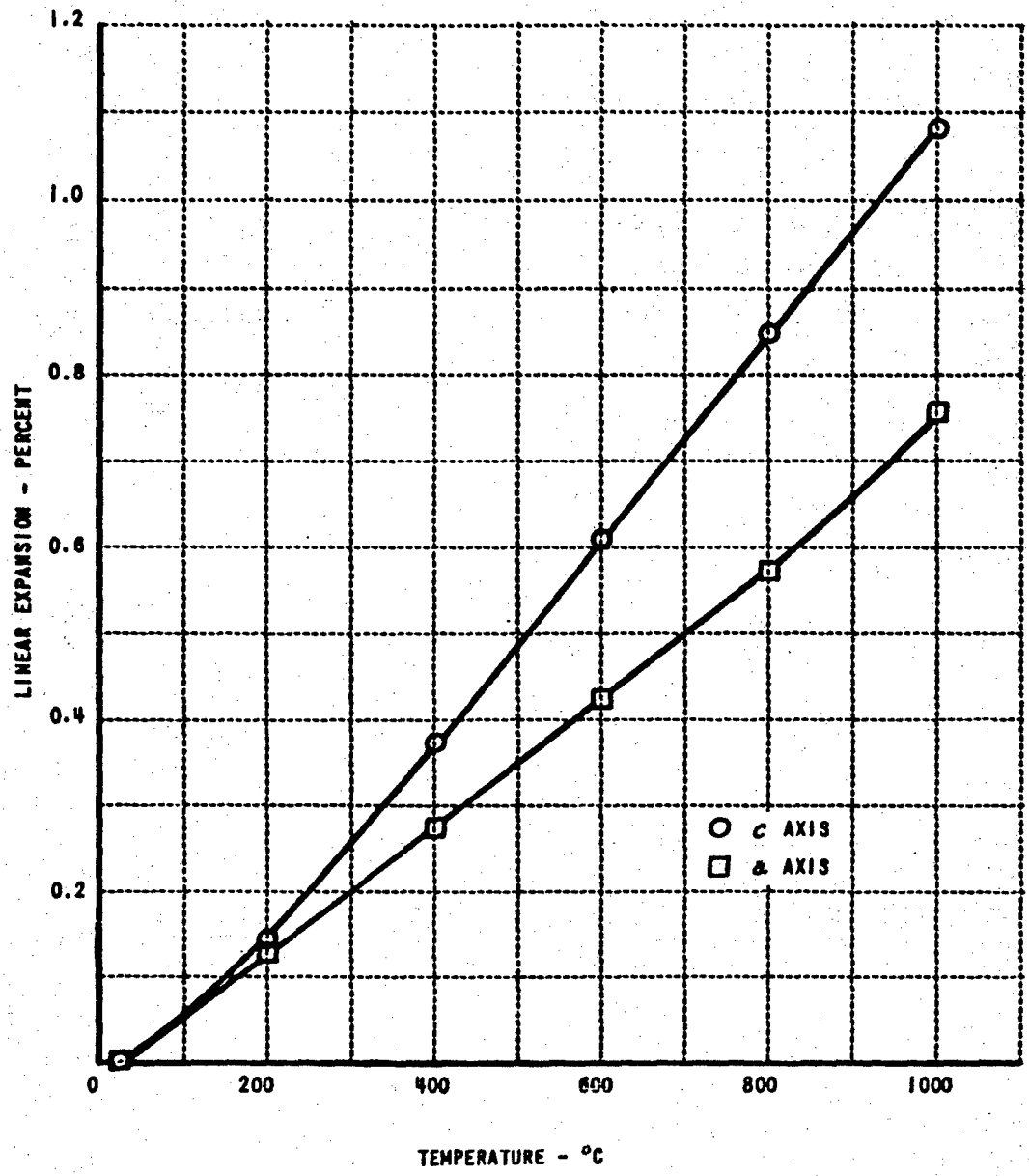

Figure 13 LINEAR THERMAL EXPANSION OF TiO_2 + (10 MOLE %) ZrO_2

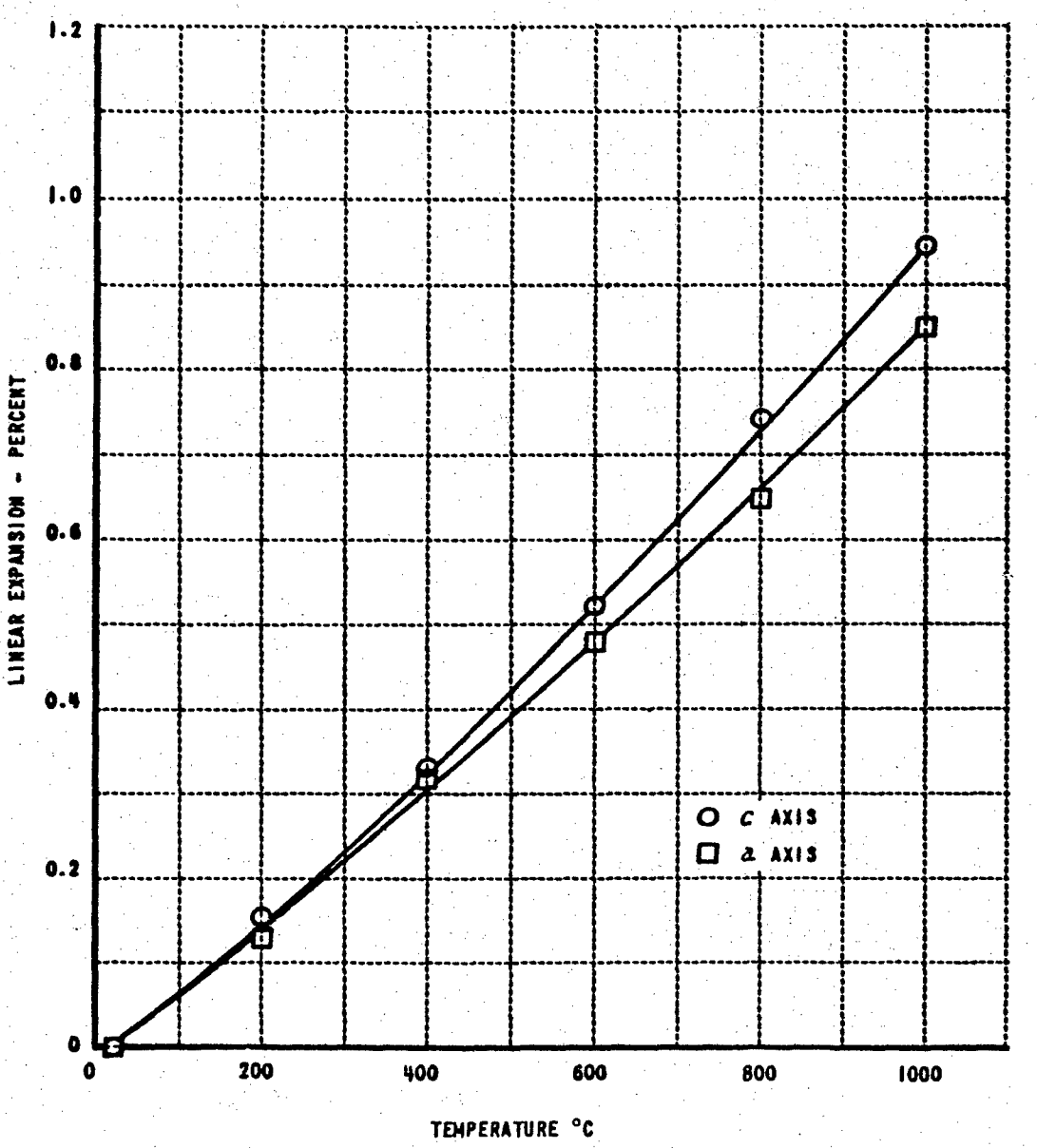

Figure 14 LINEAR THERMAL EXPANSION OF TiO_2 + 7.7 MOLE % VANADIUM

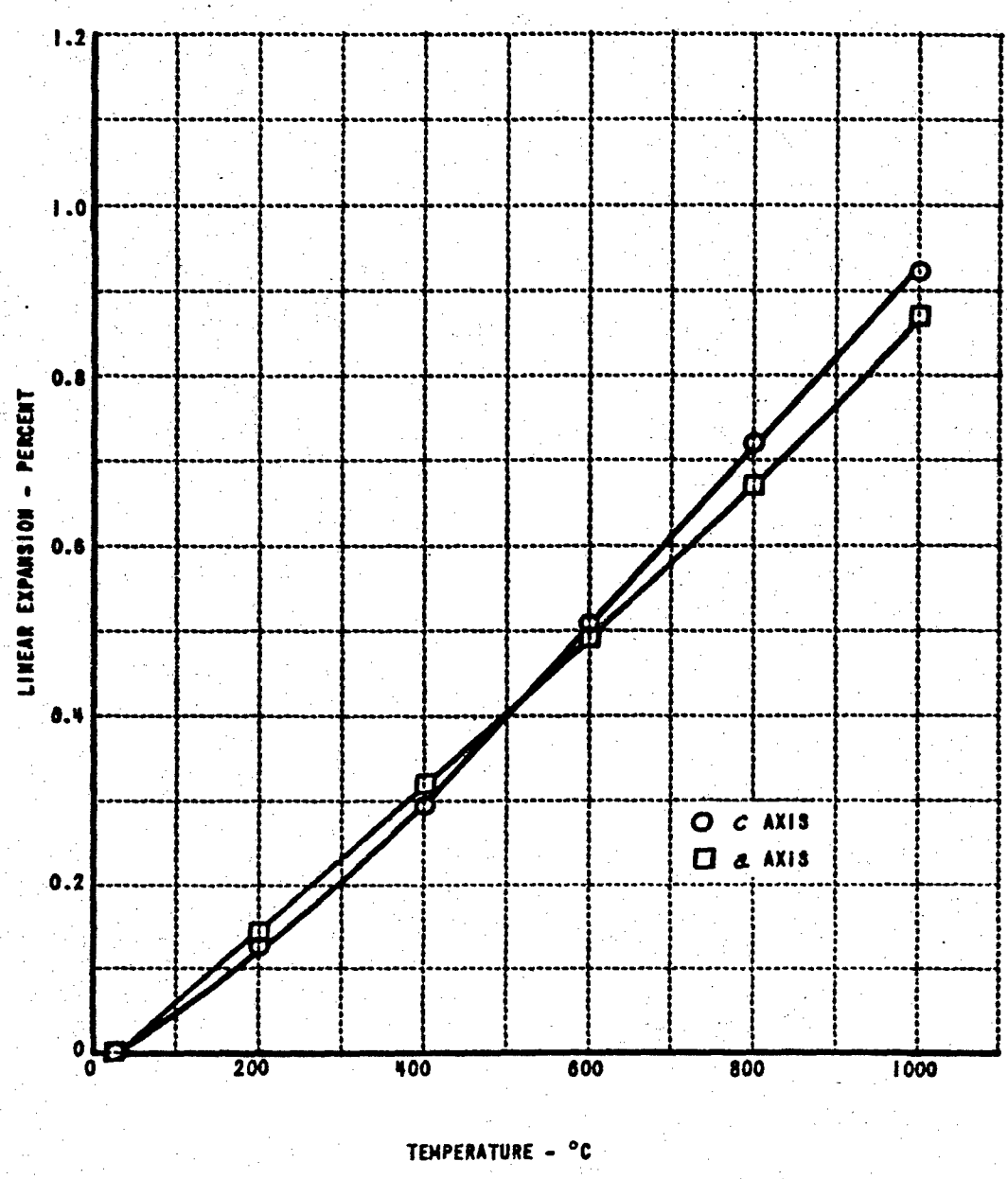

Figure 15 LINEAR THERMAL EXPANSION OF $TiO_2 + (10\ MOLE\ \%)\ V_2O_5$

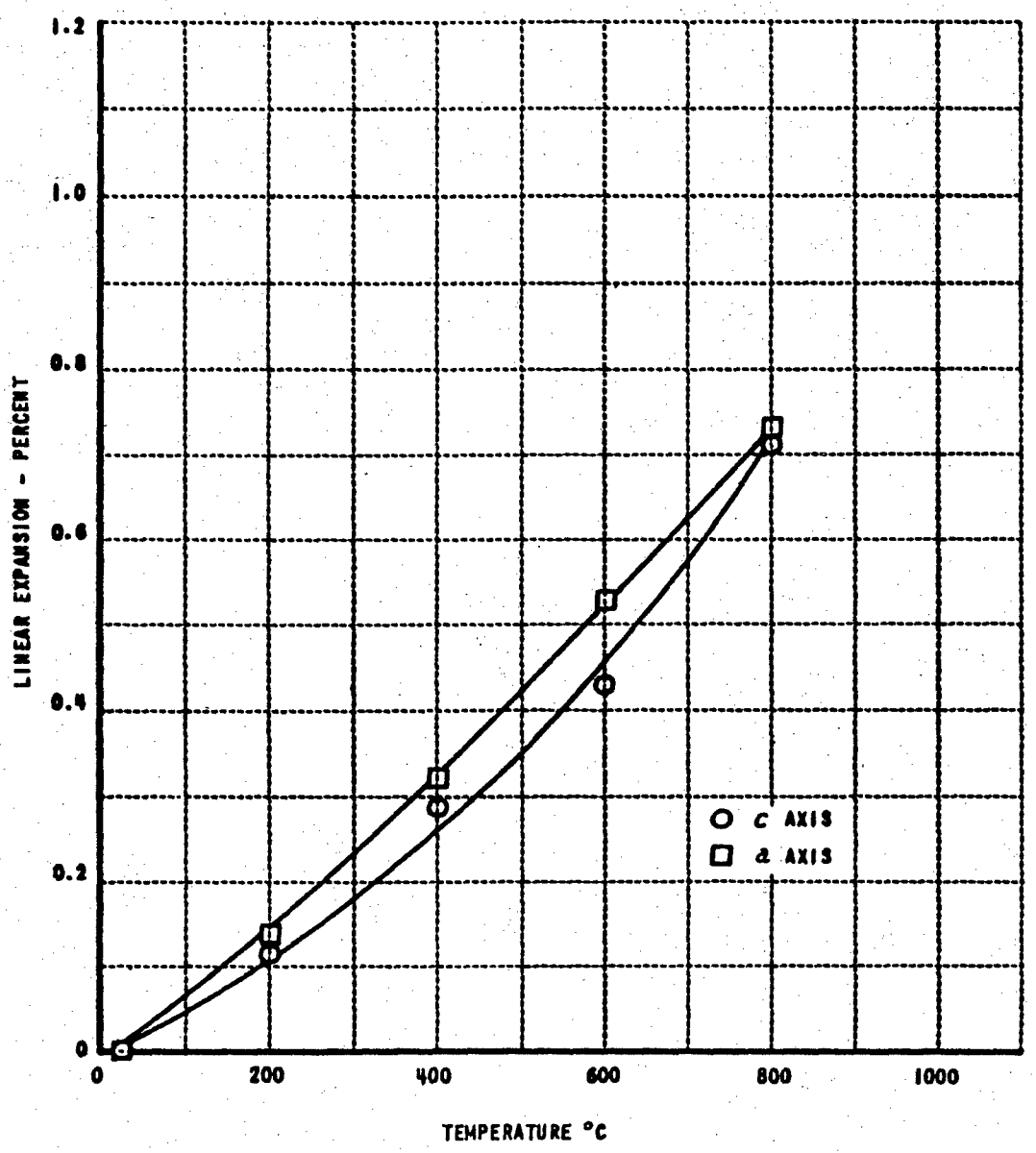

Figure 16 LINEAR THERMAL EXPANSION OF TiO_2 + 21.4 MOLE % VANADIUM

Table XI

THERMAL EXPANSION DATA FOR Al_2O_3 - Cr_2O_3 SOLID SOLUTIONS
(400°C TO 1000° C)

MOLE % ADDITIVE	LINEAR EXPANSION COEFFICIENT $^{o}C^{-1}$		EXPANSION ANESOTROPY $^{o}C^{-1}$	VOLUME EXPANSION COEFFICIENT $^{o}C^{-1}$	AVERAGE LINEAR EXPANSION COEFFICIENT $^{o}C^{-1}$
	α_{a_o}	α_{c_o}	$\alpha_{c_o} - \alpha_{a_o} = \Delta\alpha$	α_v	α_{a_v}
PURE Al_2O_3	86.2×10^{-7}	93.8×10^{-7}	7.6×10^{-7}	266.2×10^{-7}	88.8×10^{-7}
Al_2O_3 + 2.5 Cr_2O_3	87.4	95.1	7.7	269.9	89.8
PURE Cr_2O_3	78.2	72.9	-5.3	229.3	76.4
Cr_2O_3 + 10.0 Al_2O_3	78.0	72.5	-5.5	228.5	76.2

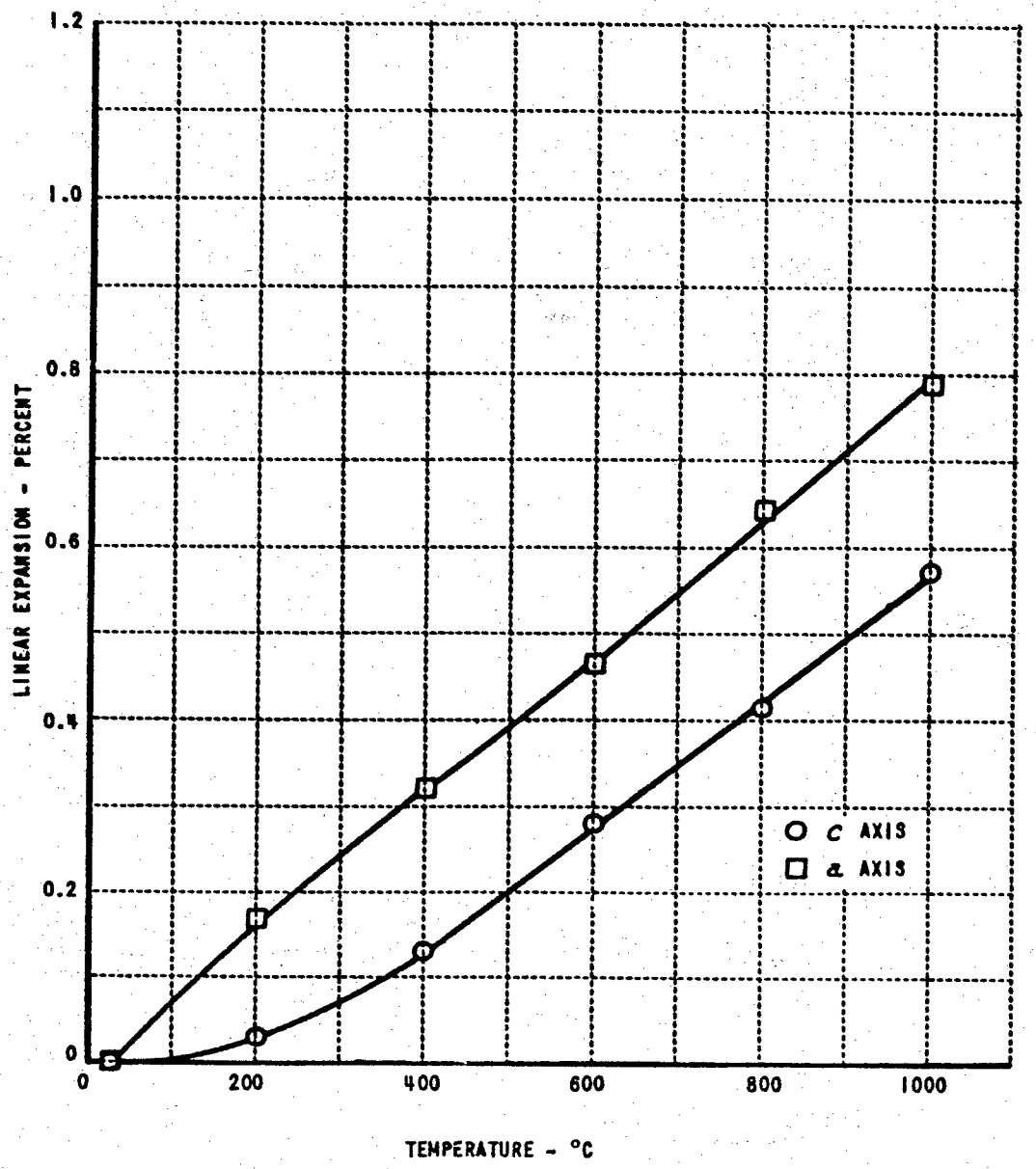

Figure 17 LINEAR THERMAL EXPANSION OF PURE Cr_2O_3

In some cases polycrystalline ceramics made from crystals having substantial thermal expansion anisotropy, show thermal expansion hysteresis. This effect was shown for rutile by Mauer and Bolz[40] and Charvat and Kingery.[28] In spite of this complication, the thermal expansion coefficient measured by Mauer and Bolz by the dilatometer method was 90.3 x $10^{-7}/^{\circ}C$ (0-1000°C) which compares favorably with the average thermal expansion coefficient calculated from the x-ray data.

The addition of vanadium to the rutile lattice results in a progressive decreases in thermal expansion anisotropy with increasing vanadium content up to 10 mole percent vanadium. At 10 mole percent vanadium, the thermal expansion anisotropy is substantially zero. Continued increase in vanadium content results in a reversal of the anisotropy so that at low temperatures the percent expansion is greater in the direction parallel to a_o than in the c_o direction. An increase in slope of the thermal expansion curve parallel to the c axis at high temperatures was observed in some cases. Little change in the volumetric expansion with increasing vanadium content was observed.

According to Cronemeyer[43] the structure of TiO_2 can be considered as made up of Ti-O-O-Ti-O-O-Ti chains oriented normal to the c axis. Therefore, replacement of titanium by vanadium with resulting decrease in a_o and slight decrease in c_o can be thought of as causing a decrease in the length of the chains but having little effect on the distance between them. To determine whether or not vanadium would have the same effect in other crystals of the rutile structure, the effect of vanadium on the thermal expansion anisotropy of cassiterite (SnO_2) was determined. In this case, too, the thermal expansion anisotropy was reduced. The results are given in Table XII and Figures 18 and 19. The thermal expansion anisotropy of crystals is important, in part, because of the effect of this anisotropy on local stresses, porosity and strength of polycrystalline bodies made from these crystals. At high temperatures during sintering, the stresses between crystals are relieved. During subsequent cooling, the crystals contract unequally causing local stresses. These stresses may cause local failures and the formation of pores that are large in two dimensions. This change in microstructure can result

Table XII

THERMAL EXPANSION DATA FOR SnO_2 - V_2O_5 SOLID SOLUTIONS

23 - 800°C

MOLE % ADDITIVE	LINEAR EXPANSION COEFFICIENT $^{\circ}C^{-1}$		EXPANSION ANESOTROPY $^{\circ}C^{-1}$	VOLUME EXPANSION COEFFICIENT $^{\circ}C^{-1}$	AVERAGE LINEAR EXPANSION COEFFICIENT $^{\circ}C^{-1}$
	α_{a_o}	α_{c_o}	$\alpha_{c_o} - \alpha_{a_o} = \Delta\alpha$	α_v	α_{a_v}
PURE SnO_2	50.6×10^{-7}	57.1×10^{-7}	6.5×10^{-7}	168.3×10^{-7}	52.8×10^{-7}
SnO_2 + 10%V_2O_5	50.9	54.5	3.6	156.3	52.1

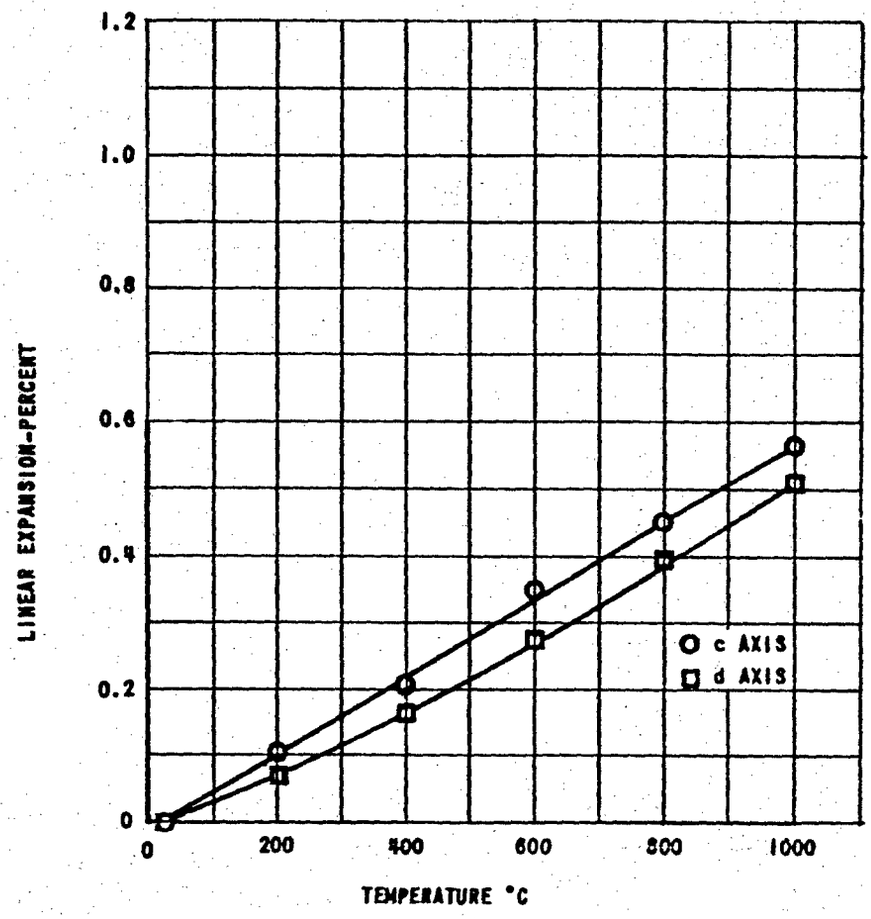

Figure 18 PERCENT LINEAR EXPANSION OF SnO_2

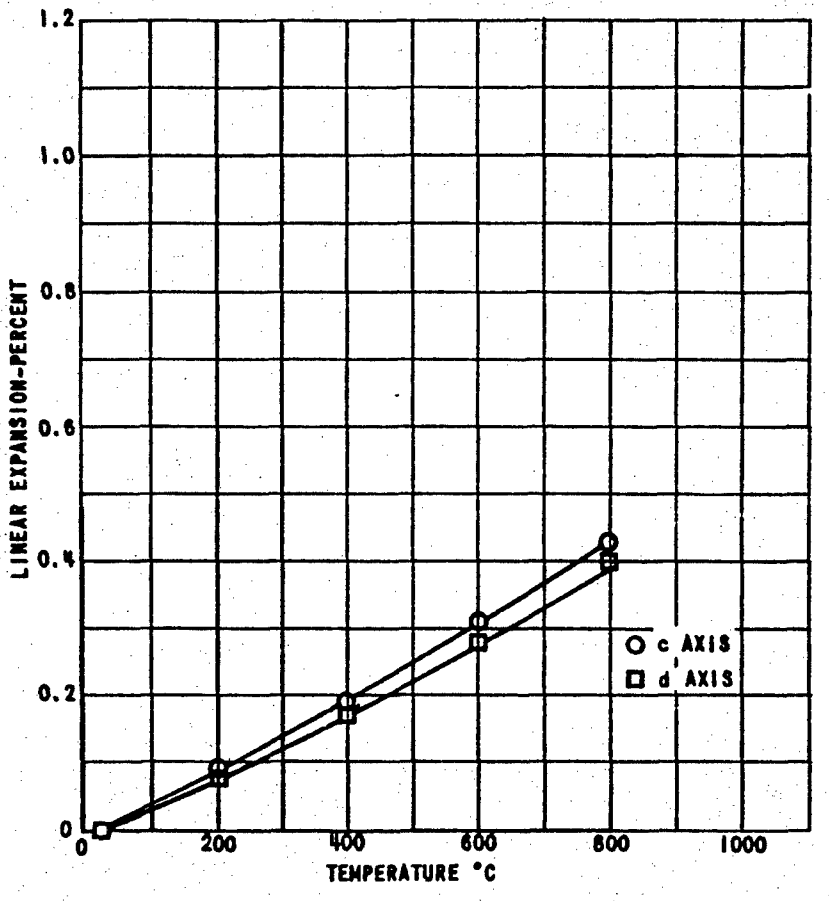

Figure 19 PERCENT LINEAR EXPANSION OF SnO_2 + 10 MOLE PERCENT V_2O_5

in low strength and low thermal conductivity. The reduction of the thermal expansion anisotropy of rutile and other crystals may make it possible to prepare ceramics with improved properties.

IV. THE THERMAL EXPANSION OF TWO-PHASE BODIES

A. Introduction

The thermal expansion of composite materials (including multiple-phase ceramics) can be predicted from the thermoelastic properties of the individual phases providing the resulting body is microscopically continuous and the phases do not enter into solid solution. The degree of validity of the theory is dependent, primarily, upon the completeness with which the internal stresses arising from thermoelastic dissimilarities are described. The case in which the composite body is homogeneous and macroscopically isotropic is of immediate interest and will be treated in this report. The results reported here are an outgrowth of research reported previously by Merz et al.[22] In this earlier research the inadequacies of available prediction methods became apparent. This led to the use of more satisfactory methods which are described in this report.

In the literature, several simplifying assumptions have been used to permit computation of the linear thermal expansion of two-phase ceramic bodies from existing data. These assumptions have been reviewed and a more complete theory for multiple-phase ceramic bodies is presented.

An important factor in improved correlation between thermal expansion theory and experiment is the determination of the intrinsic elastic properties of each ceramic phase. Gross reduction in the elastic moduli due to finite porosity resulted in attempts to produce high-density ceramic bodies. Apparatus was assembled for induction-heated hot-pressing to obtain high-density spinel and mixtures of Pyrex glass with spinel. The Pyrex-spinel system has been studied in detail both theoretically and experimentally.

B. Relationships Between Elastic Moduli and Stress Wave Velocities In Isotropic Bodies

The application of a dynamic stress at the boundary of a solid will generate a stress wave (or waves). For small disturbances, these stress waves will propagate away from the source with a velocity dependent solely upon the elastic properties, density, and geometry of the medium. Measure-

ment of elastic wave velocities in appropriately shaped specimens will provide data for computation of the elastic moduli.

Transmission of ultrasonic pulses, consisting of a burst of radio frequency (R.F.) stress waves, provides a convenient method for simultaneous measurement of stress wave velocity and attenuation over a range of frequencies. High frequency compressional waves and high frequency shear waves in ceramic specimens have been measured using the electronic test system indicated in Figure 20. The stress wave velocities (C) in semi-infinite media are given by: $C = \frac{L}{\gamma}$

where L = stress wave path length

γ = stress wave transit time

and by Kolsky[44]

compressional wave velocity $C_1 = \left[\frac{Y(1-\nu)}{\rho(1+\nu)(1-2\nu)}\right]^{\frac{1}{2}}$ for $a \gg \lambda$

shear wave velocity, $C_S = \left[\frac{G}{\rho}\right]^{\frac{1}{2}}$

where Y = Young's modulus (modulus of elasticity)

G = shear modulus (modulus of rigidity)

ρ = mass density

λ = wavelength of stress wave in medium

a = cross sectional dimension of specimen

ν = Poisson's ratio

These equations along with the relationships between the isotropic elastic constants,[45] e.g.

$$G = \frac{Y}{2(1+\nu)}$$

$$K = \frac{Y}{3(1-2\nu)}$$

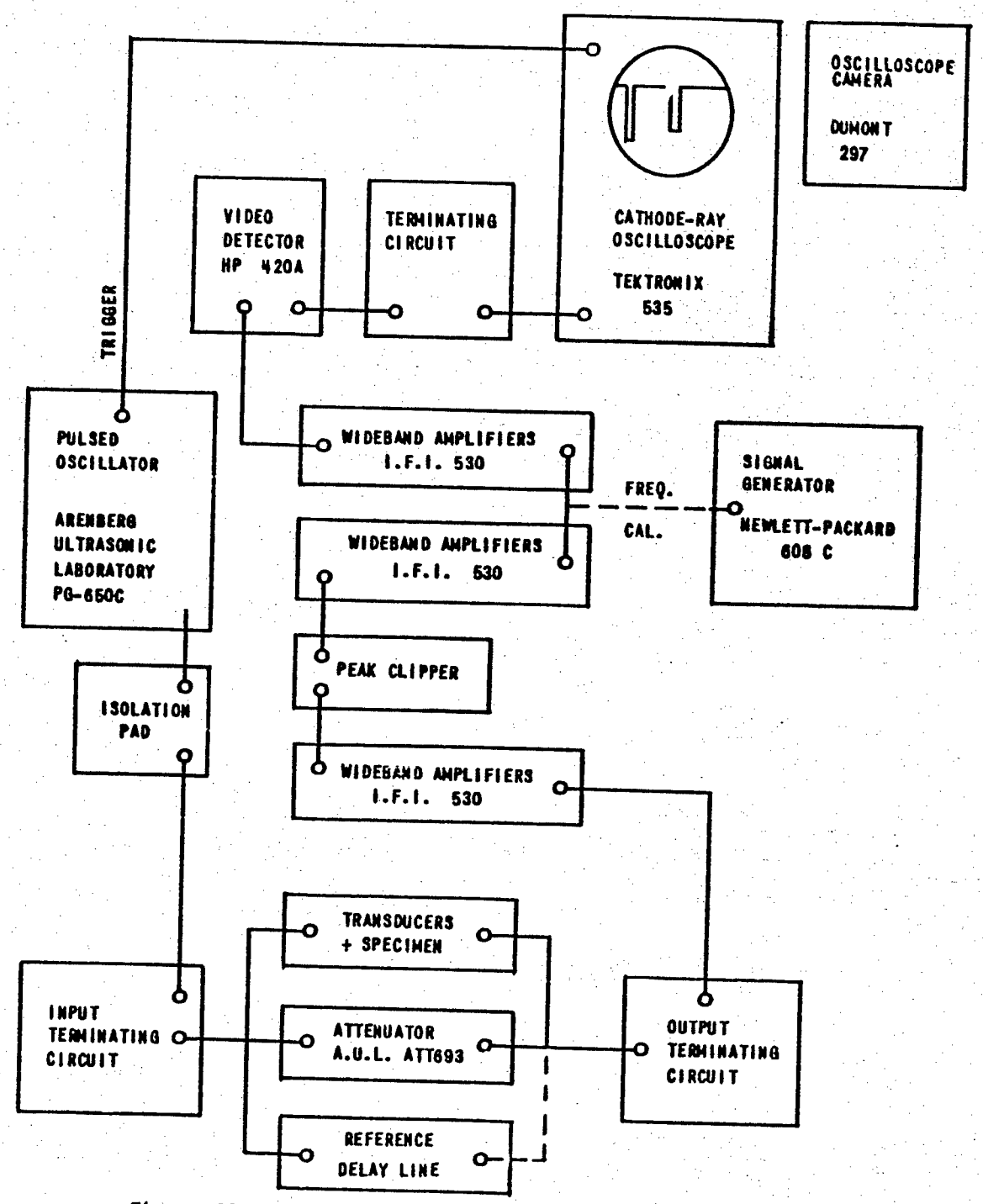

Figure 20 BLOCK DIAGRAM OF CAL ULTRASONIC TEST SYSTEM FOR STRESS WAVE PULSE TRANSMISSION MEASUREMENTS

were used to derive the following*

$$G = \rho C_s^2$$

$$\nu = \frac{\frac{1}{2} - \left(\frac{C_s}{C_1}\right)^2}{1 - \left(\frac{C_s}{C_1}\right)^2}$$

$$Y = \frac{\rho C_1^2 (1+\nu)(1-2\nu)}{1-\nu}$$

$$K = \rho\left(C_1^2 - \frac{4}{3} C_s^2\right)$$

Note that while four elastic constants may be of interest, only two independent elastic constants exist for isotropic media, hence only two different stress wave velocities need be measured.

The ultrasonic pulse method also permits convenient use of interferometric techniques for accurate determination of temperature coefficients of stress wave velocity and attenuation. By simultaneous excitation of two similar specimens maintained at different temperatures, small changes in propagation characteristics are readily observed as R. F. phase changes. Since these specimens may be excited at megacycle frequencies, detection of small phase changes constitutes a detection of velocity changes of a few parts per million or less.

- - - - - - - - - - -

* Identical relations were also given by Birch.[45]

The attenuation of megacycle stress waves in ceramics will arise from several factors:

1. Elastic anisotropy of the individual grains introduces scattering losses.
2. Elastic hysteresis within grains introduces irreversible absorption losses.
3. Relaxation effects between grains due to grain boundary motion introduces relaxation-absorption losses.
4. Thermal conduction between regions of compression and rarefaction introduces thermoelastic losses.
5. The presence of impurities within grains introduces an atomic relaxation-absorption loss.
6. The presence of pores, voids and microcracks introduces another form of acoustic scattering loss.

All together, these various losses are called internal friction losses and are intrinsic to the material (i.e. internal friction losses are independent of specimen geometry). Measurement of internal friction over a range of temperatures and frequencies provides a method for separating the several losses. Grain boundary relaxation generally produces an internal friction peak at slightly elevated temperatures while elastic hysteresis losses generally increase as a power of the absolute temperature. Scattering from microcracks, however, will tend to decrease with temperature since the size of the microcrack decreases. In some ceramics, the microcracks seem to completely close and reheal,* hence the acoustic scattering loss from such scattering centers would disappear at appropriately high temperatures. If this loss mechanism contributes significantly to the total internal friction at lower temperatures, then ultrasonics provides a method for nondestructive determination of the onset of microcracks. Such information would be immediately useful in computing the stresses required to induce microcracks.

- - - - - - - - - - -

* Private discussion with Professor W. R. Buessem, Pennsylvania State University.

Computation of the thermal stresses necessarily involves knowledge of the single crystal elastic constants for each of the ceramic phases along with their temperature dependence. Such data are generally obtained by ultrasonic pulse techniques and have been reported for a few ceramic single-crystals, e.g. sapphire, ruby, magnesium oxide, and magnetite (see Appendix C). The number of independent elastic constants increases from 3 in a cubic crystal to 13 in a monoclinic crystal. In each crystal class, the several elastic constants may be used to compute the single-crystal bulk modulus. In multiphase ceramics, the bulk modulus will be a function of the porosity and the component single-crystal bulk moduli as discussed in detail in Appendix C. Since each of these properties may be measured independently, a theory of elasticity for porous ceramic bodies will provide the basis for computation of composite elastic moduli, thermal expansion and resulting thermal stresses. A systematic computation of thermal stresses in multiphase ceramics should provide the insight toward the design of high-strength ceramic bodies.

C. Applications of Ultrasonic Measurements

1. Stress Wave Velocity Measurements

The ultrasonic equipment was arranged for use in measurement of the onset of microcracks in polyphase ceramic bodies. Because of the desire to measure stress wave losses introduced by the smallest possible crack dimension, megacycle frequencies were chosen. However, at megacycle frequencies, the acoustic scattering losses due to both elastic anisotropy of the grains and the presence of voids or pores are sufficiently great that only short path lengths through the specimens may be used successfully. In order to obtain sufficient accuracy in the determination of stress wave transit time in bar type specimens, several variations of ultrasonic interferometer techniques were employed. The most useful technique utilized a long pulse-length such that the pulse reflected twice at the fused silica-ceramic specimen interfaces as indicated on Figure 21. The twice-reflected pulse produced phase interference with the directly transmitted pulse introducing combined response nulls and peaks as the carrier frequency was varied. Observation of the

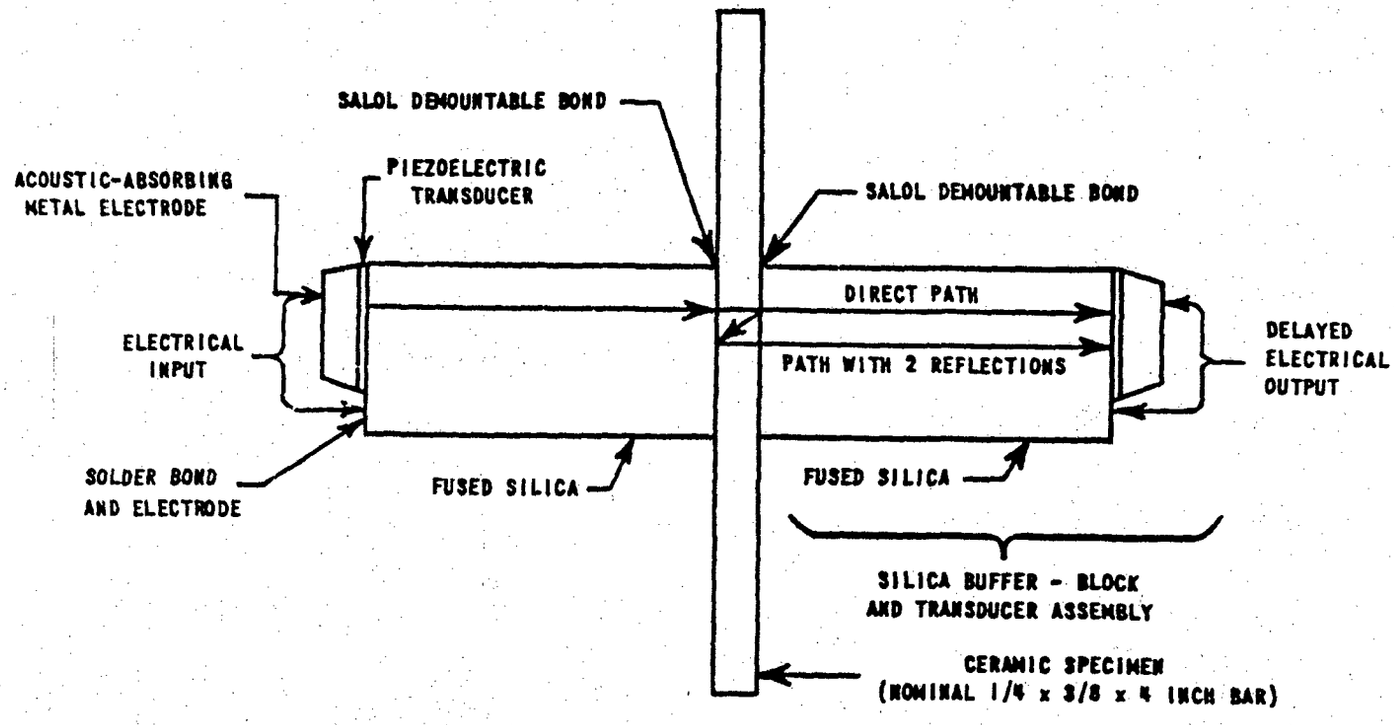

Figure 21 ULTRASONIC TRANSDUCER AND TEST SPECIMEN ASSEMBLY

frequencies at which maximum phase cancellation occurred, permitted computation of the phase velocity. The expression derived for stress wave velocity is similar to that given by McSkimin.[46]

$$C = \frac{2Lf}{n + \frac{1}{2} + \frac{2\psi}{360}}$$

where f = frequency at which a phase interference null occurs

ψ = phase shift at the specimen-buffer block interface in degrees

n = number of wavelengths in a $2L$ path length of the specimen

In the pulsed carrier measurement system, the pulse length is always chosen to include a minimum of several complete R. F. cycles in order to minimize the frequency spectrum. Thus for a given pulse length, a minimum frequency of operation exists and the value of n cannot be determined by counting from zero frequency. However, measurement of two consecutive null frequencies provides a method of evaluating both n and C. For specimens whose geometry is selected to avoid velocity dispersion,

$$\frac{2Lf}{n + 0.5 + \frac{2\psi}{360}} = C = \frac{2L(f + \Delta f)}{n + 1.5 + \frac{2\psi}{360}}$$

and $$n = \frac{f}{\Delta f} - 0.5 - \frac{2\psi}{360}$$

where Δf = frequency change between successive nulls

For all measurements made using this technique, eleven consecutive null frequencies were measured and the mean frequency change between nulls determined. In general, the stress wave velocity was accurate to three significant figures by the long pulse overlap technique which was adequate for use in thermal expansion computations.

Shear wave velocities were measured with two independent methods: 1. Total pulse transit time, and 2. The long-pulse overlap method. A summary of the data obtained with the second method is listed in Table XIII.

Table XIII
SHEAR WAVE MEASUREMENTS FOR PYREX-SPINEL SPECIMENS AT ROOM TEMPERATURE (23°-28°C)

SPECIMEN COMPOSITION BY WEIGHT	THEORETICAL DENSITY ρ_0 g/cm^3	APPARENT DENSITY ρ g/cm^3	POROSITY PERCENT	PATH LENGTH L INCHES	MEAN FREQUENCY SHIFT BETWEEN NULLS Δf, Mc	SHEAR WAVE VELOCITY 10^5 CM/SEC	DYNAMIC SHEAR MODULUS 10^6 LB/IN^3
100% SPINEL	3.58	3.28 ± .03	8.4	0.2505 ± .0001	0.365 ± .003	4.68 ± .08	10.4 ± 4%
25% PYREX	3.12	2.61 ± .03	16.2	0.2510 ± .0001	0.305 ± .003	3.92 ± .08	5.82 ± 4%
50% PYREX	2.75	2.71 ± .03	1.5	0.2560 ± .0001	0.288 ± .003	3.82 ± .08	5.73 ± 4%
75% PYREX	2.47	2.19 ± .03	11.3	0.2490 ± .0001	0.263 ± .003	3.35 ± .08	3.58 ± 4%
100% PYREX	2.23	2.23 ± .005	0	1.5585 ± .0001	0.268* ± .003	3.40 ± .08	3.74 ± 4%
100% PYREX	RESONANT ROD NEAR 10 Kc, SPINNER (22)					3.39	3.71
100% PYREX	PULSE TRANSMISSION AT 15 Mc, ARENBERG (28)					3.42	3.78

* COMPARISON MADE WITH DIFFERENT REFERENCE PULSE AS DESCRIBED IN TEXT.

A length of Pyrex cane was cut and lapped on both ends to obtain the 100% Pyrex data. For this specimen it was convenient to measure the null frequencies between two pulses, the difference being represented by

$$(1S + 3P + 1S + 2B_t + 2T + 2B_s) - (1S + 1P + 3S + 2B + 2T + 2B_s) = 2P - 2S$$

where T = path length through one transducer
S = path length through one silica block
P = path length through Pyrex specimen
B_t = path length through one transducer/silica bond
B_s = path length through one transducer/specimen bond

It can be shown that the small effects of the bonds and transducer paths completely cancel out with the interferometer technique providing that the reflection interfaces are properly identified. As a check on the accuracy of these measurements, data for Pyrex from two other investigations were obtained from the literature. The differences between these three sets of shear wave velocity measurements were about 1%. The long-pulse null frequencies were generally determined to only 1% accuracy (frequencies were read directly from the signal generator dial, higher accuracy may be obtained through the use of a frequency counter when necessary).

The total pulse transit time provides a convenient check on the stress wave velocity, but the accuracy decreases with decreasing specimen transit time. Typical values of transit times are given in Table XIV for the shear mode transducer assemblies illustrated in Figure 20.

If the total transit time was determined with $\pm$ 3% accuracy, the ceramic specimen transit time would be known to only $\pm$ 40% for the values given in Table XIV. In order to improve the attainable accuracy, a fixed delay line having a delay time near the value to be measured was used (Figure 20). By incorporating a delayed trigger circuit, the two delayed pulses could be observed, simultaneously, with an expanded sweep. With this arrangement, the delay difference could be determined with $\pm$ 3% accuracy. Thus, with the fixed delay equal to the time delay of the transducer-buffer block assembly (without the specimen), the delay difference becomes equal to

the specimen transit time and may be measured directly with ± 3% accuracy. In general, all three methods were used to determine shear wave velocities in each ceramic specimen in order to minimize operator errors.

Table XIV
SHEAR WAVE TRANSIT TIMES FOR TEST SPECIMEN COMPONENTS

SYMBOL	MEDIUM	PATH LENGTH L INCHES	SHEAR WAVE VELOCITY C_s 10^5 CM/SEC	SHEAR WAVE TRANSIT TIME γ_s MICROSECONDS
S	FUSED SILICA BLOCK	2.000	3.760	13.51
B_t	INDIUM SOLDER BOND	0.0001	0.71	0.003
B_s	SALOL BOND	0.0001	0.4	0.006
T	AC-CUT QUARTZ TRANSDUCER	0.00125	3.31	0.0096
C	CERAMIC SPECIMEN (100% SPINEL)	0.2505	4.68	1.36
$2S + 2B_t + 2B_s + 2T$	TRANSDUCER + BUFFER BLOCK ASSEMBLY	-	-	27.06
$2S + 2B_t + 2B_x + 2T + C$	TEST SPECIMEN ASSEMBLY	-	-	28.42

Compressional wave measurements were severely restricted because the transducer assemblies available consisted of one megacycle barium titanate ceramic transducers. The frequency response of these transducers was poor at the pulsed oscillator carrier frequencies (5 megacycles and above). Large response ripples due to reverberations within the ceramic transducers precluded use of interferometer techniques. The extended rise time obtained with these transducers also precluded precise determination of transit times. Preliminary measurements of compressional wave velocities in the Pyrex-spirel series were not accurate enough to provide comparison with Kerner's theory for Young's

modulus and bulk modulus of the composite bodies. Fused silica blocks and 25 megacycle x-cut quartz crystal transducers prepared with optical polished surfaces should be used.

D. Elastic Moduli of Polycrystalline Ceramics

Multiphase ceramics usually have average thermal expansion coefficients which lie between the two extreme end members. This occurs because the internal stresses present in continuous solid-phase bodies prevent the high-thermal expansion phase from dilating as much as in the isolated free-particle state. Of course, these same stresses also cause the low expansion phase to dilate more than in the isolated state. A similar effect occurs in simple compression of composite bodies as illustrated by the two-phase model in Figure 22. The important point is that the internal stresses are present within and between the individual grains. Hence, it is the elastic properties of the individual grains which should enter into the internal stress calculations. Or restated, it is the single crystal thermoelastic constants which determine the composite thermoelastic properties. Aside from the anisotropy considerations, the thermoelastic properties of available single-phase ceramics bodies differ from the single-crystal values because of the general inability to produce fully dense, pure single-phase bodies. Finite porosity causes each of the three principal elastic moduli (ν, K, G) to decrease. Lang[47], for example, found a 70% decrease in Young's modulus for a pure alumina body with 28% porosity. Because of these gross changes, it becomes important to be able to predict the porosity dependence. In fact, porosity accounts for most of the variability found between reported values of elastic moduli for single-phase ceramic bodies.

However, a comparison of static and dynamic moduli requires consideration of two additional factors. First, the measurement of elastic moduli under static conditions gives values for the isothermal moduli while sonic or ultrasonic measurements give the adiabatic moduli. The difference between these two moduli is dependent upon the ratio of specific heats ($\frac{C_p}{C_v}$) and is generally assumed to be negligible. Mason[48] has computed the elastic compliances of α-quartz under the two conditions and found the largest

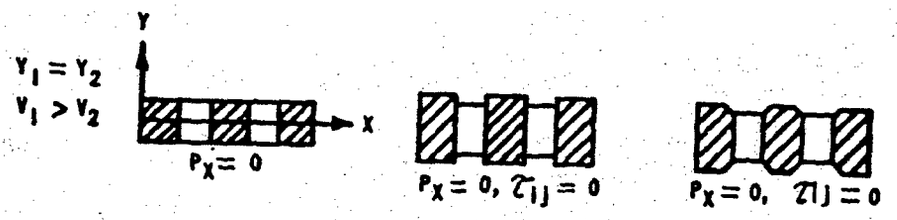

a) LINEAR ARRAY OF GRAINS WITH UNIAXIAL LOADING

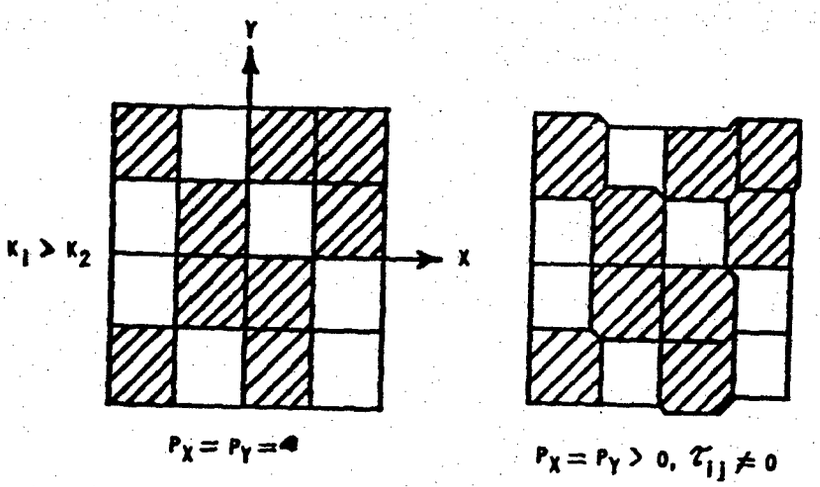

b) PLANE ARRAY OF GRAINS WITH BIAXIAL LOADING

Figure 22 DEFORMATION OF A TWO-PHASE MODEL SUBJECTED TO COMPRESSIVE LOADING

difference to be less than 2%. In rutile,[49] the differences are less than 0.3%. For isotropic solids, a relation given by Zener[50] may be used to evaluate the difference between the adiabatic Young's modulus (Y_μ , unrelaxed modulus) and the isothermal or static modulus (Y_S).

$$\frac{Y_\mu}{Y_S} = 1 + \frac{\alpha^2 T Y_\mu}{\rho C_v} \qquad \text{(IV-1)}$$

where C_v = specific heat at constant volume
ρ = density
T = absolute temperature
α = linear thermal expansion coefficient

For anisotropic solids, a relation derived by Voigt and reported by Vick and Hollander[49] may be used

$$\Delta_{ik} = -\frac{T\alpha_i\alpha_k}{\rho C_p} \qquad \text{(IV-2)}$$

where Δ_{ik} = adiabatic elastic compliance - isothermal elastic compliance
α_i, α_k = thermal expansion coefficients in the i and k directions
C_p = specific heat at constant pressure

Using the following values for MgO, $Y_\mu = 3.03 \times 10^{12}$ dynes/cm^2, $T = 288^\circ$K, $C = 0.20$ cal/g/$^\circ$C, $\alpha = 135 \times 10^{-7}/^\circ$C, and $\rho = 3.58$ g/cm^3, the dynamic modulus (Y_μ) was computed to be 0.5% greater than the static modulus (Y_S). A cursory review of the range of these physical constants for other single-phase ceramic bodies suggests that the ratio of adiabatic to isothermal elastic moduli will not differ from unity by more than a few percent.

At elevated temperatures the test specimen may deform slightly by creep producing an apparent lowering of the modulus. At sonic frequencies

and above, the period between cycles is too short to permit stress relaxation by creep. Hence, sonic measurements provide an unrelaxed modulus which is always greater than the static or relaxed modulus. Dynamic elastic moduli have been used for all computations.

Table XV is a compilation of the elastic properties of fully dense oxide ceramic bodies obtained from space averaging of single-crystal elastic constants and from extrapolation of porous body data to zero porosity.[51]

E. Theoretical Thermal Expansion of Multiple-Phase Ceramic Bodies

Turner[52] considered the thermal expansion of composite bodies by assuming that only isostatic stresses occurred within each phase due to the dissimilarities in thermoelastic properties. Hence only the modulus of volume elasticity, or bulk modulus (K), and the volume coefficient of thermal expansion (α_v) were required to define the composite thermal expansion, i.e.,

$$\alpha_v = \frac{\sum \alpha_{vi} V_i K_i}{\sum K_i V_i} \qquad \text{(IV-3)}$$

where V_i = volume fraction of the ith phase

α_{vi} = volume coefficient of expansion of the ith phase

K_i = bulk modulus of the ith phase

For isotropic bodies, the linear coefficient of thermal expansion (α) is approximately one-third of the volume coefficient (α_v)* so that equation (IV-3) remains unchanged when α is used. Previous applications of Turner's method[22,53] have resorted to an additional simplifying assumption which introduces considerable error in many systems, i.e. assuming $\nu = \nu_1 = \nu_2 = \nu_i$, then K_i may be replaced by Y_i because $Y = 3K(1-2\nu)$ where Y = Young's modulus (modulus of elasticity), ν = Poisson's ratio and

$$\alpha = \frac{\sum \alpha_i Y_i V_i}{\sum Y_i V_i} \qquad \text{(IV-4)}$$

---

* For unrestrained isotropic materials, $1+\alpha\Delta t = (1+\alpha\Delta t)^3 \simeq (1+3\alpha\Delta t)$ for $\alpha\Delta t \ll 1$, hence $\alpha_v \simeq 3\alpha$.

Table XV
ELASTIC PROPERTIES OF FULLY DENSE POLYCRYSTALLINE CERAMICS AT ROOM TEMPERATURE

CERAMIC	FORMULA	CRYSTAL FORM	YOUNG'S MODULUS PSI X 10^{-6}			SHEAR MODULUS PSI X 10^{6}			BULK MODULUS PSI X 10^{-6}			POISSON'S RATIO	THEORETICAL DENSITY g/cm^3
			VOIGT Y_V	REUSS Y_R	EXTRAP.* Y_o	VOIGT G_V	REUSS G_R	EXTRAP.* G_o	VOIGT K_V	REUSS K_R	K_o**	ν_o**	ρ_o
CORUNDUM	Al_2O_3	TRIGONAL	59.0	57.4	58.8	24.0	23.2	23.5	36.4	36.1	39.3	0.25	3.98
MAGNESIA	MgO	CUBIC	43.7	42.3	44	18.6	18.0	19	22.2	22.2	21.5	0.16	3.58
SPINEL	$MgO \cdot Al_2O_3$	CUBIC	-	-	40	-	-	15.5	-	-	31.8	0.29	3.58
MAGNESIUM ALUMINATE	$MgO \cdot 3.5\ Al_2O_3$	CUBIC	44.0	39.1	-	18.0	15.9	-	28.9	28.9	-	0.23	3.63
QUARTZ	SiO_2	TRIGONAL	14.7	13.2	-	6.80	5.96	-	5.8	5.7	-	-	2.65
FUZED SILICA	SiO_2	AMORPHOUS	-	-	10.5	-	-	4.50	-	-	5.25	0.168	2.20
PYREX	7740	AMORPHOUS	-	-	9.0	-	-	3.74	-	-	5.0	0.20	2.23
MULLITE	$3Al_2O_3 \cdot 2\ SiO_2$	ORTHO-RHOMBIC	-	-	32.	-	-	12	-	-	32	0.33	3.16
RUTILE	TiO_2	TETRAGONAL	46.0	38.2	-	18.2	14.1	-	30.8	30.6	-	-	4.24
BARIUM TITANATE	$BaTiO_3$	TETRAGONAL	23.5	18.8	17	8.70	6.89	8-9	27.0	23.6	-	0.36	6.01
MAGNETITE	Fe_3O_4	CUBIC	33.5	33.2	-	13.3	13.2	-	23.4	23.2	-	0.26	5.18
HEMATITE	Fe_2O_3	TRIGONAL	35.6	32.8	-	16.4	14.75	-	14.2	14.1	-	0.1	5.20
OLIVINE	$(Mg, Fe)_2SiO_4$	ORTHO-RHOMBIC	29.7	28.7	-	11.9	11.5	-	19.4	18.7	-	0.25	3.4
CALCITE	$CaCO_3$	TRIGONAL	16.7	11.6	-	6.81	4.48	-	10.0	9.48	-	0.25	2.71
CHROMITE	$FeO \cdot Cr_2O_3$	CUBIC	39.5	38.8	-	15.4	15.1	-	29.5	28.4	-	0.28	5.11
THORIA	ThO_2	CUBIC	-	-	35.5	-	-	14	-	-	25.5	0.27	9.82
URANIUM DIOXIDE	UO_2	CUBIC	-	-	31	-	-	12	-	-	24	0.29	10.95
ZIRCONIA	ZrO_2(5%CaO)	CUBIC	-	-	31	-	-	11	-	-	-	-	5.75
ZIRCON	$ZrSiO_4$	TETRAGONAL	5.2	6.3	-	2.3	2.6	-	3.1	3.5	-	0.2	4.67

*DYNAMIC MODULUS OF HIGH-DENSITY HIGH-PURITY POLYCRYSTALLINE CERAMIC BODIES EXTRAPOLATED TO ZERO POROSITY AS DESCRIBED BY KINGERY

**
$$K_o = \frac{Y_o G_o}{3(3G_o - Y_o)}, \nu_o = \left(\frac{Y_o}{2G_o}\right) - 1$$

It is to be noted that for the entire range of solid materials, Poisson's ratio is only required to vary from zero to 0.50 (the latter corresponds to an ideal liquid). Hence a small numerical difference in Poisson's ratio may reflect a large difference in solid state properties. The agreement between values predicted by equation (IV-4) and dilatometer measurements has generally been due to an opportune choice of values for the elastic constants. When the gross effects of porosity upon elastic moduli are ignored, the resulting apparent disparity of elastic moduli data has tended to permit a selection of those values which gave the best correlation with Turner's method.

An examination of the internal stress model used by Turner reveals that shear stresses between different grains and between similar grains with dissimilar orientations have been neglected. Assuming that shear stresses are negligible is equivalent to stating that at least one phase behaves as a liquid. Clearly, such a model is not adequate for use with ceramic bodies.

After establishing the necessary conditions for a more realistic internal-stress model, a review of the literature revealed that Kerner[69] had derived expressions for the thermoelastic properties of composite materials based upon such a model. Kerner's model incorporates both the volume dilation and the grain boundary shear stresses which arise in continuous-solid-phase composite bodies.* The linear thermal-expansion coefficient of composite bodies given by Kerner is

$$\alpha = \left(\frac{4G_o}{K_o} + 3\right) \sum' \left[\frac{\alpha_i v_i}{\frac{4G_o}{K_i} + 3}\right] \qquad \text{(IV-5)}$$

---

* Neither Turner's method nor Kerner's method is applicable to discontinuous-solid-phase bodies. Thus, the presence or occurrence of microcracks decreases the validity of both approaches.

where $\sum'$ stands for a summation excluding the index 1*

$$G_o = G_1 \left[\frac{\sum' \frac{G_1 V_i}{(7-5\nu_1)G_1 + (8-10\nu_1)G_i} + \frac{V_1}{15(1-\nu_1)}}{\sum' \frac{G_1 V_i}{(7-5\nu_1)G_1 + (8-10\nu_1)G_i} + \frac{V_1}{15(1-\nu_1)}} \right] \qquad \text{(IV-6)}$$

and

$$K_o = \frac{\sum \frac{K_i V_i}{3K_i + 4G_1}}{\sum \frac{V_i}{3K_i + 4G_1}} \qquad \text{(IV-7)}$$

The shear modulus (G_o) and the bulk modulus (K_o) refer to the moduli of the composite body, Kerner's method requires computation of these two moduli before the thermal expansion of the composite body may be determined. Since most applications of thermal expansion data also require data on elastic moduli, these intermediate steps serve dual purposes (Figure 23). Since it is generally more convenient to prepare bodies on a weight-fraction basis, the volume fractions may be replaced by $\frac{P_i}{\rho_i}$ where P_i is the weight fraction of the ith phase and ρ_i is the density of the ith phase. Note that phase-density does not effect either the internal stresses or the composite thermal expansion except by defining the fractional composition. Obviously, when the densities of each phase are equal (e.g., in the MgO-$MgO \cdot Al_2O_3$ system), the weight fractions become equal to the volume fractions. If the bulk moduli of each phase were equal, then equations (IV-3) and (IV-5) would reduce to one equation corresponding to a simple rule of mixtures, i.e.,

$$\alpha = \sum \alpha_i V_i = \sum \frac{\alpha_i P_i}{\rho} \qquad \text{(IV-8)}$$

---

* Index 1 was used for the annihilated suspending fluid.

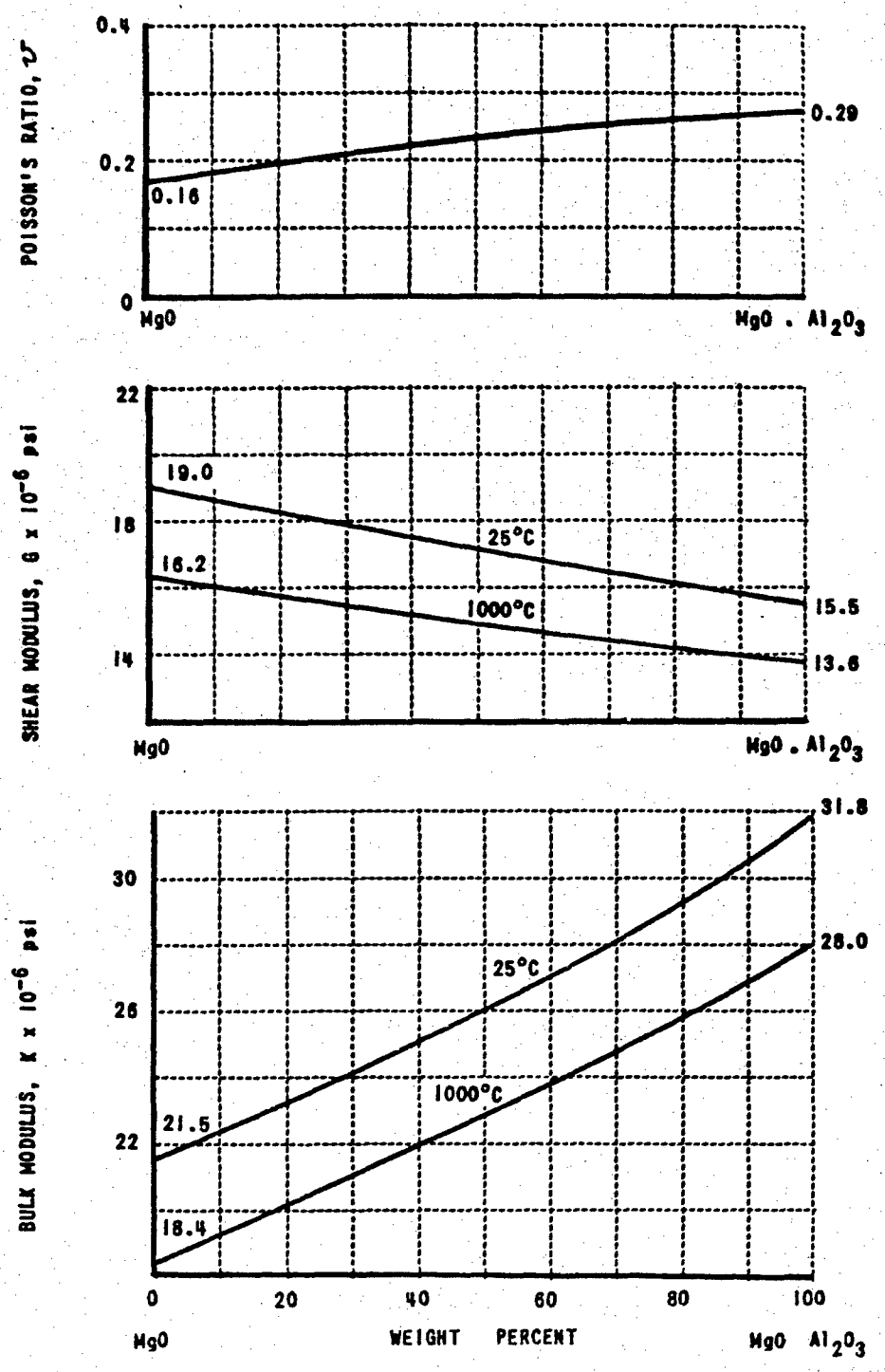

Figure 23 ELASTIC MODULI OF MAGNESIA-SPINEL CERAMICS BASED ON KERNER'S THEORY

F. Comparisons Between Theoretical and Empirical Thermal Expansion in Two-Phase Materials

1. Aluminum-Silica System

Figure 24 illustrates the differences between predictions by equations (IV-3) and (IV-5) for the aluminum-fused silica system. Measurements of thermal expansion for two different compositions as reported by Kingery[53] are included. The difference between theory and experiment may be due to stress induced microcracks. Microcracks arise when internal shear stresses exceed the local shear strength and hence the occurrence of microcracks would cause the empirical data to lie between the values predicted by equations (IV-3) and (IV-5) as was found for the aluminum-silica system.

Kingery used the oversimplified version of Turner's method (equation IV-4) to compute thermal expansion coefficients for this system. Since Young's moduli are equal for these two materials, the assumption of equal Poisson's ratio is equivalent to assuming equal bulk moduli and equation (IV-4) reduces to a simple rule of mixtures. The simple rule of mixtures is valid for a compacted mixture of powders in which no binder has been added, no sintering accomplished and hence no internal stresses developed. This model does not seem representative of the aluminum-silica system unless all aluminum-silica grain boundaries have fractured. Table XVI summarizes the differences between the several approaches to theoretical prediction of thermal expansion in composite bodies.

2. Magnesium Oxide-Spinel System

In the magnesium oxide-spinel ($MgO \cdot Al_2O_3$) system, the difference between predictions by equations (IV-3) and (IV-5) is small (Figure 25). In fact, the range of reported values for the linear thermal-expansion coefficient for the end members alone constitutes the greatest uncertainty to the predicted values for the two-phase ceramic body. Table XVII lists the values used for this analysis.

The thermal expansion coefficient of several other compositions in the MgO-spinel system were measured with a quartz tube dilatometer. However, the reproducibility of the measurements was unsatisfactory ($\pm$ 10%). These data were omitted in Figure 25 since a precision of $\pm$ 1% would be required to

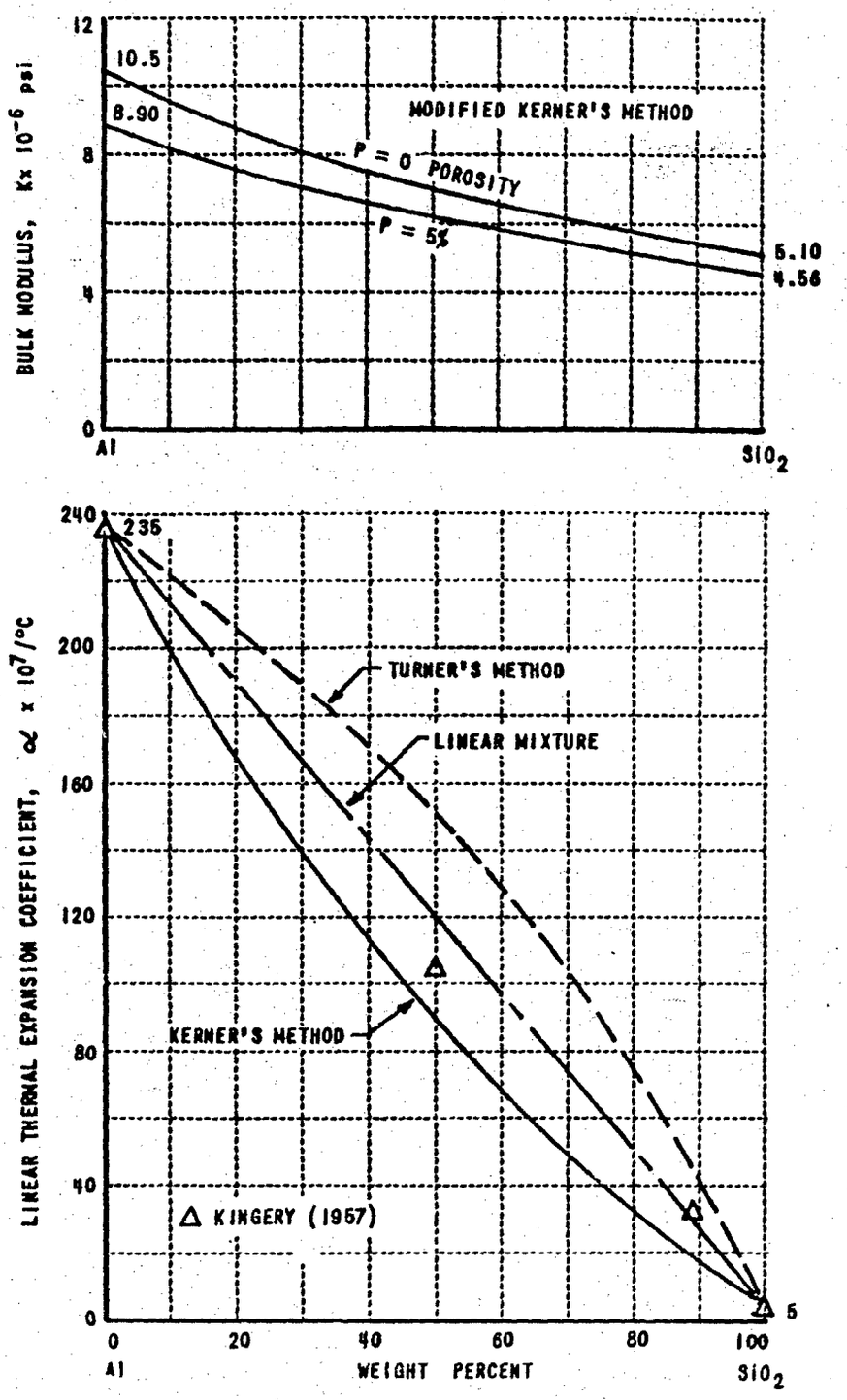

Figure 24 THERMAL EXPANSION IN THE ALUMINUM - SILICA SYSTEM

Table XVI

COMPARISON OF THERMAL EXPANSION RELATIONS FOR COMPOSITE MEDIA

FORMULA	INTERNAL STRESS MODEL	EQUIVALENT PHYSICAL INTERPRETATION
1) LINEAR MIXTURE $\alpha = \sum \alpha_i V_i$	NO INTERNAL STRESSES	HIGHLY COMPACTED POWDER MIXTURE WITHOUT BINDER AND NOT SINTERED
2) TURNER'S SIMPLIFIED METHOD $\alpha = \frac{\sum \frac{\alpha_i V_i P_i}{d_i}}{\sum \frac{V_i P_i}{d_i}}$	LONGITUDINAL (ONE DIMENSIONAL) STRESSES ONLY	SINGLE CHAIN OF PARTICLES SINTERED WITH RANDOM SEQUENCE OF PHASES AND WITH NO LATERAL RESTRAINTS
3) TURNER'S METHOD $\alpha = \frac{\sum \frac{\alpha_i K_i P_i}{d_i}}{\sum \frac{K_i P_i}{d_i}}$	ISOSTATIC STRESSES ONLY (THREE-DIMENSIONAL)	THREE DIMENSIONAL ARRAY OF REGULARLY SHAPED PARTICLES HAVING A THIN LIQUID AT EACH GRAIN BOUNDARY SUCH THAT NO PARTICLE DISTORTION OCCURS
4) KERNER'S METHOD $\alpha = \left(\frac{4G_o}{K_o} + 3\right) \sum' \left[\frac{\alpha_i V_i}{\frac{4G_o}{K_i} + 3} \right]$	LONGITUDINAL, LATERAL AND SHEAR STRESSES INCLUDED (THREE-DIMENSIONAL)	THREE DIMENSIONAL ARRAY OF RANDOM-SHAPED AND RANDOM-PHASE PARTICLES WHICH CHANGE BOTH IN VOLUME AND SHAPE DUE TO THE COMPLEX STRESS PATTERN NORMALLY PRESENT

SEE TEXT FOR G_o AND K_o RELATIONS

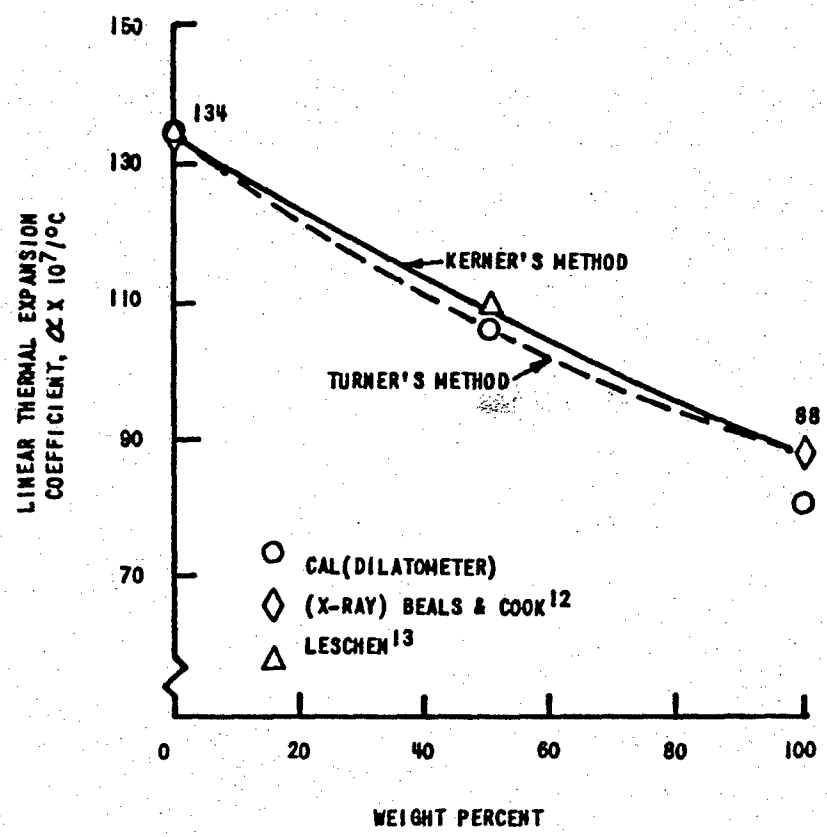

Figure 25 THERMAL EXPANSION IN THE MAGNESIA - SPINEL SYSTEM

Table XVII

THERMAL EXPANSION IN THE MgO-Mgo·Al_2O_3 SYSTEM

COMPOSITION	AVERAGE LINEAR THERMAL EXPANSION COEFFICIENT, IN/IN°C X 10^7		MEASUREMENT TECHNIQUE	REFERENCE
	OVER 25° TO 400°C	OVER 25° TO 1000°C		
100% MgO	134.7	144	X-RAY	BEALS (26)
	135	142	DILATOMETER	THIS STUDY
50% MgO	-	110*	DILATOMETER	LESCHEN(64)
50% MgO·Al_2O_3	107	118	DILATOMETER	THIS STUDY
	109	114	KERNER'S THEORY	THIS STUDY
	107	111	TURNER'S THEORY	THIS STUDY
100% MgO·Al_2O_3	88	88.3	X-RAY	BEALS (26)
	81	86	DILATOMETER	THIS STUDY

* 0.1% TiO_2 ADDED TO PRODUCE IMPERMEABLE, HIGH-DENSITY BODY (ρ = 3.50 g/cm^3)

validate the theory. Even with the several obvious improvements in the dilatometer, it is clear that it will be difficult to obtain adequate precision to establish the relative validity of equations (IV-3) and (IV-5) in the MgO-spinel system.

The concept which has been developed suggests two perturbations to the thermal expansion coefficient: 1) The thermal expansion of a single-phase polycrystalline body (having the same chemical composition as the single crystal) will depend upon porosity if the single crystal is anisotropic in thermal expansion and elastic properties, and the pore phase is continuous.* This dependence should arise from the changes in the internal stress pattern surrounding each grain as the continuous-pore phase increases. The investigation of porous alumina by Coble and Kingery[54] was made with discontinuous pore-phase bodies in which the expected change in internal stress would be small. They concluded that porosity had no effect upon the thermal expansion in alumina. 2) The thermal expansion of multiple-phase bodies will depend upon porosity if the elastic moduli and the expansion coefficient are dissimilar among the phases.

These perturbations would not be present in powder x-ray measurements. Dilatometer equipment available for this study did not provide sufficient accuracy to conclusively validate these predictions. For example, several 100% spinel bars measured during this program produced thermal expansion curves which appeared acceptable but which were not reproducible. The porosity-dependent thermal expansion of this elastically anisotropic phase could account for at least part of the data scatter, if large scale stresses induced in processing result in local stresses between grains due to elastic anisotropy (see Section IV-G).

3. Pyrex-Spinel System

Attempts to produce bars in the magnesia-spinel system with porosities of five percent or less by cold-pressing and sintering were not successful.

---

* The ratios of $\frac{Y_V}{Y_R}$ and $\frac{G_V}{G_R}$ based on data given in Table XV provide a measure of the elastic anisotropy. Isotropic crystals would have a unity ratio for each modulus.

In order to expedite development of hot-pressing equipment to produce high-density bodies at moderate temperatures, a glass-ceramic system was chosen. Pyrex and spinel were selected as representative of two-phase systems having grossly dissimilar thermoelastic properties.

Glass cane* was crushed, ball-milled, sieve-separated, and mixed with minus 325-mesh** commercial grade spinel. These mixtures were hot-pressed in an induction-heated graphite mold in the shape of 4-inch diameter disks about 3/8 inches thick. Forming data for the three disks selected are listed in Table XVIII.

Table XVIII
FORMING CONDITIONS FOR HOT-PRESSED PYREX-SPINEL DISKS

SAMPLE NO.	COMPOSITION BY WEIGHT	FORMING PRESSURE (GAUGE READING)	FORMING TEMPERATURE	TIME AT MAXIMUM TEMPERATURE
GS-4	25% PYREX	6000 PSI	1050°C	60 MIN
GS-5	50% PYREX	4000 PSI	950°C	30 MIN
GS-6	75% PYREX	4000 PSI	950°C	30 MIN

A test bar 0.2 x 0.5 x 4 inches was cut from the central portion of each disk. Densities of the rectangular prism specimens were measured by a displaced-mercury weight-change method (Table XIII).

- - - - - - - - - - -

* Pyrex Code 7740, Corning Glass Works.

** Particle size less than 44 microns.

Thermal expansion of the Pyrex-spinel series of bars was measured with a quartz-tube dilatometer over the temperature range from 20° to 300°C (Figure 26). These specimens had been subjected to no previous thermal cycling except for the initial cooling after hot-pressing. No further annealing was attempted in order to avoid the possibility of increasing the number of microcracks. Dilatometer readings were taken while the temperature increased at a nearly steady rate of 3°C per minute. The thermal expansion was found to be a nearly linear function of temperature over the temperature range of 100° to 300° C. The data below 100°C contained apparatus-originated errors and was excluded from further consideration. Contraction measurements during the cooling cycle produced a hysteresis effect indicative of non-equilibrium stress relaxation in the glassy phase. It is recognized that future measurements on glass-containing bodies will necessitate discrete measurements at stabilized specimen temperatures even when the test temperatures are well below the glass strain point. The elastic moduli for the Pyrex-spinel system as computed from equations (IV-6) and (IV-7) are shown in Figure 27.

Figure 28 is a comparison of the Pyrex-spinel thermal expansion measurements with the predictions obtained by equations (IV-3) and (IV-5). The superiority of Kerner's method is clearly demonstrated in this system. Two end points for spinel are shown. The upper point ($\alpha = 88 \times 10^{-7}/°C$) corresponds to the thermal expansion of powder specimens measured by x-ray diffraction techniques. The lower point ($\alpha = 81 \times 10^{-7}/°C$) represents dilatometer measurements on polycrystalline bars. The difference may be due to elastic anisotropy in the spinel crystal (see Section IV-G). The appropriate value to be used in prediction of thermal expansion in Pyrex-spinel mixtures is determined by consideration of the origin of the internal stresses. These stresses arise within individual grains which are surrounded, on the average, with grains having the elastic properties characteristic of the mixture. Hence, the thermal expansion of spinel powder (x-ray technique), not of the bulk ceramic, should be used in the computations. Improved correlation would be expected if Kerner's model was extended to include elastic anisotropy. Elastic anisotropy tends to lower the thermal expansion in porous bulk specimens if large scale stresses induced by the fabrication

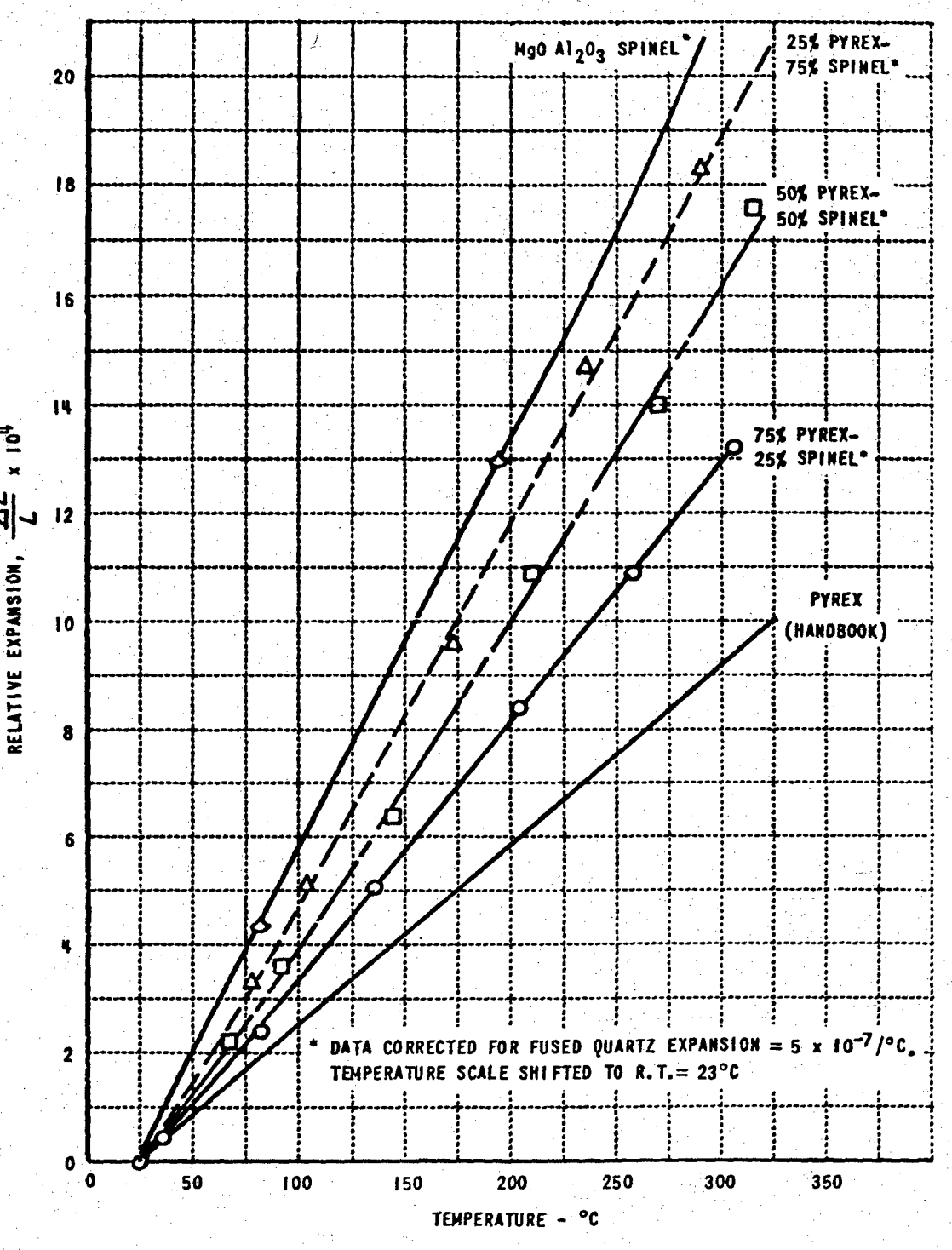

Figure 26 DILATOMETER THERMAL EXPANSION MEASUREMENTS FOR PYREX-SPINEL BARS

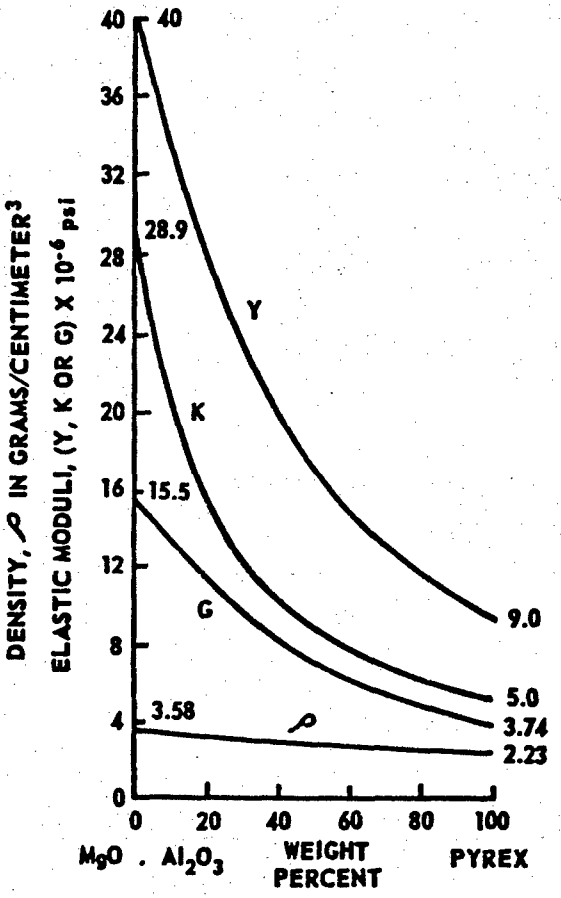

Figure 27 ELASTIC MODULI OF PYREX-SPINEL BODIES BASED ON KERNER'S THEORY

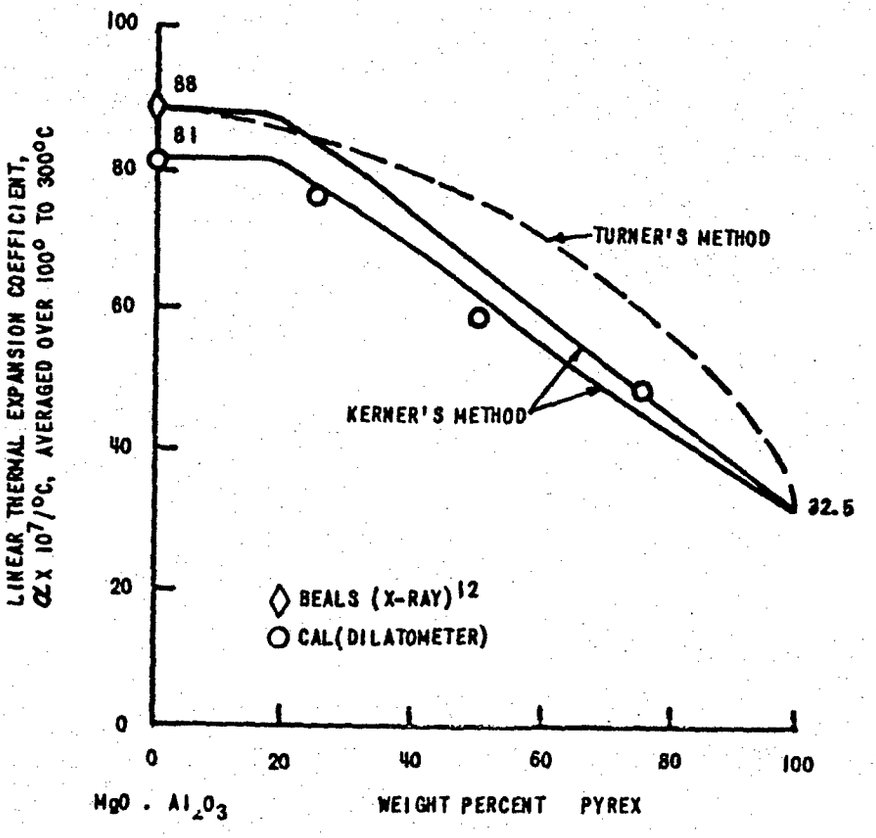

Figure 28 THERMAL EXPANSION IN THE PYREX-SPINEL SYSTEM

process, are present. This change would be dependent upon the relative amount of spinel present in the Pyrex-spinel system. It is expected that the change in thermal expansion predictions due to the addition of anisotropy terms would be similar to the differences between the two curves labeled "Kerner's Method" in Figure 27. As a reasonable approximation (and one which greatly simplifies the computations), substitution of the thermal expansion coefficient for bulk specimens (dilatometer data) could be used in equation (IV-5) to obtain the theoretical thermal expansion in a two-phase system, one of which is elastically anisotropic. This simplification would be much less valid if more than one phase were elastically anisotropic.

It is interesting to note that equation (IV-5) predicts a thermal expansion in the region of 15% Pyrex-85% spinel which is slightly higher ($\alpha = 88.5 \times 10^{-7}/^{\circ}C$) than for pure spinel ($\alpha = 88.0 \times 10^{-7}/^{\circ}C$) while equation (IV-3) predicts a continuously decreasing thermal-expansion coefficient with increasing Pyrex content. This difference serves to emphasize the importance of shear stresses to the internal stress model and to computations intended to define composition for purposes of matching thermal expansion coefficients.

G. Thermoelastic Anisotropy

In single-phase polycrystalline bodies, internal stresses may arise from either thermal anisotropy, elastic anisotropy, structural anisotropy or combinations thereof. For a cubic crystallite imbedded in a rigid, isotropic body with a matching thermal expansion coefficient, and if no restraints are present at the sintering temperature and no temperature gradients are present during forming, then the internal stresses on the crystallite reduce to zero. However, if restraints are present during forming due to temperature, pressure or compaction gradients, then stresses may arise in a polycrystalline medium even with cubic symmetry due to anisotropy of the elastic restraints.

For a spinel crystal of the type ($MgO \cdot 3.5\ Al_2O_3$) reported by Verma,[55] the anisotropy ratio is 2.1 to 1,* indicating that elastic restraints in a polycrystalline body may be anisotropic to a high degree. In a medium of this type, the anisotropy superimposes a spatial modulation upon the internal stresses. Nonhomogeneous polycrystalline bodies will generally possess regions of significant internal stress levels (e. g., cold-pressed and sintered bodies in which uniaxial pressure was employed are frequently found to have large-scale laminar-type cracks). When these internal stresses are significant, then the effects of elastic anisotropy will be significant even though the thermal expansion coefficient is isotropic. Hence, for precision dilatometer measurements upon polycrystalline bars, it is not sufficient to form a specimen in a manner which results in inhomogenities.

In general, the spatial stress function for a crystallite within a polycrystalline body will contain terms involving the direction cosines up to the fourth power.[56] The space averaged stress obtained by integration of the cosine^4 and cosine^2 functions does not reduce to zero for elastically anisotropic crystals. Hence the thermal expansion of single-phase nonhomogeneous polycrystalline bodies may be expected to differ from the average thermal expansion for the single crystal. Comparison of x-ray and dilatometer thermal expansion data for $MgO \cdot Al_2O_3$ spinel indicates that differences are often found (Table XIX).

H. Elevated Temperature Effects

Each of the internal stress theories requires the composite body to consist of a continuous solid-phase. The presence of microcracks, from any cause, seriously impairs the validity of these several predictions. Most

---

* Elastic anisotropy in a cubic crystal is proportional to the ratio of elastic compliance constants (S_{ij}) given by the expression

$$\frac{2(S_{11} - S_{12})}{S_{44}} \qquad \text{(IV-9)}$$

where a unity ratio indicates an isotropic body.

Table XIX

THERMAL EXPANSION OF $MgO.Al_2O_3$ SPINEL

TEMPERATURE RANGE	AVERAGE LINEAR THERMAL EXPANSION COEFFICIENT X 10^7/°C				
	POWDER SAMPLE, X-RAY DIFFRACTION TECHNIQUE		POLYCRYSTALLINE BAR, DILATOMETER		
			COARSE GRAIN	FINE GRAIN	OTHER SOURCES
	BEALS ET AL (1957) [26]	ZIMMERMAN (1956) [65]	WITTEMORE ET AL [66]	THIS STUDY	STUTZMAN ET AL (1959) [67]
25° - 300°C	88.2	83	52	76	67
25° - 600°C	87.8	88	75	90	73
25° - 900°C	-	89	84	90	80
25° - 1000°C	-	-	-	86	85
25° - 1200°C	88.3	90.5	91	-	-
25° - 1400°C	-	-	-	-	86
25° - 1500°C	-	-	96	-	-

microcracks arise when the internal stresses exceed the local strength of the body during cooling from forming temperatures. Hence, prediction of the elevated-temperature thermal expansion of composite bodies (where the occurrence of microcracks would be less) should provide a better opportunity for experimental validation. In order to apply equation (IV-5) to elevated temperature predictions, the temperature dependence of both the elastic moduli and the thermal expansion for each phase must be known. Wachtman, et al[57] have shown that Young's modulus for several oxide ceramics (e.g., sapphire, alumina, magnesia, and thoria) follow an exponential temperature dependence of the form

$$Y = Y_o - BTe^{\frac{-T_o}{T}} \qquad \text{(IV-10)}$$

where T = absolute temperature in ^{o}K

B, T_o are empirical constants

Y_o = Young's modulus at $0^{o}K$

Based upon Wachtman's data, Young's modulus for alumina ceramics would decrease by 10% from 25°C to 1000°C. Similar data for other ceramics show a more rapid decrease with increasing temperature. Smiley, et al[58] have compiled data on the elastic moduli versus temperature for spinel, mullite and several other ceramic phases.

A few observations related to the temperature-dependent effects can be made. Young's modulus for spinel decreases with temperature more rapidly than for MgO. Assuming both the shear modulus and the bulk modulus decrease in a similar manner, the elevated-temperature thermal-expansion coefficient for the spinel-MgO system will be everywhere higher than at room temperature. Both increasing α_{MgO} (Table XVII) and decreasing G_{spinel} would contribute to this change. An increase of 10 percent was obtained by high-temperature dilatometer measurements for the 50% MgO, 50% $MgO \cdot Al_2O_3$ specimen (Table XVII).

The elastic moduli of a few materials increase with temperature below 800°C. This is characteristic of high silica glasses, for example. In the aluminum-silica and Pyrex-spinel systems, the elastic moduli changes may be expected to produce significant differences between the room temperature and elevated-temperature thermal expansion.

I. Conclusions

Each of the several methods used to predict thermal expansion of composite bodies requires data on the elastic properties of the end members. It has been shown, that the elastic moduli which should be used for ceramics corresponds to the values for the fully-dense polycrystalline body rather than the lower values associated with the more readily available porous ceramics. The greater validity of Kerner's method over Turner's method for prediction of thermal expansion for multiple-phase ceramics has been clearly shown for three different two-phase systems. The completeness of Kerner's model for internal stresses is expected to reveal the superiority of Kerner's method for most composite bodies (which remain continuous solids).

In general, the thermal expansion coefficients of two-phase bodies will lie between the end members for all ranges of composition with one exception. When the thermoelastic properties are grossly dissimilar, the resulting thermal expansion may lie slightly outside the bracketed range for compositions which are predominantly one phase (e.g., 15% Pyrex-85% spinel).

Preliminary calculations for polycrystalline specimens composed of elastically anisotropic crystals indicate that the presence of structural inhomogenities will introduce internal stresses which will tend to lower the thermal expansion coefficient. Under these conditions, the bulk thermal expansion for polycrystalline bodies will differ from the single-crystal or the x-ray-measured thermal expansion for powder specimens. These local stresses may arise even though the single-crystal thermal expansion coefficient is isotropic, provided that large scale stresses induced during fabrication are present.

The elastic properties (e. g., K, G, Y, ν) of composite bodies, including multiple-phase ceramics, may be predicted (with small error for bodies which remain continuous solids) by a method developed by Kerner. This study appears to be the first application of Kerner's method to ceramic bodies.

V. CONCLUSIONS AND RECOMMENDATIONS

A. Conclusions

1. The relationship between the openness ratio and the thermal expansion coefficient for a number of oxides and silicates, was investigated. In these groups of materials, phases having high values of the openness ratio usually have low thermal expansion coefficients.

2. Several phases having high values of the openness ratio were synthesized and the thermal expansion coefficients were measured. The following phases have especially low thermal expansion coefficients:

$CaO \cdot CuO \cdot 4SiO_2$
$SrO \cdot CuO \cdot 4SiO_2$
$BaO \cdot CuO \cdot 4SiO_2$
} Tetragonal sheet silicates

UP_2O_7 (cubic)

3. Cubic UP_2O_7 has unique thermal expansion properties. The crystal expands with increasing temperature up to about 400°C. Above this temperature the crystal contracts, returning to its room temperature dimensions at about 1000°C. Since the peak positions and intensities of the x-ray diffraction patterns are very nearly the same at room temperature and at 1000°C, these expansion properties are not the result of a major structural change.

4. Little variation of the thermal expansion coefficient with openness ratio is observed within homologous series. These observations confirm Megaw's rule. $\left(\alpha = \frac{Ap^2}{z^2}\right)$.

5. The thermal expansion coefficients of the alkali halides were calculated based upon the change in lattice spacing with temperature at minimum free energy using the techniques of statistical mechanics. These calculations require knowledge of the atomic structure, ionic charge and atomic spacings at one temperature. The repulsion exponent was assumed to

have one value for the entire group. Comparison of the results of these calculations with experimental values gave encouraging results. Improvements can probably be made by taking into account the polarization of the ions and variation of the repulsion exponent.

6. The thermal expansion anisotropy of crystals can be varied by addition of appropriate solid solution atoms. Addition of vanadium atoms to replace titanium in rutile (TiO_2) results in a marked decrease in the thermal expansion anisotropy. At an addition of about 10% vanadium the thermal expansion anisotropy reverses so that the a axis becomes the direction of highest thermal expansion coefficient. The effect of vanadium on the thermal expansion anisotropy is not restricted to rutile since a similar reduction in thermal expansion anisotropy was observed when vanadium was added to cassiterite (SnO_2) which also has the rutile structure.

7. The thermal expansion anisotropy of Cr_2O_3 is opposite in sign from that of corundum (Al_2O_3). Since corundum and Cr_2O_3 form a continuous solid solution series, an intermediate composition must exist for which the thermal expansion anisotropy is zero.

8. Kerner's method was used to predict the thermal expansion coefficients of two-phase ceramic bodies. The predictions are satisfactory and the superiority of Kerner's method, which accounts for shear stresses was demonstrated.

9. In cases in which the thermoelastic properties of the pure phases are grossly dissimilar, the thermal expansion coefficients of some intermediate compositions may be slightly outside the range between the end members.

APPENDIX A

"Openness" Ratios of Some Ceramic Phases

In the following list the compounds are mainly covalent in character of chemical binding. Therefore, the calculation of these openness ratios is based upon the assumption of 100% covalent binding. This computation is simpler than those previously made[14] since the radius of each atom does not depend upon the other atoms present.

The information in Appendix A is printed directly by the IBM computer. This results in chemical formulae written in an unconventional form. Lower case letters were not available. Hence, for example, the abbreviation for aluminum is written AL rather than the customary Al. This will not result in confusion if one notes that the abbreviation for each single element is always enclosed between two numbers. As an illustration in line 1, one finds the formula 1AL1B2. Inasmuch as there is no number between A and L, these letters designate a single element, namely aluminum, normally written Al. The number 1 which heads this formula indicates there is one AlB_2 group in the formula. The numbers after each element have the meaning of conventional subscripts. In some cases rather unusual groups, such as 1N1N1 in line 36, appear. The formula for the compound is $LiGaN_2$. This N_2 is written 1N1N1 as a matter of convenience in programming. The number of significant figures should be two numbers in most cases. A larger number are given mainly for convenience.

CHEMICAL FORMULA	SOURCE	VOLUME OF IONS	VOLUME OF FORMULA WEIGHT	OPENNESS RATIO
1AL1 B2.	(1)	7.5073	15.3605	.5113
1BA1 B6.		27.3206	46.3303	.4103
1BA1 S4.		30.9201	88.9632	.6524
1 B4 C1.		6.3156	22.0000	.7129
1 B1 N1.		2.3129	11.3636	.7965
1 B3SI1.		7.9120	24.2063	.6731
1 B6SI1.		11.7852	37.6518	.6870
1CA1 B6.		21.0306	45.6522	.5393
1CA1 B6.		21.0306	42.8571	.5093
1CE1 B4.		16.4919	31.8815	.4827
1CE1SI2.		19.4050	34.5679	.4386
1CR1 B1.		5.3298	10.2107	.4780
1CR3 C2.		14.4186	26.9461	.4649
1CR5 C2.		22.4960	41.0405	.4519
1CO2 P1.		11.2284	23.2813	.5177
1CR1 P1.		7.3950	14.5614	.4921
1CR3SI2.		20.1935	38.5455	.4761
1CO1 B1.		5.2271	9.6552	.4586
1CO2SI1.		11.9108	13.8095	.1375
1CO1SI2.		12.0135	21.6981	.4463
1CU3 B2.		14.6983	26.1084	.4370
1CU3 P1.		15.4724	33.6364	.5400
1CU4SI1.		20.1935	37.4502	.4608
1FE1AS2.		12.9732	27.8378	.5340
1FE1 B1.		5.3298	9.3706	.4312
1FE3 C1.		13.2673	24.3243	.4546
1FE1 S2.		9.7117	24.0000	.5953
1FE4 N1.		17.1767	36.0731	.5238
1FE1 P1.		7.3950	14.3328	.4840
1FE2 P1.		11.4337	21.7988	.4755
1FE3 P1.		15.4724	29.5252	.4760
1FE1SI1.		8.0774	13.7705	.4134
1FE3 S4.		23.4622	65.0549	.6393
1LA1 B6.		19.9180	78.1609	.7452
1LI1GA1. 1 N1 N1.	(1)	11.6612	35.5224	.6717

CHEMICAL FORMULA	SOURCE	VOLUME OF IONS	VOLUME OF FORMULA WEIGHT	OPENNESS RATIO
1LI1 H1.	(1)	4.6925	9.7561	.5190
1MN1 B1.		5.3298	10.6452	.4993
1MN1 B2.		6.6209	11.1594	.4067
1MN3 C1.		13.2673	25.6894	.4835
1MN1 P1.		7.3950	15.9555	.5365
1MN3 P2.		18.8288	44.3359	.5753
1MN2SI1.		12.1161	22.2581	.4557
1MN1SI1.		8.0774	14.0678	.4258
1MN1SI2.		12.1161	21.1832	.4280
1MO1 B1.		6.7043	12.3699	.4580
1MO1 B2.		7.9954	16.5730	.5176
1MO2 B1.		12.1175	21.9222	.4473
1MO1 C1.		6.5644	12.3007	.4663
1MO2 C1.		11.9776	22.2222	.4610
1MO1 P1.		8.7695	20.5835	.5740
1MO1 P2.		12.1258	29.5327	.5894
1NI1SB1.		10.7545	23.8727	.5495
1NI1AS1.		8.3024	17.7015	.5310
1NI1 B1.		5.1262	9.4723	.4588
1NI3 C1.		12.6566	23.6181	.4641
1NI2 P1.		11.0266	23.4548	.5299
1NI2SI1.		11.7089	20.1389	.4186
1CB2 B2.		14.7169	16.4993	.1080
1CB1 N1.		7.0892	12.7381	.4435
1PD1SI1.		9.3270	18.4679	.4950
1 P3 N5.		15.1781	64.9402	.7663
1SI2 C1.		9.2286	27.2000	.6607
1SI3 N4.		16.2035	40.6977	.6019
1SR1 B6.		25.3171	46.3636	.4539
1TA1 B2.		8.6495	16.3974	.4725
1TA1 C1.		7.2186	13.1741	.4521
1TA1 N1.		7.0892	11.9632	.4074
1TH1 B4.		16.4919	32.5444	.4932
1TH1 B6.	(1)	19.0741	46.2617	.5877

CHEMICAL FORMULA			SOURCE	VOLUME OF IONS	VOLUME OF FORMULA WEIGHT	OPENNESS RATIO
1SN1 P1.			(1)	10.4251	22.8659	.5441
1SN4 P3.				38.3439	109.6525	.6503
1TI1 B2.				8.3819	15.5556	.4612
1TI1 C1.				6.9509	12.1704	.4289
1TI1 N1.				6.8216	11.4180	.4026
1TI1 P1.				9.1560	20.0000	.5422
1 W1AS2.			(2)	14.4746	48.4058	.7010
1 W2 B1.				12.3712	22.0734	.4395
1 W1 B1.				6.8312	12.3967	.4490
1 W1 B2.				8.1222	16.1569	.4973
1 W2 P1.				14.4365	76.5835	.8115
1 U1 B2.				9.8024	19.6063	.5000
1 U3 N4.				25.7480	76.3132	.6626
1 V1 B2.				7.1611	14.3137	.4997
1 V1 C1.				5.7302	10.9185	.4752
1 V1 N1.				5.6008	10.6036	.4718
1 V2SI1.				13.1966	23.7226	.4437
1 V1SI2.				12.6564	24.2081	.4772
1ZN3 P2.				21.4879	56.7033	.6210
1ZR1 B2.				10.2697	18.5550	.4465
1ZR1 C1.				8.8388	15.3046	.4225
1ZR1 N1.				8.7094	14.8096	.4119
1ZR1 P2.				14.4002	32.0755	.5511
1ZR1SI2.			(1)	15.7650	30.1230	.4766
1FE1 S2.			(2)	9.7117	24.4399	.6026
1CU1FE1.	1 S2 S2.		(3)	19.4235	37.0809	.4762
1FE2 S1.	1AS2 S1.		(3)	22.6850	53.7068	.5776
1CO1AS2.			(3)	12.8706	32.1538	.5997
1AG8SB1.	1AG8SB1.	1 S5 S6.	(3)	142.1182	380.6557	.6266
1AG5SB1.	1 S2 S2.		(3)	48.6023	254.6774	.8092
1CU3AS1.	1 S2 S2.		(3)	27.9294	177.8781	.8430
1PB2 S7.	1PB2 S7.	1FE1SB1.	(3)	87.5083	375.2727	.7668
1PB1CU1.	1SB1 S3.		(3)	28.6774	100.0000	.7132
1AG2FE5.	1 S4 S4.		(4)	55.0204	178.6223	.6920
1BE3 P2.			(5)	12.0457	39.5556	.6955

CHEMICAL FORMULA	SOURCE	VOLUME OF IONS	VOLUME OF FORMULA WEIGHT	OPENNESS RATIO
1CD3 P2.	(5)	27.9189	69.7552	.5998
1FE1 P2.	(5)	10.7513	23.6000	.5444
1FE2AS1.	(5)	12.5447	24.0051	.4774
1FE2SB1.	(5)	14.9968	28.6593	.4767
1FE4 B2.	(5)	18.7370	33.8398	.4463
1ER1 B6.	(5)	17.5050	41.7266	.5805
1AU1AL2.	(5)	15.9176	32.7676	.5142
1MG3 P2.	(5)	25.7419	65.5340	.6072
1MG3AS2.	(5)	27.9638	70.7937	.6050
1MO1AS2.	(5)	14.3477	30.4833	.5293
1ND1 B6.	(5)	18.8694	42.3077	.5540
1CB1 P1.	(-)	9.4237	20.9814	.5509
1PR1 B6.	(5)	19.0741	42.4742	.5509
1AG1 P2.	(5)	12.7800	36.5591	.6504
1AG1 P3.	(5)	16.1363	51.8041	.6885
1TI3 S4.	(5)	28.7452	74.5205	.6143
1TI3 S5.	(5)	31.5817	89.9408	.6489
1TI4 S5.	(5)	37.3814	94.1176	.6028
1SN1SB1.	(5)	13.9882	34.5821	.5955
1ZR3 S5.	(5)	37.2453	105.8537	.6481
1ZR2 S3.	(5)	23.8847	60.3896	.6045
1SI1 N1.	(6)	5.0605	13.2492	.6180
1SI2 N3.	(6)	11.1429	26.9231	.5861
1TI2SI1.	(6)	15.6381	30.8458	.4930
1SN2AS3.	(6)	27.5393	70.4268	.6090
1TH1SI2.	(6)	19.4050	36.1809	.4637
1ZN2 P2. 1 S3 S3.	(6)	33.5819	175.0000	.8081
1ZN2 S1. 1SI2 S1.	(6)	23.6007	73.6070	.6794
1CU3SE2.	(6)	20.1935	62.0996	.6748
1CU1 P1.	(6)	7.3950	18.4825	.5999
1CU2SI1.	(6)	12.1161	22.4638	.4606
1PT1SI1.	(6)	9.4519	19.1745	.5071
1PT2SI1.	(6)	14.8651	30.3623	.5104
1PT3SI2.	(6)	24.3170	45.5319	.4659

CHEMICAL FORMULA	SOURCE	VOLUME OF IONS	VOLUME OF FORMULA WEIGHT	OPENNESS RATIO
1MN5 N2.	(6)	22.2372	45.4955	.5112
1MN6 P2.		30.9449	79.3522	.6100
1MN1SB1.		10.9581	31.6071	.6533
1FE7 S8.		50.9631	140.6522	.6377
1FE2 P3.		18.1464	45.5556	.6017
1FE3 P4.		25.5414	57.9365	.5591
1FE1SI2.		12.1161	20.7407	.4158
1FE2SI1.		12.1161	20.0000	.3942
1FE3SI2.		20.1935	33.4328	.3960
1CO1AS3.		17.3378	41.8262	.5855
1CO1SI1.		7.9747	13.8095	.4225
1NI1 P2.		10.5478	26.1905	.5973
1NI1 P3.		13.9041	36.2768	.6167
1NI1AS2.		12.7696	29.4366	.5662
1NI2AS3.		21.0720	41.4758	.4919
1NI2 S1. 1AS2 S1.		22.2778	52.5397	.5760
1CR1 P1.		7.3950	14.5614	.4921
1CR2AS3.		21.4792	53.0645	.5952
1CR4 C1.		17.3061	32.5926	.4690
1CR1SI2.		12.1161	24.5455	.5064
1MO1SI2.		13.4906	24.9180	.4586
1 W2 C1.		12.2314	23.6613	.4831
1 W1SI2.		13.6175	25.8065	.4723
1 W2SI3.		23.1963	41.4679	.4406
1 U2 C3.		17.8941	45.3901	.6058
1 U1SI2.		15.2976	36.7500	.5837
1CB1 C1.		7.2186	13.4271	.4624
1TA1SI2.		14.1448	26.9536	.4752
1SI1 B6.		11.7852	37.6518	.6870
1ZR3 B4.		28.2271	85.4054	.6695
1FE2 B1.		9.3685	16.6216	.4364
1FE1 B2.		6.6209	15.4000	.5701
1CO2 B1.		9.1632	15.5696	.4115
1NI2 B1.		8.9613	16.0000	.4399
1CR3 B2.	(6)	14.6983	26.5672	.4467

CHEMICAL FORMULA	SOURCE	VOLUME OF IONS	VOLUME OF FORMULA WEIGHT	OPENNESS RATIO
1MO3 B4.	(6)	21.4039	47.2857	.5473
1AL3TI2.	(6)	26.3747	52.8358	.5008
1AL1 B6. 1 B3 B3.	(6)	20.4181	62.8000	.6749
1CA1SI1.	(6)	17.3228	28.9362	.4013
1CA3SI2.	(6)	47.9298	107.3171	.5534
1CA1SI2.	(1)	21.3615	38.4000	.4437
1CA3 P2.	(1)	46.5650	81.2500	.4269
1SR3 P2.	(6)	59.4243	121.2687	.5100
1BA1 H2.	(6)	19.5740	33.0166	.4071
1AL1 N1.	(1)	5.9469	12.5767	.5271
1AS2SE3.	(1)	21.0506	81.4737	.7416
1BA3AS2.	(1)	67.6567	137.0732	.5064
1CD3AS2.	(1)	30.1408	78.4219	.6157
1CR1 N1.	(1)	5.0605	11.1864	.5476
1GA1 N1.	(1)	5.9469	13.7705	.5681
1CU3SB1.	(1)	19.0355	36.6628	.4808
1CU3AS1.	(1)	16.5834	33.2500	.5013
1FE1AS1.	(1)	8.5060	16.7305	.4916
1LI3SB1.	(1)	20.9968	44.6875	.5301
1AL1 P1.	(7)	8.2814	20.3509	.5931
1SB4SE6.	(7)	51.9099	146.3362	.6453
1AS4 S3.	(7)	26.3786	110.0000	.7602
1BI1 S1.	(7)	11.6921	31.2987	.6264
1 B2 C1. 1SI2 C1.	(7)	12.9620	31.6770	.5908
1CD1 S1.	(7)	9.9053	29.8755	.6684
1CE1SI2.	(7)	19.4050	36.2292	.4644
1CE2 S3.	(7)	31.1647	73.7255	.5773
1CE2 S4.	(7)	34.0012	83.4694	.5927
1CR3 C2.	(7)	14.4186	26.9461	.4649
1CR1SE1.	(7)	8.0774	19.4362	.5844
1CR1 S1.	(7)	6.8752	20.4878	.6644
1CR2 S3.	(7)	16.5870	54.0541	.6931
1CO1 S1.	(7)	6.7726	16.3964	.5869
1CO2 S3.	(7)	16.3816	44.5833	.6326
1CO1 S2.	(7)	9.6091	26.0042	.6305

CHEMICAL FORMULA	SOURCE	VOLUME OF IONS	VOLUME OF FORMULA WEIGHT	OPENNESS RATIO
1CO1TE1.	(7)	10.4201	21.1299	.5069
1CU1SE1.		8.0774	21.4393	.6232
1CU2 S1.		10.9139	27.6042	.6046
1DY2 S3.		28.7820	64.7692	.5556
1ER2 S3.		28.0266	71.2397	.6066
1EU1 S1.		14.1641	31.2925	.5474
1GD2 S3.		29.5567	66.5584	.5559
1GA2SE3.		21.9663	76.4228	.7126
1GA2 S3.		18.3597	64.6575	.7160
1GA1TE1.		11.4092	36.2132	.6849
1GA2TE3.		29.3024	93.7163	.6873
1GE1SE1.		8.6176	28.6792	.6995
1GE1SE2.		12.6564	50.6579	.7502
1GE1 S1.		7.4155	31.7221	.7662
1GE1 S2.		10.2520	46.5986	.7800
1GE1TE1.		11.0630	32.2581	.6570
1IN2 S1.		19.8577	44.6337	.5551
1IN1 S1.		11.3471	28.3784	.6002
1IN2 S3.		25.5307	66.6667	.6170
1IN2TE1.		23.5052	55.1777	.5740
1IN1TE1.		14.9946	38.4738	.6103
1IN2TE3.		36.4733	106.4348	.6573
1IR1SE3.		17.1604	53.4162	.6787
1FE1SE1.		8.0774	19.9115	.5943
1FE2SE3.		20.1935	54.7022	.6308
1FE1 S1.		6.8752	18.3716	.6258
1FE2 S3.		16.5870	48.3721	.6571
1FE1 S2.		9.7117	24.4399	.6026
1FE1TE2.		17.0068	38.9724	.5636
1LA2SE3.		36.4592	84.4262	.5682
1LA2SE4.		40.4979	93.9873	.5691
1LA2 S3.		32.8526	76.9547	.5731
1LA2 S4.		35.6891	85.2941	.5816
1PB1SE1.		13.2484	35.3086	.6248
1PB1 S1.	(7)	12.0463	31.4888	.6174

CHEMICAL FORMULA	SOURCE	VOLUME OF IONS	VOLUME OF FORMULA WEIGHT	OPENNESS RATIO
1PB1TE1.	(7)	15.6938	41.0539	.6177
1LI2 S1. 1GA2 S3.		30.5812	94.6309	.6768
1LI2 S1.		12.2214	27.7108	.5590
1LI2TE1.		15.8690	43.5185	.6354
1MG1SE1.		10.3818	24.3499	.5736
1MG1 S1.		9.1796	20.0000	.5410
1MG1TE1.		12.8272	39.3782	.6743
1MN1SE1.		8.0774	23.9714	.6630
1MN1SE2.		12.1161	40.0376	.6974
1MN1 S1.		6.8752	22.1374	.6894
1MN1 S2.		9.7117	34.2939	.7168
1MN1TE2.		17.0068	50.7365	.6648
1HG1 S1.		10.3661	30.2991	.6579
1MO1 S3.		13.9227	48.8136	.7148
1MO2TE3.		30.2786	78.2313	.6130
1MO1TE2.		18.3813	46.1842	.6020
1ND2SE3.		34.3619	78.7106	.5634
1ND2 S3.		30.7553	72.0974	.5734
1NP1SI2.		8.0774	32.4474	.7511
1NI3BI2. 1 S1 S1.		34.8895	77.9621	.5525
1NI1SE1.		7.8738	16.3121	.5173
1NI1SE2.		11.9125	32.4365	.6327
1NI2 S1.		10.5067	26.3251	.6009
1NI2 S3.		16.1798	41.2371	.6076
1NI1 S2.		9.5081	28.0182	.6606
1NI1TE2.		16.8032	40.6736	.5869
1OS1 S2.		10.7173	26.7932	.6000
1PD1 S1.		8.1248	20.7773	.6090
1PD1 S2.		10.9613	35.4037	.6904
1PT1SE2.		13.4906	46.1438	.7076
1PT1SE3.		17.5293	60.4196	.7099
1PT1 S1.		8.2497	22.4752	.6329
1PT1 S2.		11.0862	33.8120	.6721
1PU1SI2.		8.0774	32.3465	.7503
1PU2 S3.	(7)	8.5095	68.2521	.8753

CHEMICAL FORMULA	SOURCE	VOLUME OF IONS	VOLUME OF FORMULA WEIGHT	OPENNESS RATIO
1 K2 S1. 1BI2 S3.	(7)	71.2466	131.3684	.4577
1 K2 S1. 1FE2 S3.		61.6129	119.5489	.4846
1 K2SE1.		46.2281	55.0877	.1608
1 K2 S1.		45.0259	63.2184	.2878
1 K2TE1.		48.6734	81.7460	.4046
1PR2SE3.		34.7713	80.0926	.5659
1PR2SE4.		38.8100	90.0602	.5691
1PR2 S3.		31.1647	72.0000	.5672
1RE1 S2.		10.9613	33.2889	.6707
1RE2 S7.		30.4322	122.5873	.7518
1RH2 S3.		18.3597	47.1875	.6109
1RH1 S2.		10.5981	26.0530	.5932
1RH2 S5.		24.0328	73.2000	.6717
1RB2 S1. 1GA2 S3.		72.0211	128.3626	.4389
1RB2 S1.		53.6614	69.7595	.2308
1RU2 S3.		18.1252	42.9185	.5777
1RU1 S2.		10.4809	26.9919	.6117
1SM2SE3.		35.1857	75.7746	.5357
1SM2 S3.		31.5791	67.8632	.5347
1SI1 S1.		6.8752	32.4324	.7880
1SI1 S2.		9.7117	45.5446	.7868
1AG2 S1. 1SB2 S3.		37.3196	109.7015	.6598
1AG2 S1. 1FE2 S3.		31.5582	99.7812	.6837
1AG2SE1.		16.1734	35.9756	.5504
3AG2 S1. 2SI1 S2.		64.3372	185.9719	.6540
1AG2 S1.		14.9712	33.8798	.5581
1AG2TE1.		18.6188	40.4005	.5391
1NA2 S1. 1BI2 S3.		48.5742	115.3996	.5791
1NA2 S1. 1GA2 S3.		40.7133	109.7902	.6292
1NA2SE1.		23.5558	48.0769	.5100
1NA2 S1.		22.3536	41.9355	.4670
1NA2TE1.		26.0011	60.0000	.5666
1SR1SE1.		21.6093	38.1279	.4332
1SR1 S1.		20.4071	32.4324	.3708
1SR1TE1.	(7)	24.0546	44.5135	.4596

CHEMICAL FORMULA	SOURCE	VOLUME OF IONS	VOLUME OF FORMULA WEIGHT	OPENNESS RATIO
1TA1 S2.	(7)	11.7404	36.1516	.6752
1TA1 S3.		14.5769	48.3421	.6985
1TL2 S1.		21.6171	52.5000	.5882
1TH1 S2.		17.0006	40.9405	.5847
1SN1SE1.		11.1075	32.0388	.6533
1SN1SE2.		15.1462	55.4000	.7266
1SN1 S1.		9.9053	28.9272	.6576
1SN1TE1.		13.5528	38.2716	.6459
1TI1 C1.		6.9509	14.1176	.5076
1TI1SE2.		13.8771	38.9414	.6436
1TI1 S1.		8.6362	19.4175	.5552
1TI2 S3.		20.1090	53.6313	.6251
1TI1 S2.		11.4727	34.7826	.6702
1TI1TE2.		18.7678	48.5577	.6135
1 W1 C1.		6.6913	12.4841	.4640
1 W2 C1.		12.2314	23.6613	.4831
1 W1 P1.		8.8964	17.4797	.4910
1 W1 P2.		12.2527	26.8266	.5433
1 W1 S2.		11.2131	33.0667	.6609
1 W1TE2.		18.5082	46.5042	.6020
1 U1 C1.		8.3714	18.3419	.5436
1 U1 N1.		8.2420	17.5978	.5316
1 U2 N3.		17.5059	46.0854	.6201
1 U3SI1.		25.6994	47.6252	.4604
1 U3SI2.		29.7381	63.1148	.5288
1 U1SI1.		11.2589	25.5769	.5598
1 U1SI2.		15.2976	32.7394	.5327
1 U1 S1.		10.0567	24.8390	.5951
1 U1 S2.		12.8932	38.2278	.6627
1 U1 S3.		15.7298	57.4871	.7264
1 V1 S1.		7.4155	19.3925	.6176
1 V2 S3.		17.6674	42.1277	.5806
1 V2 S5.		23.3404	87.3333	.7327
1YB2SE3.		36.8939	79.5362	.5361
1YB2 S3.	(7)	33.2873	73.4219	.5466

CHEMICAL FORMULA	SOURCE	VOLUME OF IONS	VOLUME OF FORMULA WEIGHT	OPENNESS RATIO
1 Y2SE3.	(7)	33.5579	80.8967	.5852
1 Y2 S3.	(7)	29.9513	71.7277	.5824
1ZN1 S1. 1CR2 S3.	(7)	24.3486	73.5802	.6691
1ZN1SE1.	(7)	8.9638	26.5683	.6626
1ZN1 S1.	(7)	7.7616	23.7745	.6735
1ZN1TE1.	(7)	11.4092	34.8375	.6725
1ZR1 S2.	(7)	13.3606	40.0517	.6664

SOURCES

1. "Handbook of Chemistry and Physics," Charles D. Hodgman, Editor, Chemical Rubber Publishing Co., Cleveland (1953).

2. "Optical Mineralogy," A. F. Rogers and P. F. Kerr, McGraw-Hill, New York (1942).

3. "Dana's Manual of Mineralogy," 15th Edition, John Wiley, New York (1949).

4. "The Microscopic Determination of the Nonopaque Minerals," E. S. Larsen and H. Berman, Second Edition, U. S. Geological Survey Bull. 848 (1934).

5. "Landolt-Börnstein Physikalisch-Chemische Tabellen," Julius Springer, Berlin (1923).

6. "International Critical Tables," E. W. Washburn, Editor, McGraw-Hill, New York (1926).

7. "Data on Chemicals for Ceramic Use," Bull. Nat. Res. Council No. 118, University of Pittsburgh (June, 1949).

APPENDIX B

THE EFFECT OF POROSITY ON THE ELASTIC PROPERTIES OF CERAMICS

The sintering of pure ceramic specimens generally results in densities lower than theoretical unless the particle size, forming pressure, sintering temperature cycle, sintering environment, and other factors affecting final density are carefully controlled and optimized for each new ceramic body. Lowering of density due to the presence of pores also lowers the elastic moduli values. In view of the difficulty of obtaining suitable ceramic specimens having maximum density, it appeared desirable to investigate methods of predicting the elastic properties of bodies having theoretical density from measurements made on specimens with finite porosity.

Mackenzie [59] derived expressions for the bulk modulus (K) and the shear modulus (G) for solids containing spherical isolated pores:

$$K = \frac{4K_o G_o (1-P)}{4G_o + 3K_o P}$$

$$G = G_o (1 - ZP)$$

where $Z = 5\left(\frac{3K_o + 4G_o}{9K_o + 8G_o}\right)$ (Table B-I)

P = volume fraction of pores = $1 - \frac{\rho}{\rho_o}$

Table B-I

DIMENSIONLESS ELASTIC CONSTANT OF OXIDE CERAMICS

(USED IN POROUS BODY COMPUTATIONS)

CERAMIC PHASE	$Z = 5\left[\frac{3K_o + 4G_o}{9K_o + 8G_o}\right]$
CORUNDUM	1.97
MAGNESIUM OXIDE	2.03
SPINEL	2.04
FUSED SILICA	2.02
α- QUARTZ	1.98

Table B-2

SHEAR MODULUS DEPENDENCE ON POROSITY

BASED ON MACKENZIE'S RELATION

POROSITY, P	G/G_o		
	Z = 1.93	Z = 1.98	Z = 2.03
0	1.000	1.000	1.000
5%	0.904	0.901	0.899
10	0.807	0.802	0.797
20	0.614	0.604	0.594
30*	0.423	0.408	0.391

Mackenzie's model consisted of a spherical pore of radius (A_o) surrounded by a spherical shell of solid with radius (r_o) which in turn was surrounded by an equivalent homogenious material having the same properties as the pore and shell combined. His solutions were obtained by expanding the function $\left(\frac{a_o}{r_o}\right)^3$ in a power series. However, the higher power terms (i.e. those above the third power) were neglected in his solution. Coble and Kingery[54] suggested the next term in Mackenzie's shear modulus expression will be of the form AP^2 where the constant (A) may be evaluated by setting $G = 0$ at $P = 1$, thus:

$$G = G_o(1 - ZP + AP^2)$$

$$A = Z - 1$$

and $$G = G_o\left[1 - ZP + (Z-1)P^2\right]$$

Table B-I lists the values of Z computed for several different ceramics. Since Z is approximately two for many ceramics, it can be seen that this term increases the predicted value of shear modulus, slightly, for porous materials over that obtained from Mackenzie's original expression as shown in Figure B-1.

Coble and Kingery[54] found reasonably good agreement between predictions using the latter expression and measurements made on specially prepared low-density alumina bodies as shown in Figure B-1. However, recent data by Lang[47] does not fit either expression. In order to investigate further the effects of Mackenzie's approximate solution, an additional term in the form was added to give

$$G = G_0 (1 - ZP + AP^2 + BP^3)$$

let $G = 0$ at $P = 1$

and $\frac{dG}{dP} = 0$ at $P = 1$

then $A = 2Z - 3$

$$B = 2 - Z$$

$$G = G_0 \left[1 - ZP + (2Z - 3)P^2 + (2 - Z)P^3\right]$$

The effect of the BP^3 term was small and the fit to Lang's data was not improved. Clearly, the finite porosity in Lang's specimens was not of the discontinuous-pore-phase considered by Mackenzie's model. In fact, with the exception of ceramic bodies purposely made low in density by foaming or "burn-out binder" techniques, normal pressing and sintering will not produce isolated spherical pores except in the final stages of sintering where the porosity will be under 5%. Mackenzie's relation involved only the elastic constants of the solid material and the bulk density of the porous solid. Hence it could not distinguish between continuous solid-phase and continuous pore-phase materials.

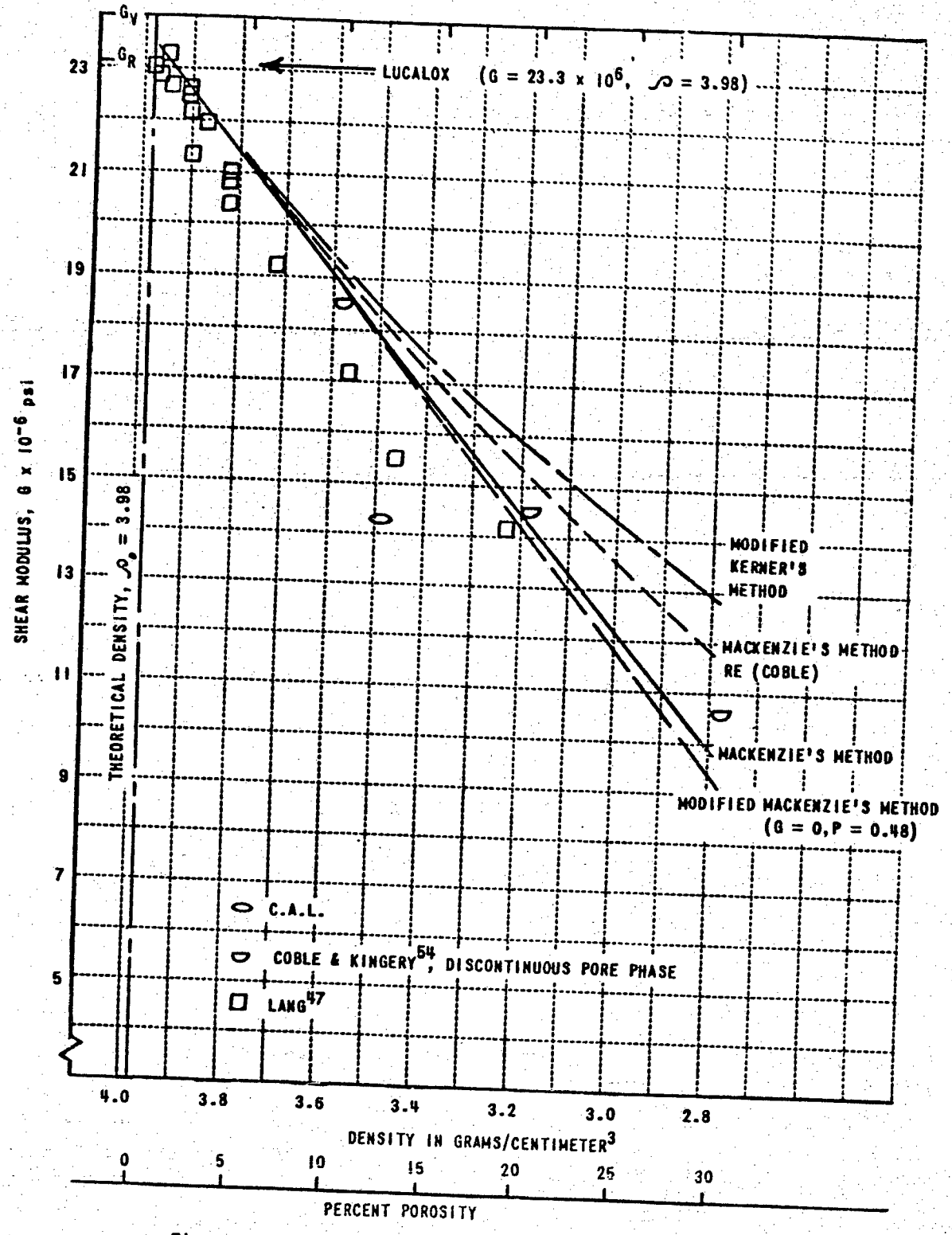

Figure B-1 SHEAR MODULUS OF POROUS ALUMINA

Continuous pore-phase materials could be represented by a simple cubic structure of equal-size spherical grains in which an uncompressed model would have a porosity of 48%. Using $G = 0$ at $P = .48$ for the boundary conditions on Cobles' extension of Mackenzie's relation gives

$$A = 1.35 - 2.09Z$$

and $$G = G_0\left[1 - ZP - (4.35 - 2.09Z)P^2\right]$$

It can be seen that the predicted shear modulus is lowered by these boundary conditions and approaches Lang's data for the continuous pore-phase boundary conditions. Therefore, if the constant A were treated as an empirical constant for continuous pore-phase bodies, Mackenzie's relation could be made to fit the experimental data. In this case, the value of A would be dependent upon the porosity of the unsintered body which is in turn dependent upon the particle size, the particle size distribution, the particle shape, the forming pressure, the percent binder and perhaps other experimental factors. Another approach to the porous body problem was made by extension of relations derived by Kerner for elastic moduli of composite bodies. Kerner derived an expression for the shear modulus of composite materials (G_0) contained within a "suspending fluid" (subscript 1) as

$$G_0 = G_1\left[\frac{\sum' \frac{G_i V_i}{(7-5\nu_1)G_1 + (8-10\nu_1)G_i} + \frac{V_1}{15(1-\nu_1)}}{\sum' \frac{G_1 V_i}{(7-5\nu_1)G_1 + (8-10\nu_1)G_i} + \frac{V_1}{15(1-\nu_1)}}\right]$$

By considering a porous body as composed of a porous phase (subscript 2) and a solid phase (subscripts $i \neq 2$), Kerner's equation may be used to derive an expression for porous solids. For a porous single-phase solid

($G_2 = 0$) and the shear modulus becomes:

$$G_p = G_1 \left[\frac{\frac{V_1}{15(1-\nu_1)}}{\frac{G_1 V_2}{(7-5\nu_1)G_1} + \frac{V_1}{15(1-\nu_1)}} \right]$$

For comparison with Mackenzie's expression, this equation may be written in terms of the bulk modulus (K_o) and shear modulus (G_o) of the fully-dense body. Collecting terms and substitution of

$$Z = 5\left(\frac{3K_o + 4G_o}{9K_o + 8G_o}\right)$$

gives

$$G = G_o\left[\frac{1-P}{PZ + (1-P)}\right].$$

Figure B-1 illustrates the dependence of shear modulus upon porosity in alumina ceramics according to the two approaches. The later expression is labeled "Modified Kerner's Method" although he did not imply applicability of his method to the porous body case.

Following a similar line of reasoning, the bulk modulus for porous single-phase materials as derived from Kerner's expression becomes:

$$K = \frac{4G_oK_o(1-P)}{4G_o + 3K_oP}$$

Young's modulus for a porous single-phase materials was derived from the expressions for bulk modulus and shear modulus and their isotropic interrelationship:

$$Y = \frac{9KG}{3K+G}$$

Young's modulus for porous media based upon Kerner's expressions becomes:

$$Y = \frac{G_0(1-P)}{\frac{G_0}{Y_0} + \frac{ZP}{3} - \frac{P}{4}}$$

Based upon Mackenzie's expressions, Young's modulus becomes:

$$Y = \frac{G_0(1-P)(1-ZP)}{\left(\frac{G_0}{Y_0} + \frac{ZP}{3} - \frac{P}{4}\right) - \left(\frac{ZPG_0}{Y_0} + \frac{ZP^2}{12}\right)}$$

A comparison of these two expressions for the case of porous alumina is shown in Figure B-2. The deviation of Mackenzie's relation from the empirical data of Coble and Kingery[54] above 30 percent porosity is probably due the higher order terms which Mackenzie neglected during his series expansion. As Mackenzie noted, his relations are valid only for small porosity.

For the application of Kerner's equations, the pore phase was considered as a simple mixture within the solid phase without regard to pore geometry. It might have been expected that such an approach would not correlate well with empirical data indicated in Figures B-1 and B-2.

The successful prediction of elastic properties of fully-dense ceramic bodies from single crystal data described in Appendix C, postponed attempts to improve the porous-body model by including terms dependent upon pore geometry. Present equations are reasonably valid for porosities of five percent or less porosity.

Young's modulus and shear modulus for porous magnesia, spinel, mullite, and thoria are illustrated in Figure B-3 through B-8. For the examples of alumina, magnesia and spinel, values of Young's modulus Y_V and Y_R and shear modulus G_V and G_R for the fully-dense ceramic body as derived from single crystal elastic constants are plotted along the ordinate. In each instance, the extrapolated porous-ceramic value lies between the two values computed from single crystal constants. This demonstrates a good correlation between two independent methods for predicting elastic properties of fully-dense single-phase ceramic bodies. The use of single crystal elastic constants is described in Appendix C.

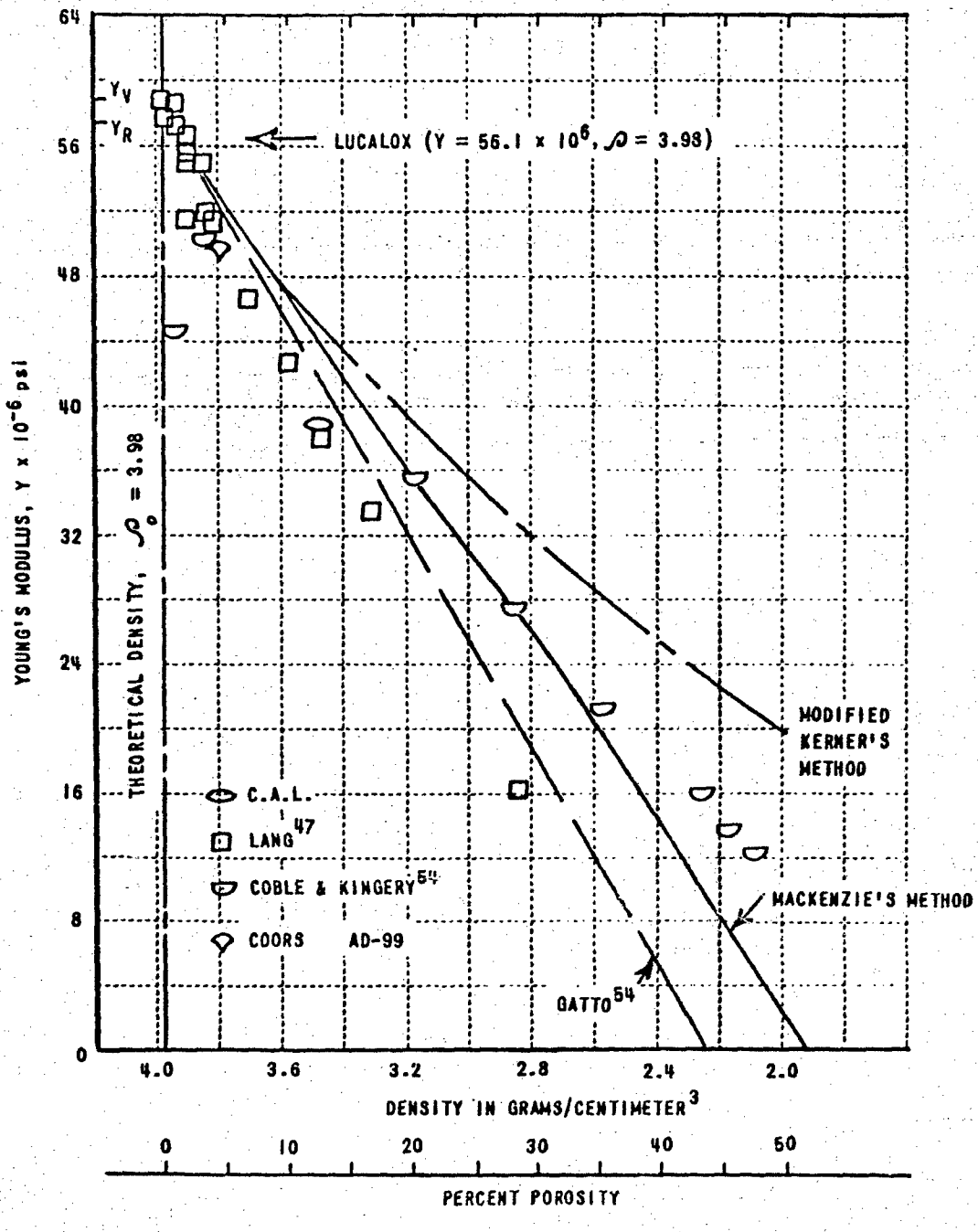

Figure B-2 YOUNG'S MODULUS OF POROUS ALUMINA

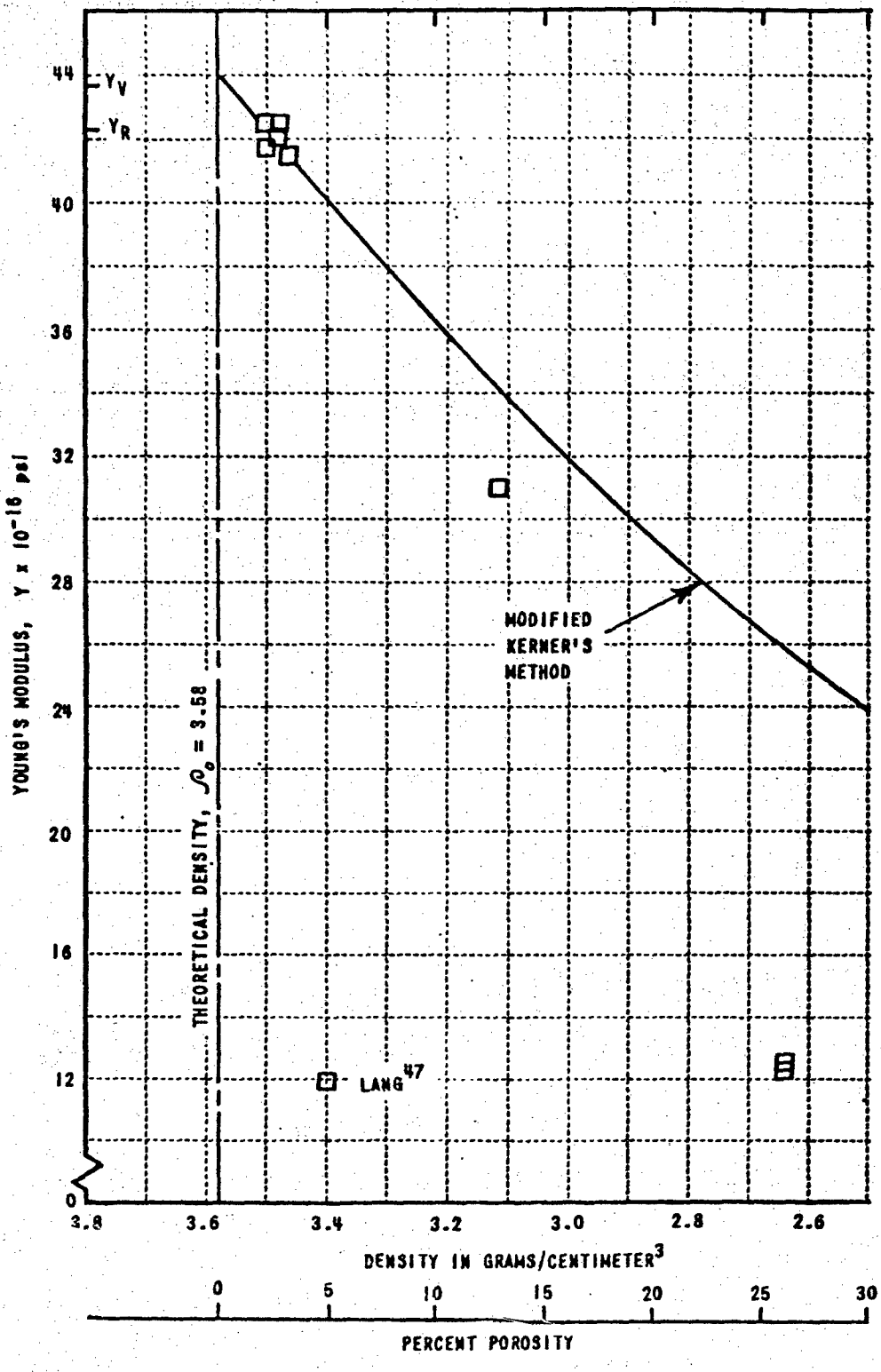

Figure B-3 YOUNG'S MODULUS OF POROUS MAGNESIA

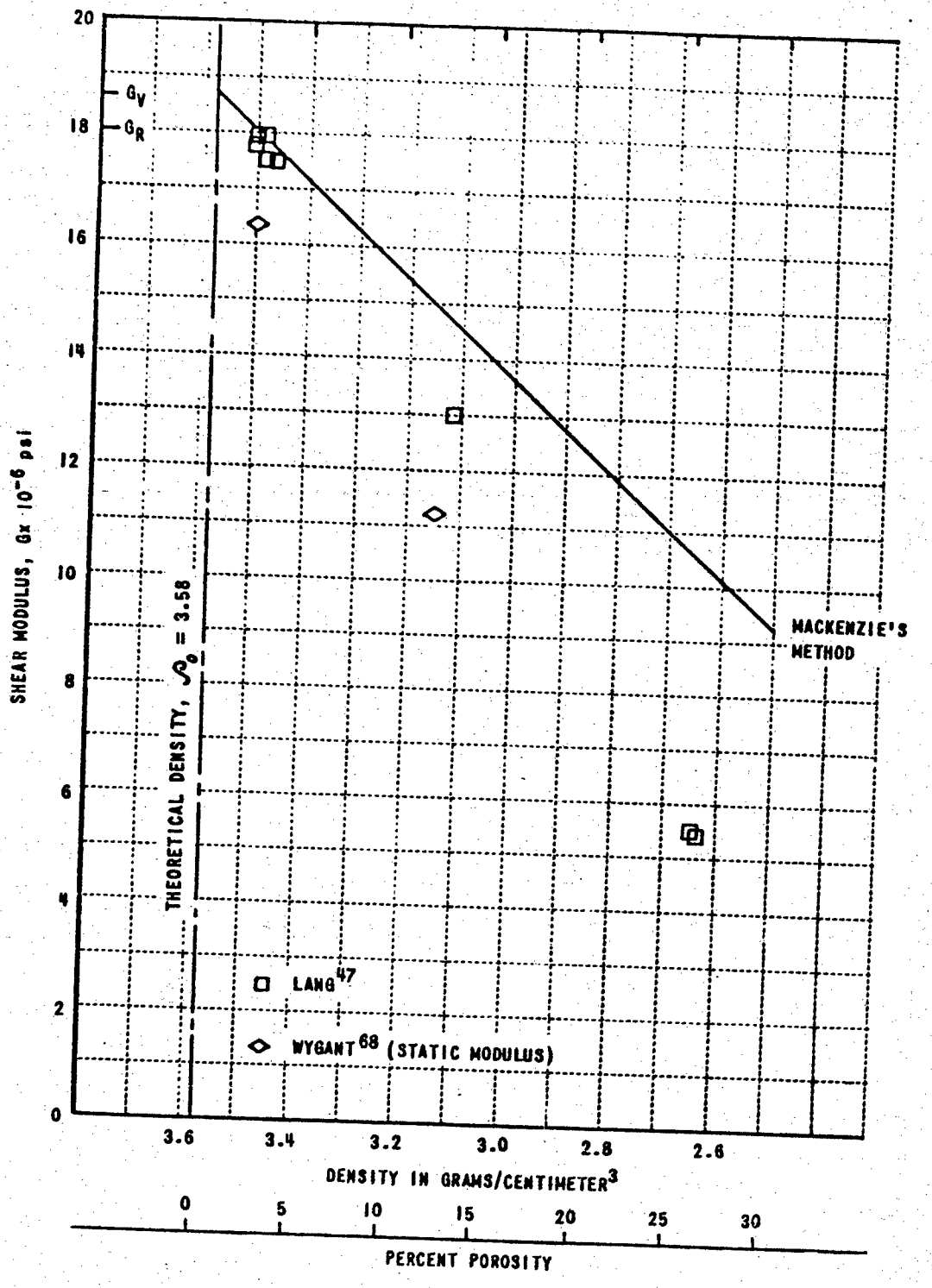

Figure B-4 SHEAR MODULUS OF POROUS MAGNESIA

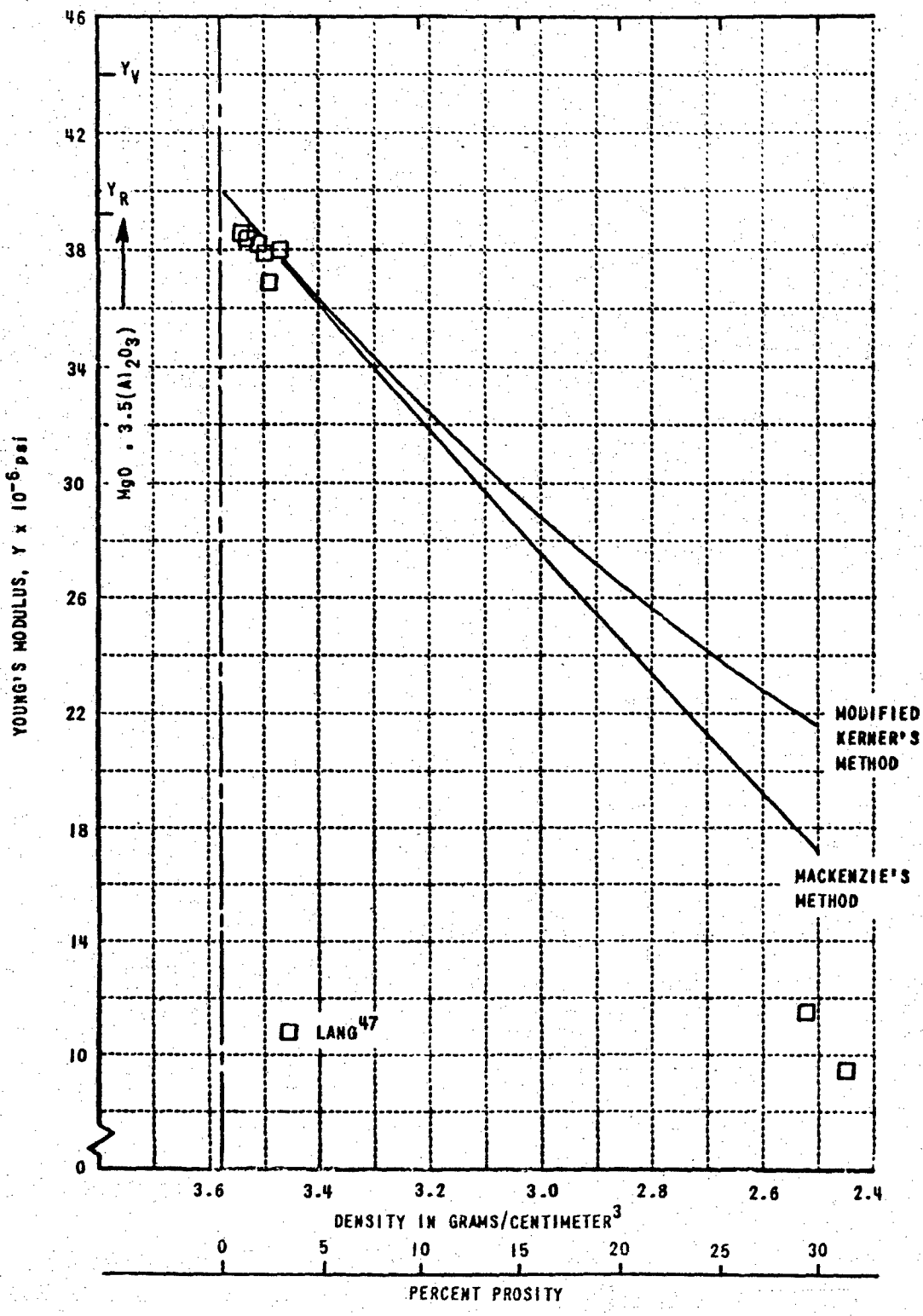

Figure B-5 YOUNG'S MODULUS OF POROUS SPINEL (MgO · Al_2O_3)

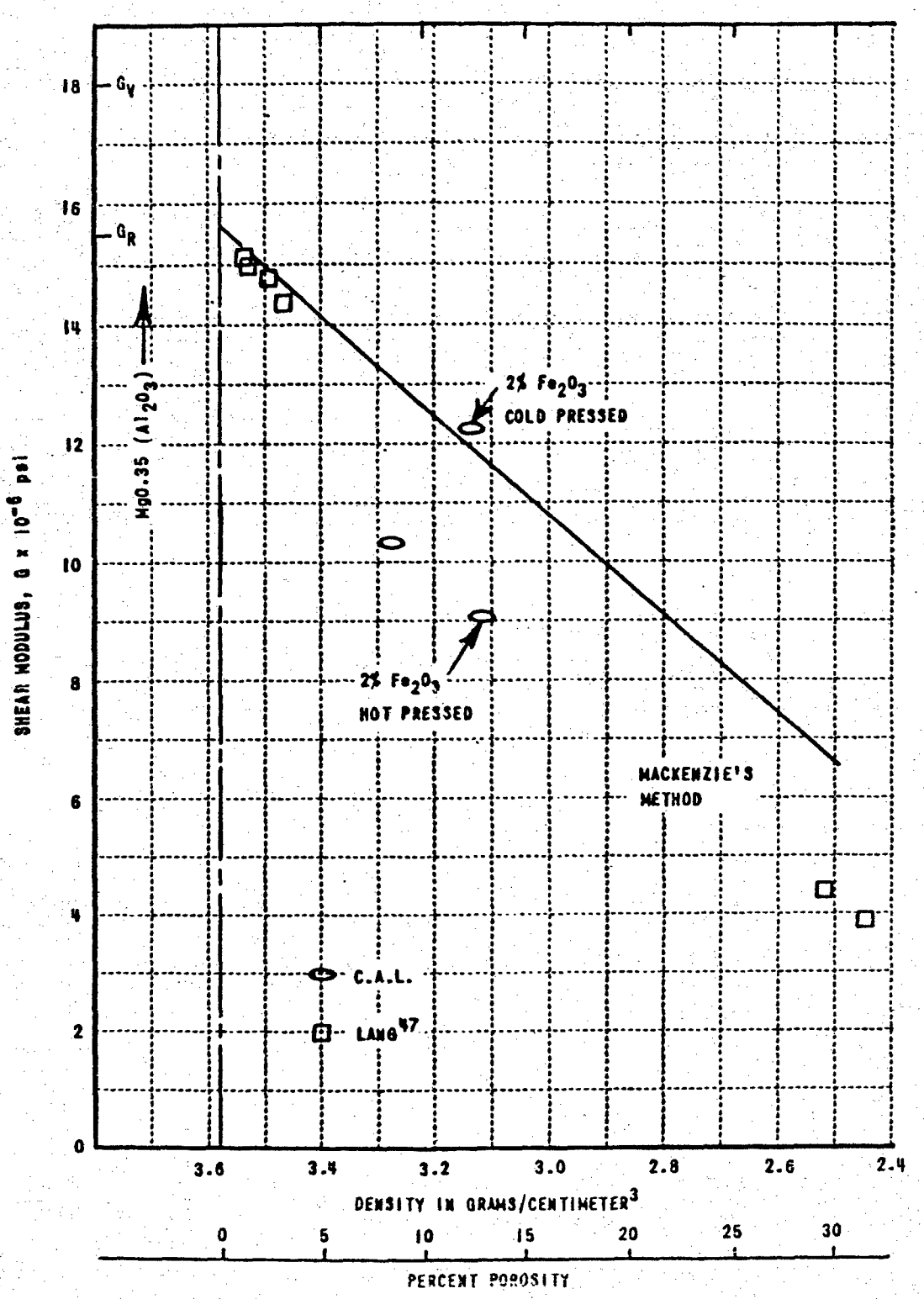

Figure B-6 SHEAR MODULUS OF POROUS SPINEL (MgO • Al_2O_3)

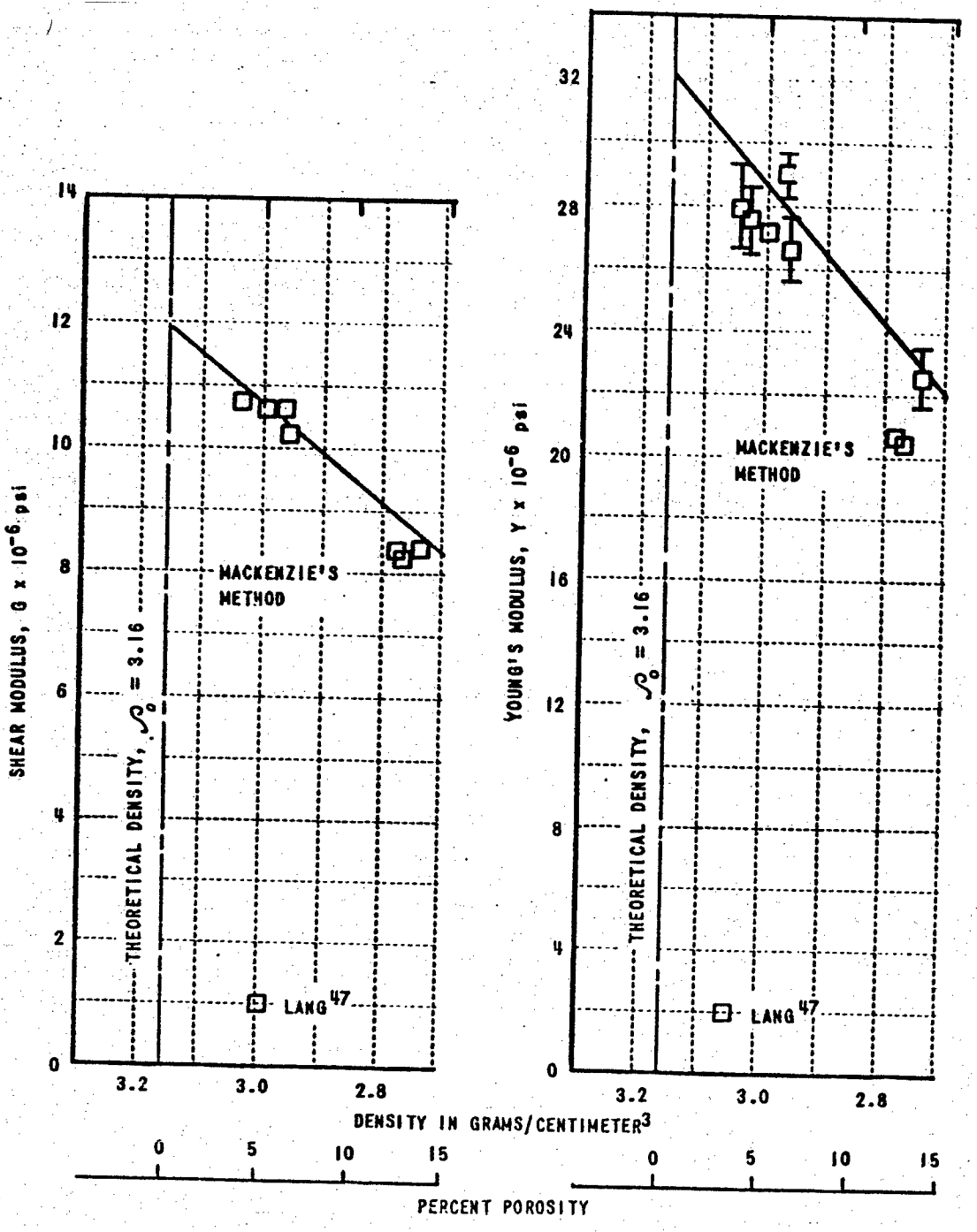

Figure B-7 ELASTIC MODULI OF POROUS MULLITE

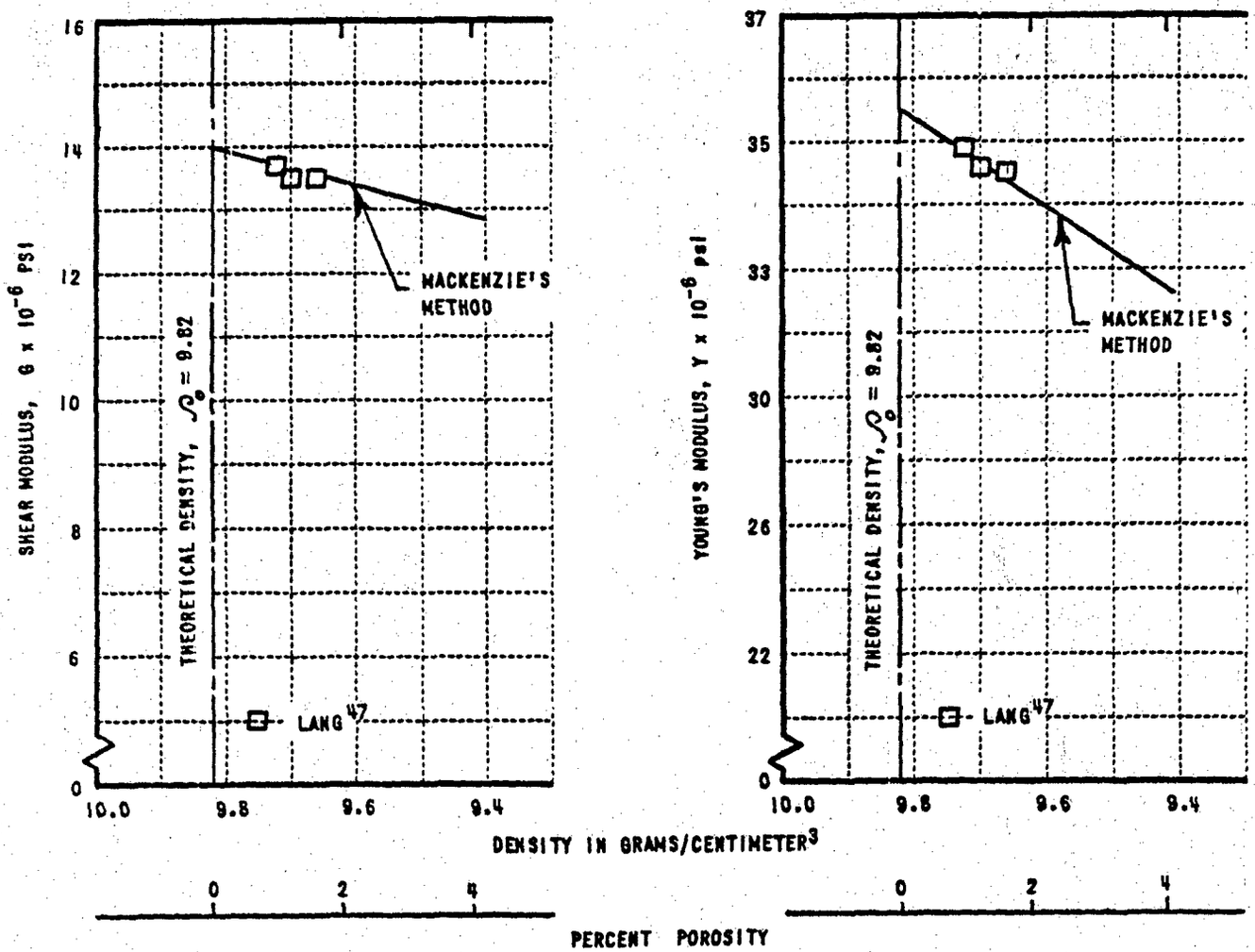

Figure B-8 ELASTIC MODULI OF POROUS THORIA (ThO_2)

Kerner's formula may also be extended to the case of porous multiple-phase ceramic bodies. For example, the bulk modulus for a porous two-phase ceramic would be given by:

$$K_o = \frac{\frac{K_1 P_1}{\rho_1(3K_1+4G_1)} + \frac{K_2 P_2}{\rho_2(3K_2+4G_1)}}{\frac{P_1}{\rho_1(3K_1+4G_1)} + \frac{P_2}{\rho_2(3K_2+4G_1)} + \frac{V_3}{4G_1}}$$

where V_3 = volume fraction of pores = porosity

subscript 1 refers to the basic matrix into which phase 2 material is added.

Application of this expression to the aluminum-silica system was illustrated at the top of Figure 24. In this system, an increase in porosity for any composition results in a decrease of the composite bulk modulus as might be expected. However, the mixture of phases with different compressibilities necessarily introduces shear stresses between the particles during compression of the composite if the mixture has been sintered or otherwise bonded together. In some systems the presence of finite porosity will not cause a monotonic decrease in the composite bulk modulus because of the independent effects of porosity upon the large-scale shear modulus. The Pyrex-spinel system, for example, has a compositional range in which small porosity produces a slight increase in the bulk modulus (Figure B-9). This rather surprising result serves to illustrate the importance of including shear stresses in any model designed to describe the thermoelastic properties of composite media. It also provides further evidence that Kerner's method for predicting thermal expansion of composite media should be superior to Turner's method in which shear stresses were neglected.

Alternatively, the bulk modulus of a porous composite body might have been computed in two steps. First, the bulk modulus of the solid composite could be computed from Kerner's equation. Then Mackenzie's relation could be applied to the composite bulk modulus to obtain the values for finite porosity. However, Mackenzie's relation always predicts a lowering of the

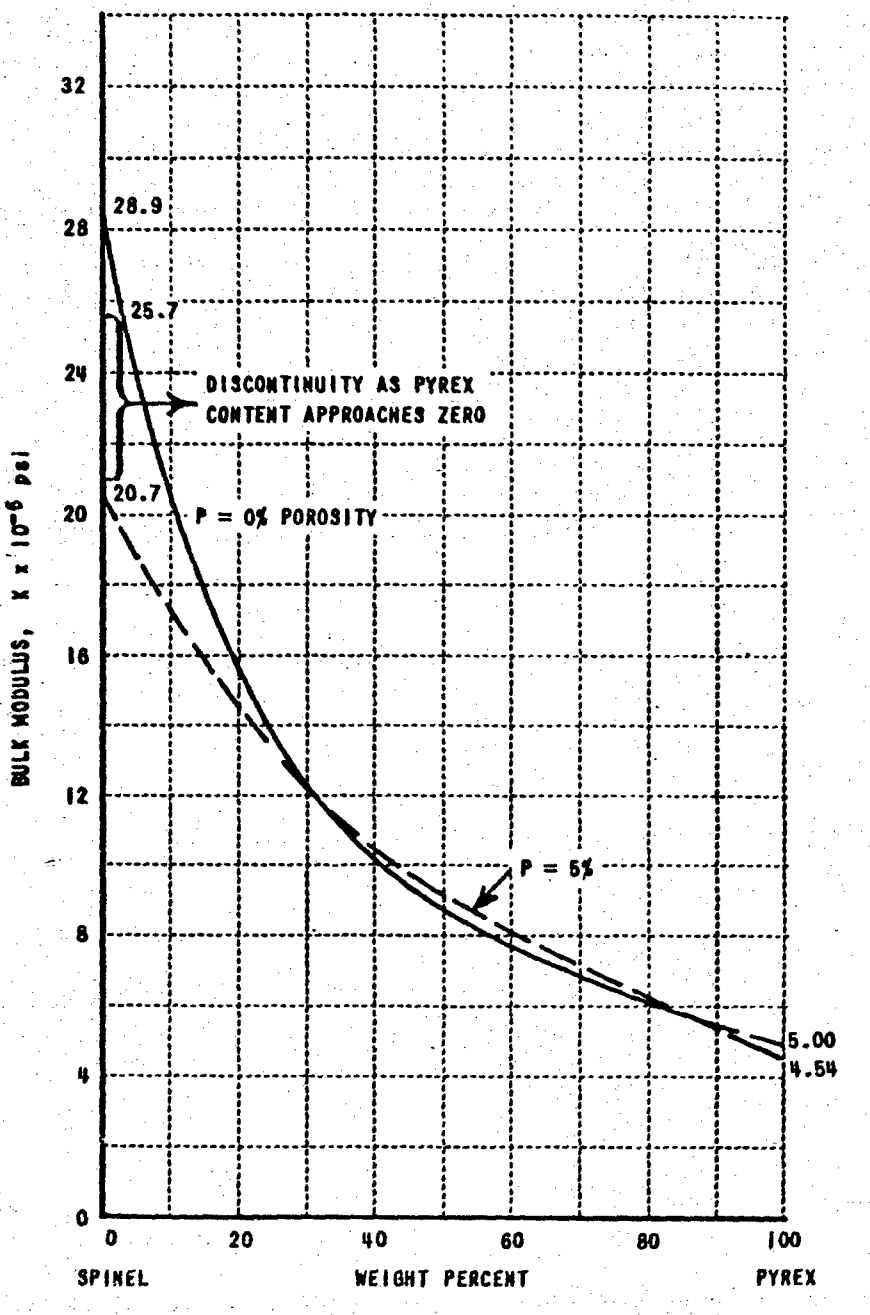

Figure 8-9 BULK MODULUS OF PYREX-SPINEL MIXTURES

moduli due to the presence of pores. Internal stresses arising from the dissimilar thermoelastic properties of the several phases would have to remain constant with increasing porosity if this approach were valid. But in the limit of high porosity, the internal stresses approach zero. Hence, Mackenzie's relation cannot be correctly applied to multiple-phase ceramics or composite bodies.

APPENDIX C

RELATIONSHIPS BETWEEN SINGLE CRYSTAL AND POLYCRYSTALLINE ELASTIC CONSTANTS INCLUDING DATA FOR SEVERAL CERAMIC PHASES

The elastic properties of fully-dense polycrystalline bodies which are macroscopically isotropic can be predicted from the elastic constants for single crystals of each of the phases present by the use of appropriate space averaging techniques. Space averaging presumes random orientation of the grains. The validity of the random grain orientation equations will be greatest if neither the particle shape nor the forming technique induce significant amounts of preferred orientation. Voigt took the stiffnesses of the aggregate to be the space average of the compliances of the single crystal. Alternatively, Reuss took the compliances of the aggregate to be the space average of the compliances of the single crystal. These two approaches are equivalent to assuming uniform strain and uniform stress respectively, for each spherical grain in the polycrystalline body. While neither condition will exist in a real body, these approaches are valuable in that they define the two extreme cases. Empirical data for polycrystalline metallic elements generally lie between these extremes according to data tabulated by Hearmon[56]. Similar results have been found for single-phase polycrystalline ceramics during the course of this study.

Hooke's law states that stress (σ) is proportional to strain (S) for sufficiently small strains. The generalized statement for an anisotropic medium may be taken as

$$\sigma_i = \sum_{j=1}^{6} C_{ij} S_j$$

where C_{ij} = elastic stiffness constants or the moduli of elasticity. Alternatively, the relation may be written in terms of the elastic compliance constants (s_{ij}) where

$$S_i = \sum_{j=1}^{6} s_{ij} \sigma_j$$

In general,

$$C_{ij} \neq \frac{1}{s_{ij}}$$

The elastic stiffness and complaince constants obtained with these relations hold for a rectangular coordinate system with one preferred crystallographic orientation. Table C-I lists reported values for oxide crystals. If the elastic constants for a more general direction are desired, equations for rotated elastic constants must be used. Hearmons[56] has tabulated the 126 equations required for the most general case. By integration of the equation for rotated elastic constants over all space, i.e.

$$\int_0^{2\pi}\int_0^{2\pi}\int_0^{2\pi} F(\phi,\psi,\theta)\, d\phi\, d\psi\, d\theta$$

the space averaged value will be obtained. This was done by Hearmon who gives Voigt's results in terms of the elastic stiffness constants as

$$\overline{C}_{11} = \frac{1}{5}(3A + 2B + 4C)$$

$$\overline{C}_{12} = \frac{1}{5}(A + 4B - 2C)$$

$$\overline{C}_{44} = \frac{1}{5}(A - B + 3C)$$

where

$$3A = C_{11} + C_{22} + C_{33}$$

$$3B = C_{12} + C_{23} + C_{31}$$

$$3C = C_{44} + C_{55} + C_{66}$$

and the overline represents an average value. Since space averaged values are macroscopically isotropic, the isotropic constants, Young's modulus (Y), modulus of rigidity (G) and bulk modulus (K) may be derived in terms of

Table C-I
ELASTIC CONSTANTS OF OXIDE-CERAMIC SINGLE CRYSTALS

		ELASTIC STIFFNESS, 10^{11} DYNES/Cm^2						ELASTIC COMPLIANCE, 10^{-12} Cm^2/DYNE						
SYMBOL	MATERIAL	C_{11}	C_{33}	C_{44}	C_{12}	C_{13}	C_{14}	S_{11}	S_{33}	S_{44}	S_{12}	S_{13}	S_{44}	REF.
CUBIC SYSTEM														
Cr_2FeO_4	CHROMITE	32.3	-	11.7	14.4	-	-	0.427	-	0.856	-0.131	-	-	72
Fe_3O_4	MAGNETITE	27.3	-	9.7	10.6	-	-	0.47	-	1.03	-0.131	-	-	72
MgO	MAGNESIA	28.6	-	14.8	8.7	-	-	0.408	-	0.676	-0.095	-	-	72
$MgO.3.5Al_2O_3$	SPINEL	30.05	-	15.86	15.37	-	-	0.509	-	0.631	-0.172	-	-	55
HEXAGONAL SYSTEM														
$BaTiO_3$	BARIUM TITANATE	16.8	18.9	5.46	7.82	7.10	-	0.818	0.676	1.83	-0.298	-0.195	-	72
TRIGONAL SYSTEM														
Al_2O_3	CORUNDUM	46.5	56.3	23.3	12.4	11.7	10.1	0.290	0.194	0.578	-0.105	-0.038	-0.171	72
$CaCO_3$	CALCITE	13.7	8.01	3.42	4.40	4.50	-2.03	1.10	1.73	3.94	-0.34	-0.43	0.86	72
Fe_2O_3	HEMATITE	24.2	22.8	8.5	5.5	1.6	-1.3	0.442	0.444	1.192	-0.102	-0.023	0.080	72
SiO_2	α-QUARTZ	8.76	10.68	5.72	0.607	1.33	1.73	1.236	0.972	2.002	-0.168	-0.138	-0.424	72
TETRAGONAL SYSTEM							C_{66}							
$BaTiO_3$	BARIUM TITANATE	28.3	17.8	8.05	18.7	14.2	11.3	0.725	1.08	1.24	-0.315	-0.326	0.884	72
$ZrSiO_4$	ZIRCON	7.35	4.60	1.38	0.90	-0.54	1.60	1.39	2.21	7.2	-0.16	-0.14	6.2	72
TiO_2	RUTILE	27.3	48.4	12.5	17.6	14.9	19.4	0.655	0.259	0.800	-0.376	-0.086	0.516	72

the elastic stiffness constants as given by Hearmon:

$$E_V = \frac{(A-B+3C)(A+2B)}{2A+3B+C}$$

$$G_V = \frac{A-B+3C}{5}$$

$$K_V = \frac{A+2B}{3}$$

where the suffix v denotes the Voigt moduli. Similarly, Hearmon derived the expressions based on the Reuss approach as

$$K_R = \frac{1}{3A'+6B'}$$

$$G_R = \frac{5}{4A'-4B'+3C'}$$

$$E_R = \frac{5}{3A'+2B'+C'}$$

where

$$3A' = s_{11} + s_{22} + s_{33}$$

$$3B' = s_{23} + s_{31} + s_{12}$$

$$3C' = s_{44} + s_{55} + s_{66}$$

Comparison of Young's modulus or shear modulus as computed by the Voigt and Reuss techniques provides a measure of the elastic anisotropy of the single crystal. For elastically isotropic bodies, Voigt's approach and Reuss' approach will give identical values.

For a cubic crystal such as MgO, only three independent elastic stiffness or compliance constants appear

$$C_{11} = C_{22} = C_{33} = 28.6 \times 10^{11} \text{ dynes/cm}^2$$

$$C_{23} = C_{31} = C_{12} = 8.7 \times 10^{11} \text{ dynes/cm}^2$$

$$C_{44} = C_{55} = C_{66} = 14.8 \times 10^{11} \text{ dynes/cm}^2$$

Hence, $K_V = \frac{C_{11} + 2C_{12}}{3} = 22.2 \times 10^6 \text{ psi}$

and $S_{11} = S_{22} = S_{33} = 4.08 \times 10^{-13} \text{ cm}^2/\text{dyne}$

$S_{23} = S_{31} = S_{12} = -0.95 \times 10^{-13} \text{ cm}^2/\text{dyne}$

$S_{44} = S_{55} = S_{66} = 6.76 \times 10^{-13} \text{ cm}^2/\text{dyne}$

$K_R = \frac{1}{3S_{11} + 6S_{12}} = 22.2 \times 10^6 \text{ psi}$

In a cubic system,

$$C_{11} + 2C_{12} = \frac{1}{S_{11} + 2S_{12}}$$

and hence the bulk moduli (K_V and K_R) will be equal for all cubic crystals. Computation of both K_V and K_R for cubic crystals provides a measure of the consistency of the reported values of elastic stiffness (C_{ij}) and (s_{ij}).

Birch[45] has applied these space averaging techniques to several ceramic crystals to obtain the compressional wave and shear wave velocities for polycrystalline bodies. For example, the shear modulus (G) for polycrystalline corundum (Al_2O_3) computed from Birch's space averaged data are:

(Voigt) = 24.0×10^6 psi

(Reuss) = 23.2×10^6 psi

Lang[47] has measured the dynamic shear modulus of a series of alumina ceramic bars with varying densities. Extrapolation of his data to theoretical density ($\rho = 3.98$ g/cm^3) gives an experimental value of 23.5×10^6 psi for the shear modulus which lies between the two predicted values. Birch[45] has

tabulated similar data for eleven other mineral or synthetic crystals. These data have been used to compute the elastic properties of fully dense ceramics listed in Table XV. However, it is to be noted that several of the ceramic phases of interest in studies of thermal expansion, internal stress due to thermal expansion anisotropy, tensile strength of multiphase ceramics and other ceramic properties have no single crystal elastic constant data reported in the literature.

APPENDIX D

REFERENCES

1. G. R. Rigby, "X Reversible Thermal Expansion From Theoretical Considerations," Trans. Brit. Ceram. Soc. 50, 175-83 (1951).
2. H. T. Smyth, "Thermal Expansion of Vitreous Silica," J. Am. Ceram. Soc. 38 (4) 140-141 (1955).
3. M. Blackman, "On Negative Volume Expansion Coefficients," Phil. Mag. 3, 8th Series, 831-838 (1958).
4. D. F. Gibbons, "Thermal Expansion of Some Crystals with the Diamond Structure," Phys. Rev. 112 (1) 136-140 (Oct. 1, 1958).
5. H. P. Kirchner, "A Preliminary Study of the Thermal Expansion of Ceramics," Cornell Aeronautical Laboratory Report No. PI-1216-M-1 (August 1, 1958).
6. L. Pauling, "The Nature of the Chemical Bond," 3rd Ed., Cornell University Press (1960).
7. S. Ganesan, "Thermal Expansion of Sodium Chlorate and Bromate," J. Indian Inst. Sci. 41 (1) Sections A and B 9-15 (1959).
8. E. Gruneisen, "The State of a Solid Body," Handbuch der Phys. 10, 1-52 (1926) Jules Springer (Berlin); NASA Republication RE-2-18-59W (Feb., 1959).
9. T. A. Kontorova, "Thermal Expansion and Thermal Conductivity of Some Crystals," Soviet Phys. 1 (9) 1959-1969 (Sept., 1957), Erglish Translation Volume.
10. L. Cartz, "Thermal Vibrations of Atoms in Cubic Crystals II: The Amplitude of Atomic Vibrations," Proc. Phys. Soc. (London) B 68, 957-967 (1955).
11. G. Borelius, "On the Connection Between the Thermal Expansion and Potential Energy in Solids and Liquids," Arkiv Fysik 11, 217-27 (1956).
12. S. Kumar, "Thermal Expansion of Simple Ionic Crystals," Proc. Nat. Inst. of Sci. of India, 25A(6) 364-372 (1959).

13. S. Kumar, "Thermal Expansion of Oxides," Central Glass and Ceramic Res. Inst. Bull. 7 (2) 58-69 (1960).

14. H. P. Kirchner, "Investigation of the Theoretical and Practical Aspects of the Thermal Expansion of Ceramic Materials," Cornell Aeronautical Laboratory Report No. PI-1273-M-3, Contract No. NOrd-18419 (May, 1959).

15. D. E. Harrison and F. A. Hummel, "High Temperature Zirconium Phosphates," J. Am. Ceram. Soc. 37 (6) 277 (1954).

16. D. E. Harrison and F. A. Hummel, "Reactions in the System TiO_2-P_2O_5," J. Am. Ceram. Soc. 42 (10) 487 (1959).

17. H. W. G. Wyckoff, "Crystal Structures," Vol. III, Interscience Publishers, Inc., New York (1953).

18. F. A. Hummel, "Observations on the Thermal Expansion of Crystalline and Glassy Substances," J. Am. Ceram. Soc. 33, 102-107 (1950).

19. J. B. Austin, "Thermal Expansion of Nonmetallic Crystals," J. Am. Ceram. Soc. 35 (10) 243-253 (1952).

20. H. D. Megaw, "The Thermal Expansion of Crystals in Relation to Their Structure," Z. Krist. 100, 56-76 (1938).

21. K. M. Merz, "Investigation of the Theoretical and Practical Aspects of the Thermal Expansion of Ceramic Materials," Cornell Aeronautical Laboratory Report No. PI-1273-M-5, Contract No. NOrd-18419 (December, 1959).

22. K. M. Merz, H. P. Kirchner and H. T. Smyth, "Investigation of the Theoretical and Practical Aspects of the Thermal Expansion of Ceramic Materials," Cornell Aeronautical Laboratory Report No. PI-1273-M-8, Contract No. NOrd-18419 (September 30, 1960).

23. J. E. Mayer and M. G. Mayer, "Statistical Mechanics," John Wiley and Sons, New York (1940).

24. N. R. Thielke, "Refractory Materials for Use in High Temperature Areas of Aircraft," WADC Technical Report 53-9, The Pennsylvania State College (January, 1953).

25. W. A. Weyl, "An Interpretation of the Thermal Expansion of the Alkali Halides and of the Structural Changes Occurring in Glass Under High Pressure," Central Glass and Ceramic Res. Inst. Bulletin (India) 6 (4) 147-74 (1959).

26. R. J. Beals and R. L. Cook, "Directional Dilatation of Crystal Lattices at Elevated Temperatures," J. Am. Ceram. Soc. 40, 279-84 (1957).

27. F. H. Gillery and E. A. Bush, "Thermal Contraction of β-Eucryptite ($Li_2O \cdot Al_2O_3 \cdot 2SiO_2$) by X-ray and Dilatometer Methods," J. Am. Ceram. Soc. 42, 175 (1957).

28. F. R. Charvat and W. D. Kingery, "Thermal Conductivity: XIII, Effect of Microstructure on Conductivity of Single-Phase Ceramics," J. Am. Ceram. Soc. 40, 306-15 (September, 1957).

29. G. R. Rigby, G. H. B. Lovell and A. T. Green, "The Reversible Thermal Expansion and Other Properties of Some Calcium Ferrous Silicates," Trans. Brit. Ceram. Soc. 44, 37-52 (1945).

30. S. Kozu and J. J. Ueda, "Thermal Expansion of Plagioclase," Proc. Imp. Acad. Tokyo 9, 262-4 (1933).

31. S. Kozu and J. J. Ueda, "Thermal Expansion of Diopside," Proc. Imp. Acad. Tokyo 7, 317-319 (1933).

32. R. W. Ricker and F. A. Hummel, "Reactions in the System TiO_2-SiO_2; Revision of the Phase Diagram," J. Am. Ceram. Soc. 34, 271-9 (1951).

33. R. S. Roth and L. W. Coughanour, "Phase Equilibrium Relations in the Systems Titania-Niobia and Zirconia-Niobia," J. Res. Nat. Bur. Stds. 55, 209 (1955).

34. L. W. Coughanour, R. S. Roth and S. Marzullo, "Solid-State Reactions and Dielectric Properties in the System Magnesia-Lime-Tin Oxide-Titania," J. Res. Nat. Bur. Stds. 54, 149, R. P. 2576 (1955).

35. F. H. Brown and P. Duwez, "The Zirconia-Titania System," J. Am. Ceram. Soc. 37, 129-32 (1954).

36. S. M. Lang, C. L. Fillmore and L. J. Maxwell, "The System Beryllia-Alumina-Titania: Phase Relations and General Physical Properties of Three-Component Porcelains," J. Res. Nat. Bur. Stds., 48, 298, R. P. 2316 (1952).

37. G. H. Johnson, "Influence of Impurities on Electrical Conductivity of Rutile," J. Am. Ceram. Soc., 36, 97-101 (1953).

38. P. W. Selwood, "Magnetochemistry," Second Edition, Interscience Publishers, Inc., New York (1956).

39. H. J. Gerritsen and H. R. Lewis, "Paramagnetic Resonance of V^{4+} in TiO_2," Phys. Rev. 119, 1010-2 (1960).

40. F. A. Mauer and L. H. Bolz, "Measurement of Thermal Expansion of Cermet Components by High Temperature X-ray diffraction," WADC TR-55-473, Supplement 1 (June, 1957).

41. J. Jaffray and J. Vilateau, "Sur l'analyse thermique et la dilatometrie du sesquioxide de chrome," Compteo Rendus (Paris) 226 (21) 1701 (May 24, 1948).

42. S. Greenwald, "Changes in Lattice Constants of Cr_2O_3 Near the Curie Temperature," Nature 4270 , 379 (September 1, 1951).

43. D. C. Cronemeyer, "Electrical and Optical Properties of Rutile Single Crystals," M. I. T. Laboratory for Insulation Research, Technical Report No. 46 ATI 118352 (August, 1951).

44. H. Kolsky, "Stress Waves in Solids," Oxford at the Clarendon Press, (1953).

45. F. Birch, "The Velocity of Compressional Waves in Rocks to 10 Kilobars, Part 2," J. Geophys. Res., 66, pp. 2199-2224 (July, 1961).

46. H. J. McSkimin, "Use of High Frequency Ultrasound for Determining the Elastic Moduli of Small Specimens," IRE Trans. Ultrasonics Engr., PGUE-5, p. 29-43 (August, 1957).

47. S. M. Lang, "Properties of High-Temperature Ceramics and Cermets - Elasticity and Density at Room Temperature," NBS Monograph 6 (March, 1960).

48. W. P. Mason, "Piezoelectric Crystals and Their Applications to Ultrasonics," D. Van Nostrand Co., New York (1950).

49. G. L. Vick and L. E. Hollander, "Ultrasonic Measurement of the Elastic Moduli of Rutile," J. Acoustical Soc. Am., 32, 947-49 (August, 1960).

50. C. M. Zener, "Elasticity and Anelasticity of Metals," The University of Chicago Press (1956).

51. H. A. Scheetz, "An Investigation of the Theoretical and Practical Aspects of the Thermal Expansion of Ceramic Materials," Cornell Aeronautical Laboratory Report No. PI-1273-M-11 (November, 1961).

52. P. S. Turner, "Thermal Expansion Stresses in Reinforced Plastics," J. Res. Nat. Bur. Stds., 37, 239-250, R. P. 1745 (1946).

53. W. D. Kingery, "Note on Thermal Expansion and Microstresses in Two-Phase Compositions," J. Am. Cer. Soc., 40, pp. 351-52 (October, 1957).

54. R. L. Coble and W. D. Kingery, "Effect of Porosity on Physical Properties of Sintered Alumina," J. Am. Cer. Soc., 39, p. 377 (1956).

55. R. K. Verma, "Elasticity of Some High-Density Crystals," J. Geophysical Research, 65, pp. 757-66 (February, 1960).

56. R. F. S. Hearmon, "The Elastic Constants of Anisotropic Materials - II," Adv. in Phys., 5, pp. 323-382 (July, 1956).

57. J. B. Wachtman; W. E. Tefft; D. G. Lam and C. S. Apstein, "Exponential Temperature Dependence of Young's Modulus for Several Oxides," Phys. Rev., 122, pp. 1754-59 (June 15, 1961).

58. W. D. Smiley; L. E. Solon, et al., "Mechanical Property Survey of Refractory Nonmetallic Crystalline Materials and Intermetallic Compounds," WADC Tech. Rept. 59-443, (January, 1960).

59. J. K. MacKenzie, "The Elastic Constants of a Solid Containing Spherical Pores," Proc. Phys. Soc. London, B63, p. 2 (1950).

60. J. Warshaw and R. Roy, "Thermal Expansion Measurements from Nonindexed High Temperature X-ray Powder Patterns," J. Am. Ceram. Soc. 44 (8) 421-422 (1961).

61. W. R. Brown and H. P. Kirchner, "Investigation of the Theoretical and Practical Aspects of the Thermal Expansion of Ceramic Materials," Cornell Aeronautical Laboratory Report No. PI-1273-M-10, Contract No. NOrd-18419 (March 31, 1961).

62. S. Stecura and W. J. Campbell, "Thermal Expansion and Phase Inversion of Rare-Earth Oxides," Bureau of Mines Report of Investigations No. 5847 (1961).

63. W. D. Kingery, "Introduction to Ceramics," J. Wiley and Sons, Inc., New York (1960).

64. J. G. Leschen, "A Titanium-Matching Silica-Free Ceramic," General Electric Res. Lab., Sci. Rept. No. 7, AFCRL-298, AD-260,363 (March, 1961).

65. W. F. Zimmerman and A. W. Allen, "X-ray Thermal Expansion Measurements of Refractory Crystals," Am. Cer. Soc. Bull., 35, pp. 271-74 (July, 1956).

66. O. J. Wittemore, Jr. and N. N. Ault, "Thermal Expansion of Various Ceramic Materials to 1500°C," J. Am. Cer. Soc., 39, pp. 443-44 (Dec., 1956).

67. R. H. Stutzman, J. R. Salvaggi and H. P. Kirchner, "Summary Report on An Investigation of the Theoretical and Practical Aspects of the Thermal Expansion of Ceramic Materials," Vol. 1 - Literature Survey, Cornell Aeronautical Laboratory, Inc., Report No. PI-1273-M-4, (August, 1959).

68. J. F. Wygant, "Elastic and Flow Properties of Dense, Pure Oxide Refractories," J. Am. Ceramic Soc. 34, 374-380 (1951).

69. E. H. Kerner, "Elastic and Thermoelastic Properties of Composite Media," Proc. Phys. Soc. London, B69, pp. 808-813, (1956).

70. W. Hume-Rothery and P. W. Reynolds, "High Temperature Debye-Scherrer Camera and its Application to the Study of the Lattice Spacing of Silver," Proc. Roy. Soc. A167, 25 (1938).

71. G. L. Ploetz, C. W. Krystyniak and H. E. Dumes, "Thermal Expansion of Four Rare Earth Oxides," KAPL-M-GLP-1, (March 28, 1957).

72. H. B. Huntington, "The Elastic Constants of Crystals" from Solid State Physics, Vol. 7, Academic Press, Inc. (1958).